Biosensors and Bioelectronics 106 (2018) 149–178

Contents lists available at ScienceDirect

Biosensors and Bioelectronics

journal homepage: www.elsevier.com/locate/bios

Progress in utilisation of graphene for electrochemical biosensors

Abdulazeez T. Lawal

Department of Chemical Sciences, Fountain University Osogbo, Nigeria

ARTICLE INFO

Keywords:
Biosensor
Electrochemical
Graphene
Metals
Pesticides, immunosensor

ABSTRACT

This review discusses recent graphene (GR) electrochemical biosensor for accurate detection of biomolecules, including glucose, hydrogen peroxide, dopamine, ascorbic acid, uric acid, nicotinamide adenine dinucleotide, DNA, metals and immunosensor through effective immobilization of enzymes, including glucose oxidase, horseradish peroxidase, and haemoglobin. GR-based biosensors exhibited remarkable performance with high sensitivities, wide linear detection ranges, low detection limits, and long-term stabilities. Future challenges for the field include miniaturising biosensors and simplifying mass production are discussed.

1. Introduction

In recent years great progress has been made in applying graphene (GR) to design novel biosensors. The use of GR offers to biosensing platforms exceptional optical, electronic and magnetic properties. GR can increase the surface of the transducing area of the sensors that in turn bring an increase in catalytic behaviors. A class of graphene-like 2D materials (2DMats) is emerging and has recently attracted the interest of researchers, because of their unique properties, which also allow applications in sensing and biosensing, energy conversion and storage (Szabó et al., 2015; Ghosh et al., 2016; Tanmoy and Suvra Prakash, 2016, Yingkui et al., 2016), catalysis (Sun et al., 2015; Wang et al., 2015; Zhai et al., 2015; Wang et al., 2016; M. Chen et al., 2017; X. Chen et al., 2017; Kong et al., 2017; Wen et al., 2017), composites, electronics (Zhang et al., 2017) and biomedical field (Pittori et al., 2015, Ji et al., 2016).

In development of new biosensors, sensitivity, selectivity, and rapid cost-effective detection of target biomolecules are often taken into paramount considerations for their use in environmental, security, agriculture or food applications, healthcare including clinic diagnosis and treatment of diseases (Zhu et al., 2015; Arduini et al., 2016b; Lebedev et al., 2016; Syedmoradi et al., 2017). Biosensors are becoming a critical part of modern life, because it can be used from diagnosis of life-threatening diseases (Arduini et al., 2016a; Arduini et al., 2016b; Lebedev et al., 2016) to detection of biological agents in warfare or terrorist attacks. Recently, the incorporation of nanomaterial into biosensors has boosted the advances in biosensors leading to great enhancements in their performance and applications (Del Valle and Bonanni, 2014; Holzinger et al., 2014; Barsan and Brett, 2015; Cernat et al., 2015, David et al., 2015; Dhull et al., 2015; Gan and Zhao, 2015; Ge et al., 2015; Perreault et al., 2015; Tonelli et al., 2015; Yang et al., 2015d; Zhang and Chen, 2015; Arduini et al., 2016a; Benvidi et al., 2016; Bilgi and Ayranci, 2016; Fenzl et al., 2016; Metters and Banks, 2016; Reverté et al., 2016; Saxena and Das, 2016; Wang et al., 2016; Zhang et al., 2016; Hasanzadeh et al., 2017; Kurbanoglu et al., 2017). Advances in the field of materials science have led to the synthesis of many new materials with unique physicochemical properties and in recent years, extensive research has been carried out on nanomaterial-based electrochemical biosensors; however, some suffer from limitations of sensitivity, electrochemical stability, production cost, detection time and biocompatibility.

Carbon-based nanomaterials such as CNTs (Barsan and Brett, 2015, Boujakhrout et al., 2015, Dago et al., 2015, Amano et al., 2016, Bai et al., 2016b, Chinnappan et al., 2016, Deb et al., 2016, Eguílaz et al., 2016a, Eguílaz et al., 2016b, Eguílaz et al., 2016c, Abdalla et al., 2017, Amatatongchai et al., 2017, Barbosa et al., 2017, Beiranvand et al., 2017, Buber et al., 2017, Dalkıran et al., 2017, Jakubus et al., 2017, Liu et al., 2017, Ma et al., 2017, Paul et al., 2017, Syedmoradi et al., 2017, Termehyousefi et al., 2017), GR (Ba Hashwan et al., 2016, Bahadir and Sezgintürk, 2016, Balamurugan et al., 2016, Castrignanò et al., 2016, Church et al., 2016, Cinti and Arduini, 2016, Dalkıran et al., 2016, Eftekhari-Sis et al., 2016; Guy and Walker, 2016, Kazemi et al., 2016, Mehta et al., 2016, Zhou et al., 2016; Arvand and Hemmati, 2017, Asadian et al., 2017, Lee et al., 2017, Liu et al., 2017, Luong et al., 2017, Mehmeti et al., 2017, Morales-Narváez et al., 2017, Syedmoradi et al., 2017), buckypaper, (Sieben et al., 2014; Chatterjee et al., 2015; Rashid et al., 2017), and nanohybrids (Li et al., 2011; Gu et al., 2016) among various other types of engineered nanomaterials have received enormous attention due to their promising sensor applications, which are widely used in the electrochemical sensing of various compounds (Amatatongchai et al., 2015; Hayat et al., 2015; Ahmadraji and Killard, 2016; Aslan and Anik, 2016; Castrignanò et al., 2016; Komathi et al., 2016; Kulkarni and Slaughter, 2017).

E-mail addresses: abdul.lawal@yahoo.com, abdu.lawal@yahoo.com.

https://doi.org/10.1016/j.bios.2018.01.030
Received 28 October 2017; Received in revised form 2 January 2018; Accepted 15 January 2018
Available online 31 January 2018
0956-5663/

Nanomaterials such as gold nanoparticles (Afkhami et al., 2014; Arkan et al., 2014; Bao et al., 2014, Aliakbarinodehi et al. 2015; Arkan et al., 2015; Bao et al., 2015; Benvidi et al., 2015; Cai et al., 2015; Cheng et al., 2015; Beiranvand et al., 2016; Boujakhrout et al., 2016; Güner et al., 2017; Kangkamano et al., 2017; Zhang et al., 2017), silver nanoparticles (Lin et al., 2014, Liu et al., 2014, Wang et al., 2014, Naghib, 2016, Tang et al. 2016, H. Wu et al. 2016, Q. Wu et al. 2016, Han et al. 2017, Li et al., 2017) magnetic nanoparticles (Arvand and Hemmati, 2017), metal nanomaterials, platinum nanoparticles (Mani et al., 2014; Amatatongchai et al., 2015; Chauhan et al., 2015; Hossain et al., 2015; Liu et al., 2015; Meng et al., 2015; Yang et al., 2015a; Borisova et al., 2016; Hossain and Park, 2016a, 2016b; Tajabadi et al., 2016; Wang et al., 2016; Xu et al., 2016; Zan et al., 2016) and quantum dots (Dong et al., 2013; Sadhukhan et al., 2014; Antonios, 2015; Benítez-Martínez and Valcárcel, 2015; Fan et al., 2015a; Goryacheva et al., 2015; Huan et al., 2015; Lou et al., 2015; Nirala et al., 2015; Yan et al., 2015; Yang et al., 2015b; Zhou et al., 2015; Ertek and Dilgin, 2016; Majumder and Mondal, 2016; Mohammad-Rezaei and Razmi, 2016; Weng and Neethirajan, 2016; Xie et al., 2016; Arvand and Hemmati, 2017; Zhu et al., 2017) have also been actively investigated for their applications in biosensor. Carbon based nanomaterials have been given special attention because of their remarkable mechanical and electrical properties. They offer diverse advantages with their unique properties, such as a high surface-to-volume ratio, high electrical conductivity, chemical stability, biocompatibility, and robust mechanical strength.

They are also advantageous for electrochemical biosensors because they increase the electroactive surface area, enhance electron transfer, and promote adsorption of molecules. GA and its composites are one of the most innovative nanomaterials with unique electronic, optical (Soleymani, 2015; Zhu et al., 2015), mechanical (Verma et al., 2014), chemical and electrochemical (Abdalhai et al., 2015; Agnihotri et al., 2015; Aliakbarinodehi et al., 2015; Ahour and Ahsani, 2016; Akiba and Anzai, 2016; Aliakbarinodehi et al., 2016) properties.

Many research groups all over the world are carrying out exciting work using graphene and its hybrids in applications such as supercapacitors (Fedorovskaya et al., 2014; Dar et al., 2015; Lu et al., 2016a; Tingting et al., 2016; Velmurugan et al., 2016; Dezfuli et al., 2017; Śliwak et al., 2017), fuel cells (S. Han et al., 2015, Y. Han et al., 2015; Ravenna et al., 2015; Sun et al., 2015; Bandodkar et al., 2016), batteries (S. Liu et al., 2015; H. Liu et al., 2015; Xie et al., 2016b; Yang et al., 2016), photocatalysis (Ali Tahir et al., 2016), photovoltaics (Jariwala et al., 2013; Ali Tahir et al., 2016; Wang et al., 2017b), chemical and biosensors (Bo et al., 2016), gas sensors (Noremberga et al., 2017), photonics (Casalino et al., 2015), solar cell (Ali Tahir et al., 2016; Zheng et al., 2017), light-emitting diodes (LEDs) (Tanmoy and Prakash, 2016), electronic (Nguyen and Zhao, 2014), optoelectronics (Jariwala et al., 2013), photo catalyst (Jaeho Shim, JungKyuKim et al., 2016), thin-film transistors (Deng et al., 2016) and field effect transistor (FET) (Chang et al., 2013; Cai et al., 2015; Green and Norton, 2015; Park et al., 2015; Pezard et al., 2015; Huang et al., 2016; B. Park et al., 2016; C.S. Park et al., 2016; Zhang et al., 2017; Zhu et al., 2017).

GR represents a class of carbon materials based on a monolayer of carbon atoms arranged in a honeycomb lattice. Graphene oxide (GO) and reduced graphene oxide (RGO) are the main representatives of this class (Figs. 1 and 2). As a novel single-atom-thick sheet of sp2 hybridized carbon atoms, GR has attracted extensive attention in recent years because of its unique and remarkable properties, such as excellent electrical conductivity, large theoretical specific surface area, and strong mechanical strength (Bo et al., 2016) Fig. 1. In recent years GR has attracted an enormous amount of interest for its use in biosensors (Xie et al., 2016a; Wang et al., 2017; Zhang et al., 2017; Zhao et al., 2017) in various transduction modes from electrical and electrochemical to optical detection (Bharath et al., 2015; Arduini et al., 2016b; Báez and Bollo, 2016; Bahadir and Sezgintürk, 2016; Asadian et al., 2017). Their excellent fluorescence quenching ability has been

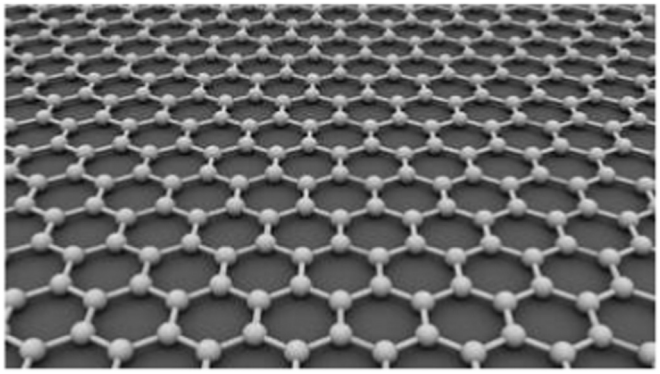

Fig. 1. Structure of the main grapheneai.

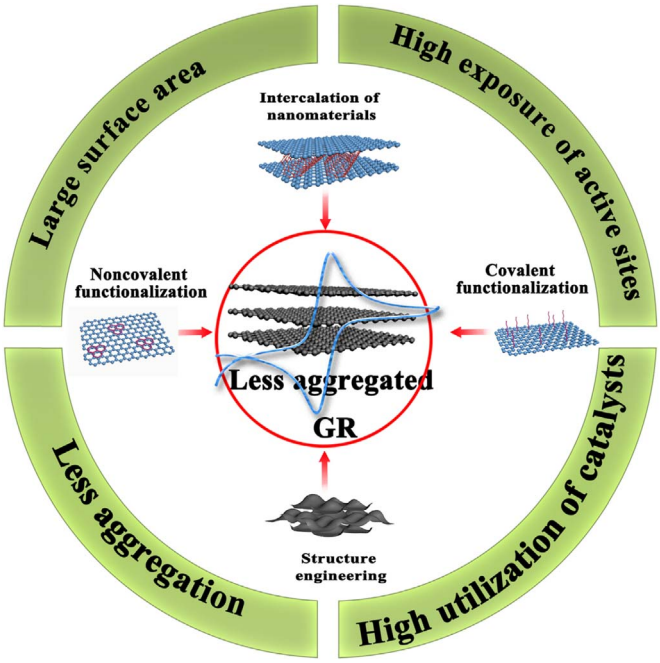

Fig. 2. Electrochemical sensors or biosensors based on less aggregated GR and their composites (Xiangjie et al., 2017).

exploited in optical sensors. Among the exceptional properties of GR, its high electrical conductivity and their very efficient electrocatalytic behavior are the most relevant for electrochemical applications. GR offers unique advantages including enhanced electronic properties, a large edge plane/basal plane ratio, and rapid electrode kinetics. Therefore, GR-electroanalytical based electrodes generally have higher sensitivities, lower limits of detection, and faster electron transfer kinetics than traditional carbon electrodes. As a result of GR high surface area, excellent electron conductivity, super hydrophobicity and enhanced mechanical strength of GR films, the research on GR films has blossomed during the recent decades and many recent biosensors have incorporated GR as sensing elements for biomolecular compound (Boujakhrout et al., 2015; Cernat et al., 2015; Chia et al., 2015; Borisova et al., 2016; Cinti and Arduini, 2016).

Different electroanalytical techniques have been employed for the development of GR electrochemical biosensors for the detection and quantification of many biomolecular species, chemical compounds, inorganic ions (Cu et al., 2014, 2015) in environmental (Hou et al., 2015; Ali Tahir et al., 2016) and biological samples. Electrocatalysts plays a critical role in the design of efficient, reliable, stable, and innovative inexpensive electrochemical biosensors which can sensitively detect a variety of biological analytes (Adhikari et al., 2015; Ali Tahir et al., 2016). Various GR electrochemical biosensors have been

developed for detecting and quantification of medical, pharmaceutical and environmental important compounds such as glucose (Amatatongchai et al., 2015; Bao et al., 2015; Bharath et al., 2015; Ambrosi et al., 2016; Aslan and Anik, 2016; Castrignanò et al., 2016; Amatatongchai et al., 2017; Luong et al., 2017), methylglyoxal, H_2O_2 (Vilian and Chen, 2014; Zor, Saglam et al., 2014; Thirumalraj et al., 2016), metal ions (Baldantoni et al., 2014; Arduini et al., 2016b), ascorbic acid (Barberis et al., 2015; J. Li et al., 2015; S.M. Li et al., 2015; Cao et al., 2016; Deb et al., 2016), uric acid (J. Li et al., 2015; S.M. Li et al., 2015), NADH (Chiang Lin et al., 2014; Govindhan et al., 2015; Li et al., 2015a; Sangamithirai et al., 2015; Mutyala and Mathiyarasu, 2016), acetaminophen (Cernat et al., 2015) and pesticides (Bao et al., 2015; Sansuk and Sritongkham, 2015; Zhang et al., 2015; Zhao et al., 2015; Zheng et al., 2015; Liu et al., 2016; Zhou et al., 2016).

GR based electrodes have been commonly used as sensors and biosensors because of their low cost, good electron transfer kinetics, large surface area, high esposure of active site and biocompatibility Fig. 2. The utilisation of GR as sensors (Justino et al., 2017), including chemical sensors (Arduini et al., 2016b; Correa et al., 2017), gas sensors, mechanical sensors, resonant sensors, humidity sensors, biofuel cells (Ravenna et al., 2015; Qiu et al., 2017; Qu et al., 2017), environment sensors and optical sensors (Bo et al., 2016) has recently gained tremendous interest.

Biomolecular detection using GR biosensor is crucial for many areas of health care, screening of new drug molecules (Yang et al., 2015a), HIV screening, clinical medicine (Mehrotra, 2016; Piro et al., 2016; Baryeh et al., 2017; Syedmoradi et al., 2017), pharmaceutical products (Ghorbani-Bidkorbeh, 2015), food safety (Malhotra et al., 2014; Malhotra et al., 2015; Rotariu et al., 2016; Song et al., 2016; Zeng et al., 2016; Dridi et al., 2017; Duffy and Moore, 2017) and environmental monitoring (Chabot et al., 2014; Ali Tahir et al., 2016; Church et al., 2016). The high surface- to -volume ratio of GAs makes it possible to obtain ultrafast detection of biomolecular species at low temperature. GR-based biosensors are ultra-sensitive, have fast response time, lower potential of redox reaction and less fouling effect. They have high stability and longer life than the commercial metal oxide, silicon and other material sensors. These enhanced characteristic have stimulated a lot of research interest in utilisation of GR as components for electrochemical biosensor. Advantages of GR-based electrochemical biosensors include: (i) high sensitivity, because of the large surface area ratio. GR can be used to immobilised enzyme, which keep high biological activity;(ii) fast response time, GR has an outstanding ability to mediate fast electron-transfer kinetics hence promote the electron-transfer reactions like NADH and H_2O_2; (iii) lower potential of redox reaction and less surface fouling effects; (iv) high stability and longer life time. These improved characteristics have stimulated the increasing research interest in the utilisation of GR as components for biosensors. Rapid development of GR used as biosensor has been successfully witnessed in the past decades and electrochemical biosensors constructed with GR have received great attention in recent years (Taranejoo and Moghri, 2014; Sun et al., 2015; Shuai et al., 2016; Sobolewski et al., 2016; Song et al., 2016; Tezerjani, Benvidi et al., 2016; Tingting et al., 2016; Arvand and Hemmati, 2017). It has also been used as bio-field-effect transistors (Zhang et al., 2015), impedance biosensors (Ding et al., 2014), electrochemiluminescence (Deng et al., 2014; Su and Lv, 2014; Feng et al., 2015; Huan et al., 2015; Shu et al., 2015; Pur et al., 2016; Chen et al., 2017b), and fluorescence biosensors (Wen et al., 2015; Zou et al., 2015; Yang et al., 2016).

They also have potential applications in nanoelectronics (B. Park et al., 2016, C.S. Park et al., 2016), composite materials (Xie et al., 2016a; Wang et al., 2017a; Xu et al., 2017; Zhao et al., 2017; Zhao et al., 2017; Cui et al., 2018a), energy (Chabot et al., 2014; Dar et al., 2015; Fan et al., 2015; Li et al., 2015c, Ghosh* et al., 2016; X. Li et al., 2016, Z.J. Li et al., 2016; Lu et al., 2016a; Majumder and Mondal, 2016; Mikmeková et al., 2016; Serry and Sakr, 2016; Shim et al., 2016; Wang et al., 2016; Xiong et al., 2016; Dahal and Gumbs, 2017; Morales-Narváez et al., 2017) and biomedicine (Reina et al., 2014; Amjad et al., 2015; Syedmoradi et al., 2017).

2. Synthesis and functionalization of graphene

2.1. Synthesis

Several kinds of GR have been synthesized and utilized in electrochemical analytical protocols The synthesis of GR can be categorized into three main techniques such as exfoliation, chemical vapour deposition and chemicals based.

Pristine GR, obtained by the mechanical cleavage of graphite, has some exceptional properties. However, this type of graphene has a low throughput, small size, and hydrophobicity in particular, which limits its application in electrochemical biosensors GO substantially increases the hydrophilicity of the graphene layers, but GO is an electrical insulator, which reduces conductivity by many orders of magnitude. By eliminating the oxygen-containing groups of GO, RGO achieves a unique combination of excellent conductivity, large surface area, high electrochemical activity and ease of functionalization. Thus, compared with pristine graphene and GO, RGO has certain overwhelming advantages for application in electrochemical analytical assays.

2.1.1. Exfoliation

Exfoliation and cleavage method is essentially based on breaking of weak Van der Waals bonds that held together layers of graphene sheets and separating them into individual graphene sheets. Different approaches based on the exfoliation principle have shown promise for large dimensions and mass production (B. Kong et al., 2015, F.-Y. Kong et al., 2015; Paredes and Villar-Rodil, 2016; Yang et al., 2016). Another way of executing the same concept includes dispersion and exfoliation of pure graphite in an aqueous media. Graphene does not contain metallic impurities and has been produced by mechanical exfoliation of graphite. Mechanical exfoliation of highly oriented pyrolytic graphite produces single or few layers of graphene, but is not suitable for mass production.

Mechanical exfoliation (repeated peeling) of highly oriented pyrolytic graphite. This method, which is called scotch-tape method, is still widely used in many laboratories to obtain pristine perfect structured graphene layer(s) for basic scientific research and for making proof-of-concept devices. The other method for producing defect-free/defect-less graphene is the mild exfoliation of graphite, but the yield so far is very low.

2.1.2. Chemical vapour deposition (CVD)

CVD is, a fabrication process where graphene is grown upon a substrate, has emerged as an important method for the preparation and production of graphene for various applications (Kakatkar et al., 2015; Osikoya et al., 2016). CVD is a simple approach that eradicates the residual metallic impurities. CVD technique preserves graphene's properties on surfaces such as Ni (Rengaraj et al., 2015), ruthenium and Cu, among others. Microwave plasma enhanced efficient synthesis of uniform multilayer graphene nanoflake films (MGNFs) on Si substrates. It is often used for low cost, largescale graphene of good quality (Lei et al., 2014). CVD is a potential mass-production method with the aim of producing graphene for electronics (Zhang and Lieber, 2016; Song et al., 2017) and biosensor (Chen et al., 2016a; Shrivastava et al., 2016; Zhang and Lieber, 2016; Zhang et al., 2016; X. Chen et al., 2017; M. Chen et al., 2017; Li et al., 2017a; Song et al., 2017) applications Fig. 3.

2.1.3. Chemicals based techniques

The chemical method is through oxidation; usually the Standenmaier method, the Brodie method and the Hummers method have been used for the disintegration of graphite to graphene layers by chemical reactants. Hummer method is a commonly used technique to prepare graphene oxide. This method essentially consists by treating

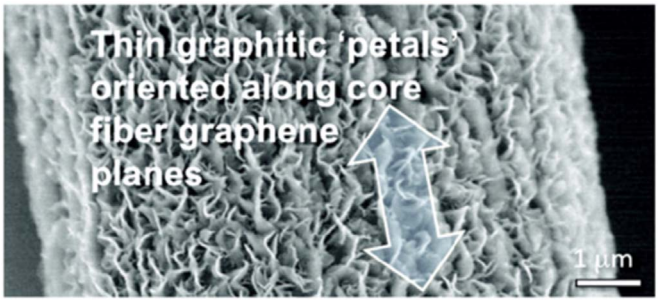

Fig. 3. Catalyst-free synthesis of cantilevered carbon nano sheet extensions, or petals, from graphite fibers by microwave plasma CVD. Results reveal that the petals grow from the fiber surface layers while preserving graphitic continuity from fiber to the petals.

graphite with a water-free mixture of concentrated sulfuric acid, sodium nitrate, and potassium permanganate.

Chemical reduction of graphite oxide is popular for electrochemical sensors because it results in graphene with structural defects and functional groups, which benefits electrochemical detection of neurotransmitters (Bahrami et al., 2016).

Graphene flowers were produced by a simple and “green” electrochemical method. The homogenous graphene flowers, with layers of petals, increased the surface area significantly and also accelerated electron transfer. However, further physical characterization of these flowers is needed to understand their properties.

Saini in his review (Saini, 2016) GR is a two-dimensional material with amazing characteristics, which grant it the title "wonder material". It has grabbed appreciable attention due to its exceptional electrical, optical, thermal, and mechanical properties. Because of these interesting properties, graphene has found its way into a wide variety of biosensing applications.

2.2. Functionalization

Functionalization of graphene has further opened up novel fundamental and applications of graphene (Saini, 2016). Various functionalization techniques have been used to modify graphene in order to attach "bioreceptor" molecules, capable of specific and selective detection of target biomarkers. Two major functionalization are currently available, direct and indirect (J. Liu et al., 2014, Y. Liu et al., 2014) functionalization technique while Deepshikha (Saini, 2016) enumerated covalent and non-covalent functionalization as the only two major methods of functionalization Fig. 2. The covalent functionalization is via the grafting of molecules onto the sp2 carbon atoms of the π-conjugated skeleton while the non-covalent functionalization is based on the adsorption of polycyclic aromatic compounds or surfactants via π-stacking and hydrophobic interactions on the carbon framework (Ji et al., 2016). The Covalent functionalisation can take place at the edges and/or on the structural alteration or functionalization can take place at the edges and/or on the basal surface while non covalent linkages between graphene and other functional groups are mainly achieved through π-π stacking, van der Waals (Macwan et al., 2017), electrostatic forces, hydrophilic (Mao et al., 2016) and hydrophobic (Baptista-Pires et al., 2014) interactions.

Some research groups reported the modification of GR or its derivatives by chemical/physical attachment of specific functional groups for application in the electrochemical sensing of biomolecules. GC electrodes modified with sulfonated GR, hydrogenated GR and GR (oritsderivatives) functionalised with ethylenediaminetetraacetic acid, ferulic acid (Han et al., 2014), L-tyrosine (Zhang et al., 2015), cetyltrimethylammonium (Yang and Li, 2014), ionic liquid (Wang et al., 2014), porphyrin (Wang et al., 2014) and 3,4,9,10-perylenetetracarboxylic acid were applied in the detection of DA. Covalent also applied for serum lactate (Manna and Retna Raj, 2016).

3. Graphene nanocomposite

Hybrid composites based on GR with inorganic nanostructures (Yan et al., 2015; Altuntas et al., 2016; Bai et al., 2017; Chauhan et al., 2017), conducting polymer (Gokoglan et al., 2017; Liu et al., 2017, Vinay Deep Punethaa, Sravendra Ranab et al., 2017, Wu et al., 2017) and organic materials (Ruecha et al., 2014; Yang et al., 2016) have been used for fabrication of electrochemical biosensors for detection of biomolecules. Nanocomposites electrodes containing GR/rGO and Iridium oxide (Kurbanoglu et al., 2017b), Au nanostructures or nanostructures (Chen et al., 2016a; Li et al., 2017b; Saeed et al., 2017; Wu et al., 2017; Xu et al., 2017; Zhao et al., 2017; Zhu et al., 2017), AgNP (Huang et al., 2015; Huang et al., 2015; Hui et al., 2015; Jamil et al., 2015; Yusoff et al., 2017), FeNP (Balamurugan et al., 2016; Teymourian et al., 2017; Yu et al., 2017), CeNP (Nayak et al., 2015; Du et al., 2017; Du et al., 2017; Tian et al., 2017), PtNPs (Liu et al., 2015a; Liu et al., 2015; Liu et al., 2015; Sun et al., 2015; Zan et al., 2016), Pd–Pt NPs (Mijowska et al., 2015; Xi et al., 2016), TiO_2 NPs (N. Liu et al., 2017; S. Liu et al., 2017; W. Liu et al., 2017; H. Liu et al., 2017; Muthuchamy et al., 2017), CuO_2 NPs (Liu et al., 2016a; Wu et al., 2016), ZrO_2 NPs (Mogha et al., 2016) or CNTs (Tran and Mulchandani, 2016; Ba Hashwan et al., 2017) have been used as electrochemical biosensors for the detection of biomolecules. These resulting nanocomposites often exhibit superior surface area and electrical conductivity, less biofouling and improved sensitivity compared to pristine GR. The combination of graphene sheets with polyvinylpyrrolidone (PVP) (Ruecha et al., 2014) or nanoparticles (Cui et al., 2017; Dalkıran et al., 2017a; Farka et al., 2017; Jain and Chauhan, 2017; H. Liu et al., 2017; N. Liu et al., 2017; W. Liu et al., 2017; S. Liu et al., 2017; Zhu et al., 2017; Cui et al., 2018; Zhan et al., 2018), can enhance the analytical response of sensors and biosensors, mainly improving their sensitivity, limit of detection, and reproducibility.

4. Biosensor

Biosensors are integrated receptor-transducer devices capable of providing selective quantitative or semiquantitative analytical information using a biological recognition element (Pacheco et al., 2017). Such biological elements include enzymes, whole cell and tissues. They are generally highly selective and offer real-time measurements for bioanalysis and bioprocess control. Graphene-based biosensor have been widely studied for the accurate electrochemical detection of many biomolecules, which is extremely vital to the development of biomedical instruments, clinical diagnosis (Bing and Wang, 2017; Campuzano et al., 2017; Hughes et al., 2017; Pan et al., 2017; Saeed et al., 2017; Wang et al., 2017a), and disease treatment (Zhang et al., 2016b) Fig. 4.

Electrochemical biosensors mainly have three types: amperometric-based, potentiometric-based and impedimetric-based, the amperometric-based mode is the most widely used. The sensing mechanism of amperometric GR-based biosensors is using the analytes, different enzymes are selected, such as NADH (Chiang Lin et al., 2014; Govindhan et al., 2015), glucose oxidase (GOx) (Bharath et al., 2015; Chen et al., 2015; Chen et al., 2015; Devasenathipathy et al., 2015; Hossain et al., 2015; Krzyczmonik et al., 2015; Wang et al., 2015; Castrignanò et al., 2016; Hong et al., 2016; Kim et al., 2017), aflatoxin-oxidase, cholesterol oxidase (Kakhki et al., 2013; Huan et al., 2015; Li et al., 2015b; Komathi et al., 2016; Nandini et al., 2016; Wu et al., 2016; Dervisevic et al., 2018), lactic acid oxidase (Dagar and Pundir, 2017) and horseradish peroxidase (Vilian and Chen, 2014; Komori et al., 2016; Wu et al., 2016; Liu et al., 2017b) (Feng et al., 2014; Guo et al., 2015; Chen, Hong et al., 2016; Komori et al., 2016). Oxidizable H_2O_2 or NADH is easily generated as a result of these enzymes, as described in Eqs. (1) and (2):

$$\text{Substrate} + O_2 \xrightarrow{\text{oxidase}} \text{Product} + H_2O_2 \quad (1)$$

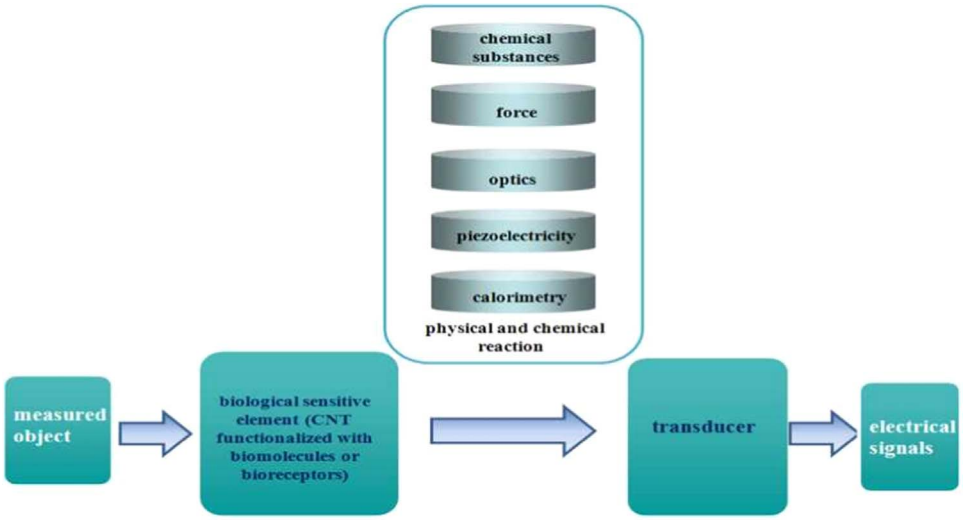

Fig. 4. Schematic depictions of different GR-based biosensors. The physical or chemical reaction is transformed into electrical signals after the target molecule was detected by detection device (Yang et al., 2015a, 2015b, 2015c, 2015d).

Substrate + NADdehydeogenase → Product + NADH..... (2)

4.1. Direct electrochemistry of graphene and enzymes

The direct electrochemistry of enzyme refers to the direct electron communication between the electrode and the active center of the enzyme without the participation of mediators or other reagents direct electrochemistry of redox enzymes on common electrodes is very difficult because the active centers of most redox enzymes are located deeply in a hydrophobic cavity (Yu et al., 2014; Liang et al., 2015; Zhao et al., 2015; Lee et al., 2016; Luong et al., 2017). Functionalized graphene promotes the electron transfer between electrode substrates and enzymes.

4.2. Enzymatic biosensor

Enzymatic sensors play an important role in human daily life. Extensive studies of enzymatic sensors are focused on improving the activity, stability, and direct electrochemistry of enzymes. Enzymatic biosensors have been valuable bioanalytical devices for analysis of diverse targets in disease diagnosis, biological and biomedical research (G. Chen et al., 2015; Y. Chen et al., 2015; Liepmann et al., 2015; Nanda et al., 2015; Z.J. Li et al., 2016; X. Li et al., 2016; Lee et al., 2017).

Since the first enzymatic electrode proposed by Clark and Lyons more than 40 years ago, electrochemical biosensors based on the use of enzymes have received considerable attention due to the advantages of the association of the biocatalytic activity of enzymes with the high sensitivity and versatility of the electrochemical transduction. The enzyme immobilization step is critical, since the biocatalyst has to remain active to perform an efficient biorecognition of the substrate and several methods have been used to immobilise these enzymes on GR and its composites. The other aspect to consider is that the transducer where the enzyme is immobilised has to allow a fast charge transfer to ensure a rapid and sensitive response. Several strategies for immobilising proteins on GR modified electrodes have been proposed,

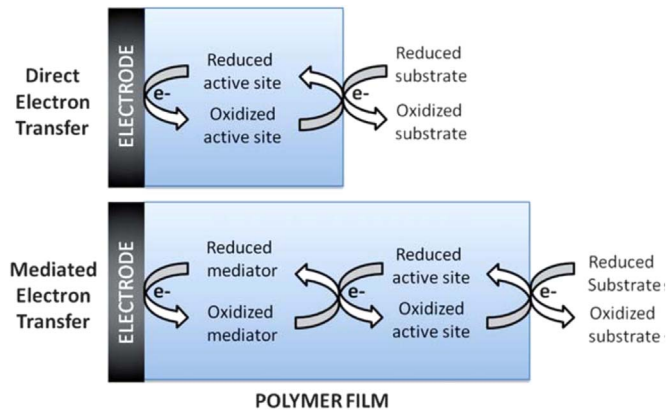

Fig. 5. Anodic direct electron transfer and mediated electron transfer.

Direct electrochemistry of enzymes involves direct electron transfer (DET) between the electrode and the active center of the enzymes without the participation of mediators or other reagents (Wang and Bi, 2014; Yu et al., 2014; Liang et al., 2015; Qu et al., 2015; Šakinyte et al., 2015; Terse-Thakoor et al., 2015; Lee et al., 2016; Mutyala and Mathiyarasu, 2016; Luong et al., 2017; Pakapongpan and Poo-arporn, 2017) Fig. 5. The favorable electron transfer kinetics and high sensitivity are originated from the good conductivity and large surface area of graphene favouring immobilization of enzymes (Song et al., 2016). New mediator-free (or reagentless) biosensors, enzymatic bioreactors, and biomedical devices employ DET by immobilising enzymes on conducting substrates. But, the redox centers of the biomolecules are usually embedded deep in their large three dimensional structures. GR and metal nanoparticles have exhibited excellent performance in enhancing the DET between enzymes and electrodes, and are now widely used. Recent research has shown that GR can enhance DET between enzymes and electrodes. Graphene offers high enzyme loading capacity that sharply increases the sensitivity. Graphene also offers a direct electron transfer between the functionalized graphene and active site of bioreceptor without involvement of any mediator and all these features make graphene a suitable material for electrochemical sensors.

4.3. Non enzymatic biosensor

Enzymatic biosensors face a serious problem of enzyme inactivation and enzyme loss which affects the biosensor performance. There are several disadvantages of enzyme-modified electrodes, such as their instability, the high cost of enzymes and the complexity of immobilization. Activity of enzymes can be affected by temperature, pH, and toxic chemicals. In attempts to eliminate such problems, several researchers now pay considerable attention to nonenzymatic electrodes.

4.4. Graphene based biosensors

Graphene based biosensors are available for sensing glucose, hydrogen peroxides, dopamine, ascorbic acid, uric acid, cholesterol, pesticides, metal ions and reduced b-nicotinamide adenine dinucleotide (NADH) molecules (Table 1).

Table 1
The specific electrochemical biosensors for sensing of small biomolecules (DA, AA, UA, APAP, H_2O_2, glucose and NADH) (Celine et al., 2017).

Molecule	Sensor	Method	Detection limit/μM	Linear range/μM	Reference
DA	Pristine G/GCE	CV	2	5.00–710	(Qi et al. 2015)
	PVP/G/GCE	CV	0.0002	0.0005–1130	
	solution-gate transistor	CV	0.001	/	(Zhang et al. 2014a)
	Fe3O4/rGO/GCE	CV	0.08	0.4–3.5	
	3DNG	CV	0.001	3–100	(Feng et al., 2015)
	CD/3DNG	CV	/	10–140	(Liu et al., 2015b)
	MWCNTs/GO/GCE	CV	0.022	0.2–400	
	G/Chitosan/GCE	CV	0.05	0.1–140	
	Fe3O4/G/GCE	CV	0.007	0.01–100.55	(Salamon et al. 2015)
	3DrGO/GCE	CV	0.17	5–1000	(Yu et al. 2014a)
	PEDOT/rGO/GCE	CV	0.039	0.1–175	(Wang et al., 2014d)
	MWNTs bridged mesocellular G/GCE	DPV	0.06	0.3–10	(Li et al., 2014a)
	G/platelet/ILs/chitosan/GCE	DPV	0.04	0.05–240	
	G/PEI/Au NPs/GCE	DPV	0.2	2–48	(Ponnusamy et al. 2014)
	G nanosheets/CTAB	DPV	0.6	4–52	
	ErGO/GCE	DPV	0.5	0.5–60	(Yang et al., 2014)
	Au NPs/Ppy/rGO/GCE	DPV	0.0000183	0.0001–5	(Qian et al., 2014)
	Au NPs/rGO/GCE	DPV	1.4	6.8–41	(Wang et al., 2014a)
	PPy/G/GCE	DPV	0.022	/	
	NG/GCE	DPV	0.25	0.5–170	
	GO/SiO2/MIPs/GCE	DPV	0.03	0.05–160	
	Fe3O4/Au-S-Fc/GS/chitosan/GCE	DPV	0.1	0.5–50	
	Screen-printed G	DPV	0.12	0.5–2000	
	Hemin/GO/GCE	DPV	0.17	0.5–40	(Zou et al., 2015)
	G/MIPs	LWV	0.1	0.1–830	
	G/Au Ag	SWV	0.205	0.3–300	(Pruneanu et al. 2015)
AA	Pristine G/GCE	CV	6.45	9.00–2314	(Qi et al. 2015)
	G/CPE	CV	0.07	0.1–106	(Li et al. 2011a)
	Au NPs/GO/GCE	CV	0.1	/	(Song et al., 2014)
	Fe3O4/rGO/GCE	CV	200	160–7200	
	CuO/3DG	CV	0.43	0.43–200	(Ma et al. 2014)
	Screen-printed G	DPV	0.95	4.0–4500	
	Hemin/GO/GCE	DPV	0.3	1–100	(Zou et al., 2015)
	MWNTs bridged mesocellular G/GCE	DPV	18.28	100–6000	(Li et al., 2014a)
	G/platelet/ILs/chitosan/GCE	DPV	14.8	0.12–260	
	ErGO/GCE	DPV	250	500–2000	(Yang et al., 2014)
	Au NPs/rGO/GCE	DPV	51	240–1500	(Wang et al., 2014a)
	NG/GCE	DPV	2.2	5–1300	
	Fe3O4/Au-S-Fc/GS/chitosan/GCE	DPV	/	6–350	
UA	Pristine G/GCE	CV	4.82	6.00–1330	(Qi et al. 2015)
	G/Chitosan/GCE	CV	0.1	1.0–125	
	Screen-printed G	DPV	0.2	0.8–2500	
	Hemin/GO/GCE	DPV	0.17	0.5–50	(Zou et al., 2015)
	Fe3O4/PDDA/rGO/GCE	DPV	0.08	0.5–20	
	MWNTs bridged mesocellular G/GCE	DPV	0.93	5–100, 300–1000	(Li et al., 2014a)
	G/platelet/ILs/chitosan/GCE	DPV	0.1	0.12–260	
	ErGO/GCE	DPV	0.5	0.5–60	(Yang et al., 2014)
	Au NPs/rGO/GCE	DPV	1.8	8.8–53	(Wang et al., 2014a)
	NG/GCE	DPV	0.045	0.1–20	
	PTCA/G/MWCNTs/ILs/GCE	DPV	0.0012	0.03–3820	
	Fe3O4/Au-S-Fc/GS/chitosan/GCE	DPV	0.2	1–90	
APAP	MWCNTs/GO/GCE	CV	0.047	0.5–400	
	CD/3DNG	CV	/	10–350	(Liu et al., 2015b)
	PEDOT/GO/GCE	CV	0.57	/	(Si et al. 2014)
	Fe3O4/PDDA/G/GCE	DPV	0.037	0.1–100	
	Fe3O4/Au-S-Fc/GS/chitosan/GCE	DPV	0.05	0.4–32	
	NMP-exfoliated G/GCE	DPV	0.0025	/	(Wu et al. 2015a)
	G/TiN	DPV	0.02	0.06–660	(B. Kong et al., 2015; F.-Y. Kong et al., 2015)
	G/Ni2O3-NiO/GCE	DPV	0.02	0.04–100	(J. Liu et al., 2014; Y. Liu et al., 2014)
	SWCNTs/G/GCE	DPV	0.038	0.05–64.5	
	rGO/PEDOT/GCE	DPV	0.4	1.0–35.0	(Huang et al. 2014b)
	Nafion/TiO2-GR/GCE	DPV	0.21	1–100	
	G/CoFe2O4/CPE	SWV	0.025	0.03–12	(Afkhami et al., 2014)
	G/ZnO/GCE	SWV	0.000033	0.0001–20	(Jiang et al. 2014)
H_2O_2	PB/nitrobenzene/RGO/GCE	Amperometric	0.4	1.2–15250	
	Ag NPs/NG/GCE	Amperometric	1.2	100–126400	(Tian et al., 2014)
	Ag/NG/ITO	Amperometric	0.26	100–80000	(Tajabadi et al. 2015)
	RGO/ZnO/GCE	Amperometric	/	0.02–22.48	
	GPs/G/CS/GCE	Amperometric	1.6	5–35000	(Jia et al. 2014)
	Cu2O/G/GCE	Amperometric	20.8	300–7800	
	Pt/G/CNT paper electrode	Amperometric	0.01	/	(Sun et al. 2015b)
	3DG/Pt NPs	Amperometric	0.125	0.167–7.486	
	AuNPs/PMS/rGO/GCE	Amperometric	0.06	0.5–50000	(Mani et al., 2014)
	DNA/Ag/G/GCE	CV	3	15–23000	

(*continued on next page*)

Table 1 (*continued*)

Molecule	Sensor	Method	Detection limit/μM	Linear range/μM	Reference
	Fe3O4/rGO/GCE	CV	0.006	0.02–0.28	
	Pt NPs/G/GCE	CV	0.5	1–1477	(Liu et al., 2015a)
	Au Pd NPs/NG	CV	0.02	0.1–20	(Shang et al. 2015)
	rGO/SWCNT/GCE	CV	1.3	0.5–5	
	Fe3O4/Au/HRP/G/Nafion/SPCE	CV	12	20–2500	
	Ag NPs/rGO/ITO	CV	5	100–100000	
	G/MWCNTs/GCE	CV	9.4	20–2100	
	G/CS/PB/GCE	CV	0.213	10–400	
	G/Nafion/Azure I/AuNPs/GCE	CV	10	30–5000	
	Pd NPs/G/GCE	CV	0.05	0.1–1000	
	BGs/GCE	CV	3.8	1000–20000	(Yeh et al. 2015)
	Cu NPs/G/GCE	CV	0.35	1–1000	(Mani et al. 2015)
	PANI/HRP/G/CNT/Nafion/Au Pt NPs/GCE	CV	0.17	0.5–100	
	SPAnH/HMGO/CLC/GOD	CV	/	10–1000	
Glucose	CuO NPs/G/GCE	Amperometric	0.09	0.5–2000	(Alizadeh and Mirzagholipur, 2014)
	Co Pt/G/GCE	Amperometric	14.6	16.7–1600	(Wang et al., 2015a)
	Cu2O/G/GCE	Amperometric	3.3	300–3300	
	rGO/Cu2O/GCE	Amperometric	0.05	10–6000	(Zhou et al., 2014)
	Pt NPs/G/GCE	Amperometric	30	1000–25000	(Chang et al., 2015)
	NiO NPs/GO/GCE	Amperometric	1	3.13–3050	
	Cu NWs/G/GCE	Amperometric	1.6	5–6000	
	CuO NPs/SG	Amperometric	0.08	100–10500	(Tian et al., 2015a)
	Nafion/NiO NF/GO/GCE	Amperometric	0.77	2–600	
	NiO HS/rGO/Nafion/GCE	Amperometric	0.03	0.6246–258.4, 258.4–10500	(Lu et al. 2015)
	$MnCo_2O_4$/G/GCE	Amperometric	0.001	0.005–800	(Zhang et al., 2015a)
	3DG/Co3O4	Amperometric	0.025	/	
	GO-PEDOT/Pt NPs/MGPN	Amperometric	0.3	10–50000	
	ErGO/GCE	CV	1	5–12000	
	Nafion/GO/G-APTES/GCE	CV	/	1400–27900	
	Nafion/G-GO/GCE	CV	/	500–4000	
	Cu NPs/G/GCE	CV	2.1	10–5500	(Mani et al. 2015)
	SPAnH/HMGO/CLC/GOD	CV	/	100–1400	
	CS/PB/G/GCE	CV	10	25–3200	
	AuNPs/G/GCE	CV	4	10–16000	
	ConA-DexP/GO/GCE	CV	0.34	5–9000	
	ErCG/GOD/GCE	CV	20	2000–18000	
	G/CNT/ZnO/GCE	DPV	4.5	10–6500	(Hwa and Subramani, 2014)
	rGO/SWCNT/GCE	CV	0.078	20–400	
NADH	G/GCE	CV	1.9	45–360	
	Fe3O4/rGO/GCE	CV	40	2.0–15	
	DNA tetrahedron/G/AuNPs/GDE	DPV	/	1fM~10 p.M.	(S.M. Li et al., 2015; J. Li et al., 2015)

4.4.1. Enzymatic glucose graphene-based biosensor

Diabetes is a major health problem causing 4 million deaths each year and 171 million people suffering worldwide. Although there is no cure for diabetes, nevertheless, the blood glucose level of diabetic patients should be monitored tightly to avoid further complications. Thus, monitoring of glucose in blood has become an inevitable need leading to fabrication of accurate and sensitive advanced blood sugar detection devices for clinical diagnosis, personal care contributing to diagnosis, monitoring and formulation of a treatment plan for diabetes mellitus patients. It also led to the development of enzymatic and non-enzymatic glucose sensing approach in food quality control and human blood (Zaidi and Shin, 2016; Qin et al., 2016)

Recently, several researches on the preparation and application of a glucose enzyme biosensor based on novel graphene materials have been reported by various research groups.

Jiang et al. (2018) proposed a label-free biosensor based on graphene oxide (GO) and glucose oxidase GOx functionalized tilted fiber grating (TFG) with large tilted angle for low concentration glucose detection. Taking advantages of sufficient binding sites of the GO with oxygen-containing groups, the enzymes GOx are covalently immobilized onto GO-deposited TFG via 1-ethyl-3-(3-dimethylaminopropyl) carbodiimide and N-hydroxyl succinimide cross-liner. Surface characterizations with optical microscopy, scanning electron microscopy, Raman and infrared spectroscopy provide detailed assessments and evidences about the homogeneity of GO deposition and the effectiveness of enzyme modification. Through the specific catalysis reaction of GOx on the glucose, a considerable refractive index change in local microenvironment around the TFG results in the resonant wavelength shifts of cladding modes. The detection results of the low-concentration glucose demonstrate that the resonant wavelength has a linear response to the glucose concentration in the range of 0–8 mM with a response coefficient of ~0.24 nm/mM, showing an enhanced sensitivity and bioselectivity compared with the pristine TFG.

Pakapongpan and Poo-arporn (2017) fabricated a novel approach of the immobilization of a highly selective and stable glucose biosensor based on direct electrochemistry by a self-assembly of GOx on reduced graphene oxide (RGO) covalently conjugated to magnetic nanoparticles (Fe3O4 NPs) modified on a magnetic screen-printed electrode (MSPE). The RGO-Fe3O4 nanocomposite has remarkable enhancement in large surface areas, is favorable environment for enzyme immobilization, facilitates electron transfer between enzymes and electrode surfaces and possesses super para magnetism property. The morphology and electrochemical properties of RGO-Fe3O4/GOx were characterized by SEM, FTIR, Raman spectroscopy, CV and amperometry. The modified electrode was a fast, direct electron transfer with an apparent electron transfer rate constant (ks) of 13.78 s^{-1}. The proposed biosensor(showed fast amperometric response (3 s) to glucose with a wide linear range from 0.05 to 1 mM, a low detection limit of 0.1 μM at a signal to noise ratio of 3 (S/N = 3) and good sensitivity (5.9 μA/mM). The resulting biosensor has high stability, good reproducibility, excellent selectivity and successfully applied detection potential at −0.45 V.

Palanisamy et al. (2015) developed a simple glucose biosensor based on direct electrochemistry of GOx immobilized on the reduced graphene oxide (RGO) and β-cyclodextrin (CD) composite. A well-

defined redox couple of GOx appears with a formal potential of ~-0.459 V at RGO/CD composite. A heterogeneous electron transfer rate constant (K_s) has been calculated for GOx at RGO/CD as 3.8 s^{-1}. The fabricated biosensor displays a wide response to glucose in the linear concentrations range from 50 μM to 3.0 mM. The sensitivity and limit of detection of the biosensor is estimated as 59.74 μA mM^{-1} cm^{-2} and 12 μM, respectively.

Park et al. (2015) reported a rapid-response and high-sensitivity field-effect transistor (FET)-based sensor with specificity towards glucose, based on reduced graphene oxide (rGO)-carboxylated polypyrrole (C-PPy) nanotube (NT) hybrids as the conductive channel. The rGO, C-PPy NTs, and rGO/C-PPy NT hybrids were characterized using Raman spectroscopy, FT-IR spectroscopy, XRD, TEM, and SEM. The results indicate that a well-organized structure was successfully prepared, based on specific interactions between the C-PPy NTs and the graphene sheets. Reliable electrical contacts were developed between the rGO/CPPy NTs and the patterned-microelectrodes, which remained stable when exposed to the liquid-phase electrolyte. Liquid-ion-gated FETs composed of these rGO/C-PPy NT hybrids exhibited hole-transport behavior with higher conductivity than those of graphene sheets or C-PPy NTs because the C-PPy NTs formed a bridge between the graphene layers, resulting in effective electron transport. GOx was used as the capture probe, and was tightly combined with C-PPy NTs via a chemical coupling reaction, and glucose detection was performed via GOx, which catalyzes the oxidation of glucose in the rGO/C-PPy NTs hybrid FET biosensor. The FET biosensor provided a rapid response (< 1 s) with high sensitivity toward glucose with a limit of detection of 1 nM. This result is ca. 2–3 orders more sensitive than previous reported glucose sensor.

Pepłowski et al., (2015) analyzed various methods and materials for enzyme stabilization within screen-printed graphene sensor. Main goal was to develop technology allowing immediate printing of the biosensors in single printing process. Factors being considered were: toxicity of the materials used, ability of the material to be screen-printed (squeezed through the printing mesh) and temperatures required in the fabrication process. Performance of the examined sensors was measured using chemical amperometry method, and then appropriate analysis of the measurements was conducted. The analysis results were then compared with the medical requirements. Parameters calculated were: correlation coefficient between concentration of the analyte and the measured electrical current (0.986) and variation coefficient for the particular concentrations of the analyte used as the calibration points. Variation of the measured values was significant only in ranges close to 0, decreasing for the concentrations of clinical importance. These outcomes justify further development of the graphene-based biosensors fabricated through printing techniques.

Qi et al. (2016) successfully prepared AuNP decorated GO nanocomposites (GO-Ph-AuNP) via aryldiazonium salt chemistry, which can be used as the immobilization matrix for loading GOx towards a sensitive glucose sensor. The fabricated nanocomposite was characterized by field emission scanning electron microscopy, UV–Vis and electrochemistry. The direct electrochemistry of GOx was successfully realized on GO-Ph-AuNP modified GC electrodes with a heterogeneous electron transfer rate constant of 8.3 s-1, revealing fast direct electron transfer of GOx. The GOx immobilized on GO-Ph-AuNP nanocomposite modified electrode retained good electrocatalytic activity toward glucose over a linear concentration range from 0.3 to 20 mM with the sensitivity of 42 mA mM^{-1} cm^{-2} and enzyme turnover rate of 112 s^{-1}. In addition, the fabricated biosensor was capable of monitoring glucose consumption by live cells.

Rabti et al. (2016) reported the preparation of a nanoporous flat electrode by drop casting a nanocomposite consisting of rGO and chitosan onto a polyester substrate. An underlying conductive surface is not required. The nanocomposite was characterized by scanning electron microscopy and electrochemical impedance spectroscopy. The 3D network of the composite was used as a scaffold for the immobilization of GOx. A well-defined signal related to direct GOx electrochemistry was registered and used to monitor levels of glucose. The resulting biosensor displays a linear response to glucose with a detection limit of 5 μM (at an S/N ratio of 3) and a sensitivity of 41.7 μA·mM^{-1}·cm^{-2}. The sensor was applied to the determination of glucose in artificial saliva.

Rafighi et al. (2016) reported a novel approach for the fabrication of a third generation glucose biosensor based on the immobilization of GOx on graphene-polyethyleneimine-gold nanoparticles hybrid (GNS-PEI-AuNPs) using glutaraldehyde as cross-linking reagent. A pair of well-defined redox peaks with the formal potential and peak separation value of −0.38 V and 60 mV was observed for the immobilized GOx on a gold electrode modified with GNS-PEI-AuNPs hybrid. The heterogeneous electron transfer rate (ks) for the redox center of the immobilized GOx, flavin adenine dinucleotide (FAD), was found to be 5.4 s^{-1}. An increase for the anodic peak current and a decrease for the cathodic peak current were recorded for the immobilized GOx on the modified electrode in the presence of glucose and the absence of oxygen. The obtained results confirmed that the prepared modified electrode presented bioelectrocatalytic activity towards glucose through a DET mechanism. The response of the fabricated glucose biosensor was linear towards glucose in the concentration range between 1 and 100 μM with the sensitivity about 93 μA mM^{-1} cm^{-2}. The limit of detection (LOD) for glucose sensing was estimated to be 0.32 μM (S/N = 3).

Altuntas et al. (2016) prepared graphene sheets and three different graphene-metallic nanocomposites including graphene-copper (graphene-Cu), graphene-nickel (graphene-Ni) and graphene-platinum (graphene-Pt) and characterized in the first place. Then the electrochemical performances of these nanocomposites were tested in glucose biosensor transducers, which were formed by combining these metallic nanocomposites with GOx enzyme and glassy carbon paste electrode (GCPE). This is the first work that includes the usage of these graphene-Me nanocomposites as a part of glucose biosensor transducer. Fabricated amperometric biosensors linear ranges were obtained as follow: For the plain graphene, the linear range was found in the concentration range between 50 μM and 800 μMwith the RSD n = 3 for 50 μ (glucose) value of 12.86% and LOD value of 7.2 μM. For graphene-Pt modified glucose biosensor, the linear range was between 10 μM and 600 μM with the RSD (n = 3 for 50 μM glucose) value of 3.45% and LOD value of 3.06 μM. In the case of graphene-Ni modified glucose biosensor, the values were 250–600 μM with the RSD (n = 3 for 50 μM glucose) value of 8.76% and LOD value of 24.71 μM and for graphene-Cu modified glucose biosensor linear range was 25 μM to 400 μM with the RSD (n = 3 for 50 μM glucose) value of 3.93% and LOD value of 2.87 μM.

Raicopol et al. (2016) reported a new strategy to create glucose amperometric biosensors with improved analytical characteristics using graphene as support for GOx. First, a reduced graphene oxide film was obtained on the glassy carbon electrode surface by direct electrochemical reduction of graphene oxide from a suspension in water. For facilitating the oxidation of the enzymatically generated H_2O_2, in a second step, Pt nanoparticles were electrodeposited on the graphene modified electrodes. The obtained biosensors showed good analytical performances in terms of high sensitivity and wide linear range.

Ravenna et al. (2015) prepared a novel composite material for the encapsulation of redox enzymes. Reduced graphene oxide film with adsorbed phenothiazone was used as a highly efficient composite for electron transfer between flavin adenine dinucleotide (FAD)-dependent glucose dehydrogenase and electrodes. Measured redox potential for glucose oxidation was lower than 0 V vs Ag/AgCl electrode. The fabricated biosensor showed high sensitivity of 42 mA M^{-1} cm^{-2}, a linear range of glucose detection of 0.5–12 mM, and good reproducibility and stability as well as high selectivity for different interfering compounds. In a semibiofuel cell configuration, the hybrid film generated high power output of 345 μW cm^{-2}. These results demonstrate a promising potential for this composition in various bioelectronic application.

Ren et al. (2016) prepared triethylenetetramine-functionalized graphene (TFGn) using GO and triethylenetetramine as raw materials through a one-step reaction under alkaline condition. The triethylenetetramine-functionalized graphene was then applied to fabricate glucose biosensors with IO_4^- oxidized GOx through layer-by-layer (LBL) self-assembly by the covalent bonding between the aldehyde groups of GOx and amino groups of TFGn. The gold electrodes modified with the $(GOx/TFGn)_n$ multilayer films were studied by CV and showed outstanding electrocatalytical response to the oxidation of glucose when ferrocenemethanol was used as an artificial redox mediator. The response increased with an increasing number of GOx/TFGn bilayers, indicating that the analytical performance, such as the sensitivity of the glucose biosensor, could be adjusted by tuning the number of deposited GOx/TFGn bilayers. The linear response range of the biosensor constructed with six bilayers of GOx/TFGn to the concentration of glucose can extend to at least 8 mM with a sensitivity of 19.9 μA mM^{-1} cm^{-2}. In addition, the sensor exhibited good stability due to the covalent interactions between the GOx and TFGn.

Sağlam and Dilgin (2017) developed a photoamperometric glucose biosensor based on GOx in flow injection analysis (FIA) system using ZnS-CdS quantum dot (QD) modified multiwalled carbon nanotube/glassy carbon electrode (ZnS-CdS/MWCNT/GCE). Cyclic voltammograms of the proposed electrode (GOx/ZnS-CdS/MWCNT/GCE) showed a pair of well-defined reversible redox peak attributing that direct electron transfer between the protein and electrode. The current of the reduction peak became more cathodic in the presence of O_2 due to the electrocatalytic activity of the electrode towards the reduction of dissolved O_2, but reduction current shifted to a less negative value upon addition of glucose in the solution. The obtained CV currents were affected by the irradiation of the electrode surface. Thus, the photoelectrochemical biosensing of glucose in the FIA system was studied by monitoring of the changes in the electrocatalyzed reduction peak current of dissolved O_2 at the proposed electrode dependent on glucose concentration. The proposed photoelectrochemical FIA method has a linear response to glucose ranging from of 0.01–1.0 mM with detection limit of 3.0 μM under optimized conditions.

Shanbhag and Prasadi (2016) addressed and discuss the emerging highly sensitive graphene and its derivative (graphene oxide and reduced graphene oxide) biosensors, which exhibit promising results in monitoring of glucose concentrations in saliva through a non-invasive way, thereby contributing to diagnosis, monitoring and formulation of a treatment plan for diabetes mellitus patients.

Thirumalraj et al. (2015) fabricated a glucose biosensor based on the direct electrochemistry of GOx at glassy carbon modified with a RGO and fullerene-C60 (C60) composite. The reduced graphene oxide/fullerene (RGO-C60) composite was prepared by electrochemical reduction of a GO and C60 composite at −1.4 V for 200 s in pH 5 solution; while the GO-C60 composite was prepared by a simple sonication of C60 in GO solution for 6 h at 45 °C. A well-defined and enhanced reversible redox peak of GOx was observed at RGO-C60 composite compared with other modified electrodes. The heterogeneous electron transfer rate constant (Ks) and the surface coverage concentration of GOx at RGO-C60/GOx modified electrode were calculated to be 2.92 s^{-1} and 1.19 × 10^{-10} mol cm^{-2}, respectively. Under optimum conditions, the amperometry response of the biosensor was linear against the concentration of glucose from 0.1 to 12.5 mM with a response time of 3 s. The limit of detection was estimated to be 35 μM based on S/N = 3 with a high sensitivity of 55.97 μA mM^{-1} cm^{-2}. In addition, the fabricated biosensor showed a good practical ability for the detection of glucose in human blood serum samples

Xue et al. (2015) described a simple process in which a graphene oxide (GO)–Prussian Blue (PB)-3, 4, 9, 10-perylenetetracarboxylic dianhydride derivative (PTC-NH2) nanocomposite film is spread onto a glassy carbon electrode (GCE). GOx was adsorbed on the modified glass carbon electrode via the specific structure of hollow Pt nanospheres. To characterise the sensors, several techniques were employed, including TEM, FT-IR s, CV, electric EIS and chronoamperometry. The resulting amperometric glucose biosensor exhibited a fast response time (within 5 s) and a good linear calibration range from 0.01 ± 0.06 mM to 5.23 ± 0.04 mM with a lower limit of detection of 3.3 μM (S/N = 3).

Vijayaraj et al. (2016) fabricated a disposable glucose biosensor on the surface of a cost-effective pencil graphite electrode (PGE) by an electrochemical method, using glucose GOx and rGO. Electrochemical pre-treatment of the PGE enables the adsorption of the rGO-GOx biocomposite. The biocomposites of GOx and rGO were simply prepared by the electrochemical potential cycling method. Efficient immobilization of rGO-GOx is confirmed by field emission scanning electron microscopy, attenuated total reflectance-Fourier transform infrared spectroscopy, X-ray photoelectron spectroscopy, and CV measurements. The rGO nanosheets enhance direct electron transfer (DET) between GOx and the electrode surface. Determination of glucose indirectly by O_2 reduction was achieved, which showed high sensitivity, selectivity, reproducibility and stability without a redox mediator. The sensor exhibits a linear current response for a wide range of glucose concentrations between 1.0 × 10^{-5} and 1.0 × 10^{-3} M (R = 0.998), and a dynamic range up to 10.0 × 10^{-3} M with a detection limit of 5.8 mM. The rGO-GOx biosensor showed an excellent anti-interference ability against electroactive species and proved to be useful for the determination of glucose in human serum samples.

Liu et al. (2016b) successfully synthesized a novel composite of graphene/MnO_2 (GR/MnO_2) by a simple one-step hydrothermal method. The as-synthesized MnO_2 and the composite were characterized by scanning electron microscopy (SEM), X-ray diffraction (XRD), X-ray photoelectron spectroscopy (XPS) and Fourier transform infrared spectroscopy (FTIR). The results showed that MnO_2 was nanorods and the two materials were perfectly composited. The composite was decorated on a GCE and used for the entrapment of GOx. Electrochemical results showed that the composite modified electrode showed a pair of well-defined redox peaks, and the direct electron transfer between GOx and the electrode surface was accelerated. The sensor fabricated by the composite modified electrode showed an excellent response to the oxidation of glucose with a wide linear range (0.04–2 mM), low detection limit (10 μM), and high sensitivity (3.3 μA mM^{-1} cm^{-2}).

4.4.2. Non enzymatic glucose graphene-based biosensor

Glucose is one of the most important human biomarkers, because of the large number of diseases correlated to alterations in its blood concentration. In diabetes mellitus, for instance, hyperglycaemia is related to a deficiency of insulin. A number of secondary factors can also contribute to high blood glucose concentrations. These include pancreatitis, pituitary orthyroiddys-function, renal failure and liver disease. Hypoglycaemia is less frequently observed but also in this case a variety of conditions may cause low blood glucose levels, such as insulinemia, hypopituitarism and neoplasms.

There has been increasing demand for the development and improvement of glucose sensors. Not only has the number of people requiring these sensors significantly increased over the last decade, the demand to make sensors which are both biocompatible and have increased sensing capabilities as compared to current technologies. In order to meet these needs, a move towards nonenzymatic glucose sensors has begun. These new sensors have garnered significant interest due to their capacity to achieve continuous glucose monitoring, their high stability compared to traditional glucose sensors, and the ease of their fabrication. Research has been extensively geared towards the preparation of these nonenzymatic glucose sensors from novel materials, often with unique micro- or nano-structures, which possess ideal properties for electrochemical biosensor applications. In recent years, a variety of materials including noble metals, metal oxides, carbon nanotubes, graphene, polymers, and composites have been explored for their electrocatalytic response to the oxidation of glucose. In this review, the most recent advances in nonenzymatic glucose sensors are visited, with the focus being on the last four years of research (Tian

et al., 2014). Noble metals such as Pt and Au and their composites were usually chosen to develop nonenzymatic sensors in early research studies. Recently, researchers have reported and fabricated several non enzymatic glucose biosensors:

Benjamin et al. (2017) reported the design and preparation of nonenzymatic biosensor based on an ionic liquid tagged cobalt-salophen metal complex (Co-salophen-IL) immobilized on electrochemically reduced graphene oxide (ERGO) for the detection of glucose via an electrochemical oxidation. The bioinspired Co-salophen-IL complex has been synthesized and immobilized on ERGO, which was previously deposited on a screen printed carbon electrode (SPE) to form the Co-salophen-IL/ERGO/SPE nonenzymatic biosensor. The electrochemical behavior of this modified electrode was studied using CV and EIS. Notably, the Co-salophen-IL/ERGO/SPE biosensor exhibited excellent electrocatalytic activity towards glucose oxidation in 0.1 M NaOH, based on which an amperometric sensor has been developed. The modified electrode has shown prominent performance towards glucose detection over a wide linear range from 0.2 μM to 1.8 mM with a detection limit and sensitivity of 0.79 μM and 62 μA mM^{-1} respectively. The detection was carried out at 0.40 V and such a less working potential excludes the interference from the coexisting oxidizable analytes.

Mazaheri et al. (2017) presented a novel hybrid electrode based on reduced graphene oxide/nickel/zinc oxide heterostructures. The sensor was fabricated by template-free hydrothermal growth of ZnO nanorod arrays on conductive glass substrates (FTO) followed by conformal electrodeposition of nickel nanoparticles with an average size of 18 nm. Then, in-situ reduction and electrophoretic deposition of graphene oxide (GO) nanosheets on the structured ZnO/Ni electrode was performed. The prepared three-dimensional nanostructure exhibited fast electrocatalytic response (< 3 s) towards glucose oxidation due to the large surface area and high electro-activity. The prepared biosensor possessed a wide linear range over 0.5 μM to 1.11 mM, a low detection limit of 0.15 μM at signal/noise ratio (S/N) of 3, and a sensitivity of 2030 μA cm^{-2} mM^{-1}. Wu et al. (2017)) prepared a Ni plasma-modified graphene-based glucose sensor on a glassy carbon electrode. The Ni plasma-modified graphene, which has structural integrity and good conductivity after the plasma treatment, shows excellent glucose sensing ability as confirmed by electrochemical assessment of the GC-G-Ni electrode. The GC-G-Ni sensor exhibits a high glucose sensitivity of 2213 μA mM^{-1} cm^{-2}, low detection limit of 1 μM, short response time of less than 1 s, good selectivity, long-term stability, and reproducibility.

Zhao et al. (2017) prepared a novel ultrasensitive nonenzymatic sensor by in-situ growing layered CuS/RGO/CuS (RGO) nanostructure on the Cu foam surface through a hydrotherm-assisted process. The CuS/RGO/CuS nanocomposite was characterized with X-ray diffraction (XRD), Raman spectroscopy, X-ray photoelectron spectrometer (XPS) and field emission scanning electron microscopy (FESEM). This CuS/RGO/CuS/Cu was directly used as electrochemical sensor of glucose, and its performance was evaluated by CV and amperometry techniques. The nonenzymatic biosensor exhibited ultrahigh linear sensitivities of 22.67 and 10.54 mA mM^{-1} cm^{-2} in the concentration ranges of 1–655 μM and 0.655–1.055 mM, respectively. The detection limit was determined to be 0.5 μM with the signal-to-noise of three.

Wang et al. (2016) fabricated a novel, stable and sensitive non-enzymatic glucose biosensor based on bimetallic hollow Ag/Pt nanoparticles and the rGO. The hybrid of bimetallic hollow Ag/Pt nanoparticles-reduced graphene oxide (HAg/PtNPs-rGO) was prepared by a galvanic replacement reaction and the thermal reduction of graphene oxide. Thermal reduction has been highly effective in producing graphene-like films which can render a stable substrate for hollow Ag/Pt nanoparticles. The morphology and composition of the prepared samples were characterized by SEM, TEM, XRD, energy-dispersive X-ray spectrometry and FTIR. CV measurements demonstrated that the biosensor decorated by HAg/PtNPs-rGO can directly detect glucose and show a superior electro catalytic activity. The results of amperometric method showed a desirable amperometric response with a sensitivity of 129.32 μA mM^{-1} cm^{-2}, a linear range of 0.003–7.72 mM (R^2 = 0.9943), a fast response time (less than 3 s) and a low detection limit of 1.8 μM (S/N = 3). In addition, the fabricated sensor also had good selectivity, reproducibility and long-term stability.

Another electrochemical non-enzymatic glucose was prepared by (Yan et al., 2015) using graphene as a spacer, multilayer ultrathin films composed of Prussian blue nanoparticles and glucose oxidase have been fabricated on a glass carbon electrode via electrostatic layer-by-layer (LbL) assembly technique to construct glucose biosensors. This work demonstrated the capability of graphene as the spacer to form electrochemically functionalized inorganic and organic hybrid nanoarchitecture. The buildup and electrochemical properties of the multilayer nanoarchitecture were investigated by UV–Vis spectroscopy, atomic force microscopy technique and CV, respectively. It was found that the developed glucose biosensor allowed rapid and sensitive determination of glucose. The amperometric response exhibited a linear correlation to glucose concentration over a range from 0.1 to 6.5 mM and the response time and detection limit were determined to be 2 s and 6 μM, respectively.

C.S. Park et al. (2016), B. Park et al. (2016) demonstrated the use of a RGO based glucose sensor using a radio frequency (RF) signal. An RGO with outstanding electrical property was employed as the interconnector material between signal electrodes in an RF electric circuit, and it was functionalized with phenylbutyric acid (PBA) as a linker molecule to bind glucoses. By adding glucose solution, the fabricated sensor with RGO and PBA showed detecting characteristics in RF signal transmission and reflection. Frequency dependent electrical parameters such as resistance, inductance, shunt conductance and shunt capacitance were extracted from the RF results under the equivalent circuit model. These parameters also provided sensing characteristics of glucose with different concentrations. Using these multi-dimensional parameters, the RF sensor device detected glucose levels in the range of 1^{-4} mM, which ordinarily covers the testing range for diabetes or medical examination.

Yang et al. (2016) directly deposited highly efficient electrocatalytic polyoxometalate (POM) on polymeric ionic liquid (PIL)-functionalized rGO in a simple manner. The nano-sized POM with PIL functional groups was uniformly distributed on the surface of rGO sheets. The unique nanostructure of the resultant POM-g-rGO nanohybrids enabled well-defined multiple redox reaction of POMs and rapid electron transfer. In particular, as-prepared nanohybrids demonstrated high electrocatalytic activity for the electrochemical detection of H_2O_2 and glucose molecules in flow-injection biosensor device with high sensitivity, rapid response time, and low detection limit.

Gao et al. (2014) fabricated a nonenzymatic sensor based on Ni(OH)2/electroreduced graphene oxide (ERGO)–multiwalled carbon nanotube (MWNT) nanocomposites via convenient electrodeposition of Ni(OH)2 nanoparticles on ERGO–MWNT film modified GCE. Graphene oxide (GO) sheets can serve as surfactants to stabilize the dispersion of pristine MWNTs in aqueous solution, rendering a fine coverage of ERGO–MWNT film on GCE during the fabrication process. MWNTs perform as conducting bridges between ERGO sheets to enhance the electron transfer rate in the substrate. By combining the advantages of ERGO and MWNTs, together with electrocatalytic effect of $Ni(OH)_2$ nanoparticles, the well-designed nanocomposites exhibit excellent sensing behavior towards glucose and H_2O_2. The linear detection ranges for glucose and H_2O_2 are 10–1500 μM and 10–9050 μM while the detection limits are 2.7 μM and 4.0 μM, respectively. Furthermore, a very high sensitivity is achieved with 2042 μA m M^{-1} cm^{-2} estimated for glucose and 711 μA m M^{-1} m^{-2} for H_2O_2.

Wang et al. (2016) reported the easy electrochemical fabrication of graphene aerogel/platinum nanoparticle (GA/PN) hybrid materials with a three-dimensional interconnected pore composite-modified electrode. The GA/PN product was characterized by scanning electron microscopy, transmission electron microscopy, X-ray diffraction, and X-

ray photoelectron spectroscopy. CV measurements show that GA/PN can directly catalyze the oxidation of glucose and exhibit enhanced current responses. This biosensor exhibits remarkable sensitivity (84.92 μA·mM^{-1}·cm^{-2}), an approximate linear detection range of glucose concentration (50 μmol·L^{-1} to 500 μmol·L^{-1}), and a detection limit of 0.561 μmol·L^{-1}.

4.4.2.1. Enzymatic hydrogen peroxide graphene-based biosensor. H_2O_2 is one of the most important analytes to be detected, because of its presence in many enzymatic reactions·H_2O_2 is the product of several oxidases, e.g. glucose, cholesterol, and alcohol oxidase, and for its occurrence in food, pharmaceutical, clinical, industrial and environmental analysis.

The high levels of H_2O_2 are closely associated with cancer and progressive neurodegenerative diseases such as Parkinson. Therefore, the accurate and sensitive detection of hydrogen peroxide is of great importance. Several researches on the preparation and application of a H_2O_2 enzyme biosensor based on novel graphene materials have been reported by various research groups:

Liu et al. (2017b) constructed a viable and simple method for preparing porous graphene network using silver nanoparticles (AgNPs) etching based on the porous graphene (PGN) and HRP to measure the release of H_2O_2 from living cells. Owing to the large surface area and versatile porous structure, the use of nanoporous materials can significantly improve the analysis performance of the biosensor by loading large amounts of enzyme and accelerating diffusion rate. Meanwhile, the constructed electrode exhibited excellent electrochemical performance toward H_2O_2 with a determination limit as low as 0.0267 nM and wide linear range of 7 orders of magnitude, which was superior to other H_2O_2 electrochemical sensors. Thus, this novel biosensor can detect the H_2O_2 release from living cells not only under normal physiological conditions (10^{-8}–10^{-7} M) but also in emergency state with the increased concentration (~10^{-4} M).

Yoon et al. (2017) fabricated an electrochemical biosensor composed of myoglobin (Mb) on molybdenum disulfide nanoparticles (MoS2 NP) encapsulated with GO was fabricated for the detection of H_2O_2. Hybrid structure composed of MoS2 NP and GO (GO@MoS2) was fabricated for the first time to enhance the electrochemical signal of the biosensor. As a sensing material, Mb was introduced to fabricate the biosensor for H_2O_2 detection. Formation and immobilization of GO@MoS2 was confirmed by transmission electron microscopy, ultraviolet-visible spectroscopy, scanning electron microscopy, and scanning tunneling microscopy. Immobilization of Mb and electrochemical property of biosensor were investigated by CV and amperometric i-t measurements. Fabricated biosensor showed the electrochemical signal enhanced redox current as −1.86 μA at an oxidation potential and 1.95 μA at a reduction potential that were enhanced relative to those of electrode prepared without GO@MoS2. Also, this biosensor showed the reproducibility of electrochemical signal, and retained the property until 9 days from fabrication. Upon addition of H_2O_2, the biosensor showed enhanced amperometric response current with selectivity relative to that of the biosensor prepared without GO@MoS2.

Mercante et al. (2017) reported the development of a graphene-based ternary nanocomposite of poly(3,4-ethylenedioxythiophene)-poly(styrenesulfonate), reduced graphene oxide and gold nanoparticles (PEDOT: PSS-rGO-AuNPs) for the detection of H_2O_2. The hybrid nanocomposite was assembly with horseradish peroxidase (HRP). The PEDOT: PSS-rGO-AuNPs-HRP modified electrode was used for the amperometric detection of H_2O_2 and exhibited a high sensitivity of up to 677 μA mM^{-1} cm^{-2}, with a wide linear range from 5 to 400 μM and a low detection limit of 0.08 μM (S/N = 3). This developed enzymatic biosensor showed to be highly stable and unresponsive to potentially interfering substances, and it could be used for sensing H_2O_2 in real samples, including tap water and bovine milk samples.

Fan et al. (2015b) developed amperometric H_2O_2 biosensor using biomimetic graphene capsules (GRCAPS). HRP was initially encapsulated in GRCAPS using porous $CaCO_3$ as sacrificial templates to mimic the existence form of bio-enzymes in the organisms, and then GRCAPS and graphene-poly(sodium 4-styrenesulfonate) were alternatively assembled onto the substrate of indium tin oxide for constructing multilayer films of the biosensor. Transmittance electron microscopy and field-emission scanning electron microscopy analyses proved that the GRCAPS and multilayer films were prepared. Electrochemical experiment results indicated that easy, direct electrochemistry and good catalytic activity toward H_2O_2 oxidation can be achieved with this biosensor. The resulting biosensor presented a wide linear range of 0.01–12 mmol l^{-1}, a low detection limit of 3.3 μmol l^{-1} (S/N = 3), excellent anti-interference ability, and long-term stability as well.

J. Huang et al. (2015), W. Huang et al. (2015) developed an efficient and eco-friendly microwave-assistant method to synthesize a ternary composite of polypyrrole-hemin-reduced graphene oxide (PPY-He-RGO). The polymerization of the pyrrole monomer and the reduction of graphene oxide are performed simply by microwave heating without using a strong reducing or oxidizing agent in an isopropanol/H_2O mixed medium. Hemin molecules are immobilized on reduced graphene oxide (RGO) sheets and can still retain high electrocatalytic activity toward the reduction of H_2O_2 in the final composite. The conducting RGO and polypyrrole with a well-controlled nanostructure provide a highly conductive network to the ternary composite, which can promote the electron transfer between hemin, analytes and electrodes, leading to an improved electrocatalytic activity. The PPY-He-RGO can act as a third-generation mediator and mimic enzyme for the fabrication of a hydrogen peroxide biosensor. The as-prepared PPY-He-RGO electrode exhibits a high sensitivity to H_2O_2 with a low detection limit of 0.13 μm. The efficient microwave heating provides an opportunity for large-scale production of PPY-He-RGO ternary nanocomposites as a kind of mimic enzyme for biosensors.

F.-Y. Kong et al. (2015), W. Kong et al. (2015) fabricated a hydrogen peroxide biosensor based on the cytochrome c (Cyt c) immobilized graphene-L-cysteine modified GC electrode. The obtained film of Cyt c/graphene-L-cysteine was investigated by scanning electron microscopy (SEM) and electrochemistry method. The direct electrochemistry of Cyt c was realized at the Cyt c/graphene-L-cysteine modified GC electrode and thoroughly investigated. The electrocatalysis oxidation of hydrogen peroxide on Cyt c/graphene-L-cysteine/GC electrode was also studied. At the optimized condition, a linear range from 0.1 to 480 μM (R2 = 0.996; n = 12) was obtained with the detection limit of 0.015 μM at the signal-to-noise ratio (S/N) of 3. The apparent Michaelis-Menten constant (Km) was calculated to be 0.83 ± 0.02 mM. Moreover, the modified electrode displayed rapid response (5 s) to H_2O_2, good stability and reproducibility. Based on the composite film, a third-generation reagentless biosensor could be constructed for determination of H_2O_2.

Radhakrishnan and Kim, (2015) described cerium oxide-reduced graphene oxide (CeO2-rGO) prepared by a facile one-pot hydrothermal approach and its assembly with HRP for the detection of H_2O_2 at traces levels. The prepared nanocomposite was characterized by Fourier transform infrared spectroscopy, field-emission scanning electron microscopy, X-ray diffraction, and voltammetry. Furthermore, the direct electrochemistry of HRP/CeO_2-rGO composite has been studied. The immobilized enzyme retained its bioactivity and exhibited a pair of well-defined redox peaks, confirming the direct electron transfer (DET) of HRP with CeO_2-rGO composite modified electrode. A significant enzyme loading (4.270 × 10^{-10} mol cm^{-2}) has been obtained on CeO_2-rGO composite as compared to the bare glassy carbon (GC), CeO_2, and rGO modified surfaces. This HRP/CeO_2-rGO film has been used for the sensitive detection of hydrogen peroxide by voltammetry and it exhibited a wide linear range of H_2O_2 from 0.1 to 500 μM with a detection limit of 0.021 μM. The apparent Michaelis-Menten constant (KMapp) of HRP on the CeO_2-rGO composite was estimated as 0.011 mM.

Wang et al. (2015) fabricated homogeneously distributed self-assembling graphene aerogel/gold nanoparticles (GA/GNs) hybrid with

3D interconnected pores through a simple hydrothermal route. A highly sensitive cytochrome c (Cyt c) sensor based on this GA/GNs hybrid was developed. The porous structure of the GA/GN hybrid favored the high-density immobilization of the enzyme and the penetration of water-soluble molecules, which provided a biocompatible sensing platform for the immobilization of Cyt c. CV results, indicated that the GA/GN film promoted direct electron transfer between Cyt c and the underlying electrode. The immobilized Cyt c exhibited excellent electrocatalytic activity towards the reduction of H_2O_2. The fabricated biosensor exhibited fast response and good electrochemical activity for H_2O_2 with a comparable linear range from 5 μmol·L^{-1} to 150 μmol·L^{-1} and low detection limit of 1.75 μmol·L^{-1}. Moreover, the modified electrode displayed rapid response to H_2O_2 and possessed good stability and reproducibility.

Mohammad-Rezaei and Razmi (2016) investigated electron transfer performance and direct electrochemistry of haemoglobin immobilized on graphene quantum dots-chitosan nanocomposite (Hb-GQDs-Chit) for biosensing purposes. Transmission electron microscopy, UV–Vis, photoluminescence, SEM, XRD, electrochemical impedance spectroscopy and CV techniques were used for characterizing of the prepared biosensor. Electron transfer coefficient (α) of the Hb-GQDs-Chit was calculated to be 0.56, indicating good activity and fast heterogeneous electron transfer rate between the Hb and electrode surface. The biosensor exhibited good linear response to hydrogen peroxide over the concentration range 1.5–195 μM with a detection limit of 0.68 μM and sensitivity of 0.53 μA μM^{-1} cm^{-2}. Due to the unique electron transfer ability and high surface-to-volume ratio of GQDs, and also good biocompatibility of chitosan, the fabricated biosensor shows good stability, short response time and high sensitivity.

4.4.3. Nonenzymatic hydrogen peroxide (H_2O_2) graphene-based biosensor

Enzymeless detection of H_2O_2 and glucose offers a more reliable and accurate detection route given the absence of enzyme that is sensitive to temperature, pH, poisoning chemicals, and humidity. Recently, researchers have reported and fabricated several non enzymatic H_2O_2 biosensors:

He et al. (2017) reported that $La_{0.6}Sr_{0.4}CoO_{3-\delta}$ (LSC) perovskite oxide can provide comparable performance to these noble metal nanomaterials. LSC provides superior electrooxidation activities (to H_2O_2 and glucose) over $La_{0.6}Sr_{0.4}Co_{0.2}Fe_{0.8}O_{3-\delta}$ (LSCF) and $LaNi_{0.6}Co_{0.4}O_3$ (LNC) that translates to good H_2O_2 or glucose detection performance. They proposed parallel pathways for H_2O_2 and glucose oxidations on LSC perovskite, which proceeds via Co^{3+}/Co^{4+} redox couple and via oxygen vacancies formation. Additionally, reduced graphene oxide (RGO) can be added to optimize the detection performance. The best electrode, i.e., LSC + RGO/GCE provides sensitivity of 500 and 330 μA mM^{-1} cm^{-2} for H_2O_2 and glucose, respectively, and limit of detection of 0.05 and 0.063 μM for H_2O_2 and glucose, respectively (at S/N = 3). Its respective linear ranges are 0.2–3350 μM and 2–3350 μM for H_2O_2 and glucose.

Lorencova et al. (2017) demonstrated that an extensive characterization of pristine and oxidized Ti3C2Tx (T: O, OH, F) MXene showed that exposure of MXene to an anodic potential in the aqueous solution oxidizes the nanomaterial forming TiO_2 layer or TiO_2 domains with subsequent TiO2 dissolution by F− ions, making the resulting nanomaterial less electrochemically active compared to the pristine Ti3C2Tx. The Ti3C2Tx could be thus applied for electrochemical reactions in a cathodic potential window i.e. for ultrasensitive detection of H_2O_2 down to nM level with a response time of ~10 s.

Sookhakian et al. (2017) electrochemically deposited efficient and excellent non-enzymatic electrochemical sensors for H_2O_2 detection, consisting of rGO and palladium (Pd) nanowalls with different rGO loadings, in a layer-by-layer fashion onto indium tin oxide (ITO) glass. The structure and morphology of the as-fabricated non-enzymatic sensor electrodes were confirmed by XRD, field-emission electron microscopy, and Raman spectroscopy. The effective combination of Pd nanowalls and rGO nanosheets provides many benefits in electrochemical detection, such as charge carriers with rapid transport and a greater number of sensing sites; thus, the Pd-rGO-modified ITO electrode with 0.5 mg mL^{-1} rGO displays the best electrochemical sensitivity with regard to H_2O_2 detection. The responses to H_2O_2 differ linearly with the concentration (from 100 μM to 12 mM). These devices showed a lowest detection limit of 0.24 μM, excellent stability, and high reproducibility. The enhanced sensitivity of the sensor electrode is due to the synergistic effect between the electrocatalytic activity of the Pd nanowalls and the high conductivity and large surface area of rGO.

Zhu et al. (2017) employed polydopamine (PDA) as an adhesive agent to integrate the GQDs and gold nanoparticles (Au NPs) tightly through a green, facile and rapid method. The synergistic effect of Au-PDA-GQD nanocomposite presented an excellent electrocatalytic activity towards the reduction of H_2O_2. Hence, the H_2O_2 biosensor based on Au-PDA-GQD exhibited better sensing performances, such as wide linear range (0.1–40 μM and 40–20,000 μM), low detection limit (5.8 nM) and fast response time (< 2 s) at low applied potential (− 0.1 V). Also, it presented a wonderful stability, reproducibility (RSD = 1.01%) and anti-interference.

Mutyala and Mathiyarasu (2016) reported a simple, facile and reproducible non-enzymatic hydrogen peroxide H_2O_2 sensor using ERGO modified GCE. The modified electrode was characterized by FT-IR, UV–Visible, SEM and AFM techniques. CV analysis revealed that ERGO/GCE exhibited virtuous charge transfer properties for a standard redox systems and showed excellent performance towards electroreduction of H_2O_2. Amperometric study using ERGO/GCE showed high sensitivity (0.3 μA/μM) and faster response upon the addition of H_2O_2 at an applied potential of −0.25 V vs. Ag/AgCl. The detection limit is assessed to be 0.7 μM (S/N = 3) and the time to reach a stable study state current is < 3 s for a linear range of H_2O_2 concentration (1–16 μM). In addition, the modified electrode exhibited good reproducibility and long-term stability.

Asif et al. (2017) effectively designed graphene oxide nanocomposite based sensing system which exhibited remarkable electrocatalytic performance towards the recognition of key biomolecule, i.e., H_2O_2 in a single step which reflects strong interaction between graphene oxide based nanocomposite and H_2O_2. Graphene oxide based nanocomposite was prepared by low cost and low temperature facile method and characterized by different spectroscopic techniques. The electrochemical sensing of as prepared nanocomposite towards H_2O_2 was assessed using CV and DC potential amperometry (DCPA at potential −0.570 V vs. Ag/AgCl reference electrode) in a phosphate buffer (pH = 7.0). The designed H_2O_2 biosensor displayed high sensitivity (−0.2844 ± 0.0169 μA nM^{-1} cm^{-2}), low detection limit (5 nM) with wide linear dynamic range (0.01–0.05 μM) and fast response time of less than 3 s. The performance of the sensor was optimized with various pH and different scan rates.

Tajabadi et al. (2016) fabricated an efficient non-enzymatic biosensor electrode consisting of nitrogen-doped graphene (N-graphene) and platinum nanoflower (Pt NF) with different N-graphene loadings on indium tin oxide (ITO) glass using a simple layer-by-layer electrophoretic and electrochemical sequential deposition approach. N-graphene was synthesized by annealing graphene oxide with urea at 900 °C. The structure and morphology of the as-fabricated non-enzymatic biosensor electrodes were determined using X-ray diffraction, field emission electron microscopy, transmission electron microscopy, Raman and X-ray photoelectron spectra. The as-fabricated Pt NF-N-graphene-modified ITO electrodes with different N-graphene loadings were utilized as a non-enzymatic biosensor electrode for the detection of H_2O_2. The behaviors of the hybrid electrodes towards H_2O_2 reduction were assessed using chronoamperometry, CV and electrochemical impedance spectroscopy analysis. The Pt NF-N-graphene-modified ITO electrode with a 0.05 mg mL^{-1} N-graphene loading exhibited the lowest detection limit, fastest amperometric sensing, a wide linear response range, excellent stability and reproducibility for the non-

enzymatic H_2O_2 detection, due to the synergistic effect between the electrocatalytic activity of the Pt NF and the high conductivity and large surface area of N-graphene.

Yan et al. (2016) reported a facile hydrothermal fabrication of graphene aerogel/platinum nanoparticle (GA/Pt NPs) nanocomposites with three-dimensional (3D) interconnected pores. The GA/Pt NPs product were first characterized by SEM, TEM, XRD, and XPS. CV measurements reveal that GA/Pt NPs can directly catalyze the reduction of H_2O_2 and display enhanced current responses. The biosensor exhibits remarkable sensitivity (138.23 μA mM^{-1} cm^{-2}), an approximate linear detection range of H_2O_2 concentration (1 μmol·L-1 to 2785 μmol·L^{-1}), and a detection limit of 0.33 μmol·L^{-1}. Moreover, good anti-interference property, reproducibility, and long-term stability of the enzymeless sensor were achieved. These results indicate that GA/Pt NPs is a good candidate for H_2O_2 detection. Due to these remarkable analytical advantages, the as-made sensor was applied to determine the H_2O_2 released from PC12 cells with satisfactory results.

Xue et al. (2016) prepared Pd nanoparticles/porous graphene (Pd/PGR) by simultaneous reduction GO and Pd precursor in sodium borohydride ($NaBH_4$) solutions at the electrode surface. In this preparation, the positively charged ZnO with high isoelectric point is used as templates for the adsorption of negatively charged GO in water. Then, the poly(diallyldimethylammonium chloride) (PDDA) is added into the ZnO/GO through the electrostatic interaction between the negative charge of GO and positive charge of PDDA. Subsequently, PDDA/ZnO/GO is employed as a support material for the adsorption of chloropalladic acid ions ($PdCl_4^{2-}$), via the self-assembly between the negative Pd precursor and positively charged functional groups of PDDA. One-step reduction of Pd precursor/PDDA/ZnO/GO in $NaBH_4$ solutions and the subsequent removal of the ZnO produce Pd/PDDA/PGR with a porous structure at the electrode surface. With a porous morphology and large surface area for both efficient exposure of Pd nanoparticles and enhanced electrolyte-reactant diffusion, a sensitive enzymeless sensor of H_2O_2 is constructed. Compared with the nonporous Pd/PDDA/GR, the Pd/PDDA/PGR displays high electrocatalytic activity towards H_2O_2, exhibiting a high sensitivity of 57.7 μA mM^{-1} and low detection limit of 0.9 μM towards the reduction of H_2O_2. The improved activity and simple preparation method makes Pd/PDDA/PGR promising for being developed as an attractive robust and new electrode material for electrochemical sensor and biosensor fabrication.

J. Bai et al. (2016), Z. Bai et al. (2016) developed a highly sensitive non-enzymatic electrochemical sensor based on platinum nanoparticles/reduced graphene oxide-chitosan-ferrocene carboxylic acid nano-hybrids (Pt NPs/RGO-CS-Fc biosensor) for the measurement of H_2O_2. The RGO-CS-Fc nano-hybrids was prepared and characterized by UV–vis spectrum, FTIR spectroscopy, TEM, Raman spectrometer and EIS. Under optimal experimental conditions, the Pt NPs/RGO-CS-Fc biosensor showed outstanding catalytic activity toward H_2O_2 reduction. The current response of the biosensor presented a linear relationship with H_2O_2 concentration from 2.0×10^{-8} M to 3.0×10^{-6} M with a correlation coefficient of $R^2 = 0.9968$ and with logarithm of H_2O_2 concentration from 6.0×10^{-6} M to 1.0×10^{-2} M with a correlation coefficient of $R^2 = 0.9887$, the low detection limit of 20 nM was obtained at the signal/noise (S/N) ratio of 3. Moreover, the Pt NPs/RGO-CS-Fc biosensor exhibited excellent anti-interference capability and reproducibility for the detection of H_2O_2.

Behera et al. (2016) developed a facile and highly sensitive platform for synthesizing branched Pt nanostructures on graphene. Graphene support has been employed to enhance the performance of platinum nanostructures (PtNs) in electrochemical sensing/biosensing. The graphene supported PtNs (GPtNs) modified electrode efficiently oxidizes the H_2O_2 at a lower potential in neutral phosphate buffer solution without employing the enzymes or redox mediators. The GPtNs electrode shows high sensitivity and can detect very low nanomolar concentrations (1 nM) of H_2O_2. It can linearly sense H_2O_2 from 0 to 0.32 mM, and the sensitivity of the sensor was estimated to be 811.26 μA mM^{-1} cm^{-2}. The sensor shows excellent reproducibility, long time storage and operational stability. The sensor successfully estimates the H_2O_2 concentration in the real sample (rainwater) for practical analysis.

Gu et al. (2016) synthesized a facile and effective strategy is demonstrated for the synthesis of ternary reduced graphene oxide-Hemin-Au (rGO-H-Au) nanohybrids. The nanohybrids through a one-pot in situ reduction of GO and $HAuCl_4$ under alkaline conditions using GO, Hemin and $HAuCl_4$ as the starting materials. The synthesis process can be finished within 1 h in a solution phase, without adding any additional surfactant, stabilizing agent and toxic or harsh chemical reducing agents. The resulting nanohybrids were characterized by UV–vis spectroscopy, Raman spectroscopy and TEM. Electrochemical measurements showed that the rGO-H-Au nanohybrids exhibited good electrocatalytic activity for the reduction of H_2O_2. Based on this property, a simple and highly sensitive amperometric biosensor for H_2O_2 had been developed. The linear relationships were obtained from 0.1 μM to 40 μM and the detection limit was estimated to be 30 nM.

S.M. Li et al. (2015), J. Li et al. (2015) explored a high-sensitive nonenzymatic H_2O_2 biosensor based on cuprous iodide and graphene (CuI/Gr) composites for the detection of H_2O_2 released by living cells and monitoring the oxidative stress of cells under excellular stimulation. The biosensor properties were evaluated by CV, electrochemical impedance spectroscopy (EIS), amperometric i-t curve, and the redox-competition mode of scanning electrochemical microscopy (SECM). The CuI/Gr nanocomposites modified GCE exhibits excellent catalytic activity for H_2O_2 with relatively low detection limit and a wide linear range from 0.5 μM to 3 mM.

Low et al. (2015) synthesized Graphene/zinc oxide nanocomposite via a facile, green and efficient approach consisted of novel liquid phase exfoliation and solvothermal growth for sensing application. Highly pristine graphene was synthesized through mild sonication treatment of graphite in a mixture of ethanol and water at an optimum ratio. The XRD affirmed the hydrothermal growth of pure zinc oxide nanoparticles from zinc nitrate hexahydrate precursor. The as-prepared graphene/zinc oxide (G/ZnO) nanocomposite was characterized comprehensively to evaluate its morphology, crystallinity, composition and purity. All results clearly indicate that zinc oxide particles were homogenously distributed on graphene sheets, without any severe aggregation. The electrochemical performance of graphene/zinc oxide nanocomposite-modified screen-printed carbon electrode (SPCE) was evaluated using CV and amperometry analysis. The resulting electrode exhibited excellent electrocatalytic activity towards the reduction of H_2O_2 in a linear range of 1–15 mM with a correlation coefficient of 0.9977. The sensitivity of the graphene/zinc oxide nanocomposite-modified H_2O_2 sensor was 3.2580 μA mM^{-1} with a limit of detection of 7.4357 μM.

Govindasamy et al. (2016) grew flower-like MoS_2 nanostructure on graphene and carbon nanotubes (GR-MWCNTs) via in-situ hydrothermal method and the resulting composite was employed for determination of H_2O_2. The MoS2/GR-MWCNTs composite was characterized by scanning electron microscopy, Energy-dispersive X-ray spectroscopy and electrochemical methods. MoS2/GR-MWCNTs possess three dimensional nanostructure, large electrochemically active surface area, porosity, and high conductivity and it was used for the enzymeless electrochemical determination of hydrogen peroxide. MoS_2/GR-MWCNTs composite film modified electrode showed excellent electrocatalytic ability to the reduction of H_2O_2. The composite delivered significantly improved electrocatalytic ability to H_2O_2 in comparison with control electrodes. Furthermore, the electrode exhibited low overpotential, high faradaic current and fast response time. MoS2/GR-MWCNTs composite film modified electrode responds quickly to H_2O2 over wide working concentration range of 5–145 μM, sensitivity of 5.184 μA μM cm^{-2} and detection limit of 0.83 μM.

Thirumalraj et al. (2016) prepared a highly active and stable composite of hemin (HN) supported by reduced graphene oxide/gold nanoparticles (HN-RGO/AuNPs) by one-pot hydrothermal method. The

physicochemical properties of the as-prepared composites were characterized by field emission scanning electron microscopy (FESEM), TEM, UV–vis spectroscopy, Raman spectroscopy and XRD. The HN-RGO/AuNP-modified electrode shows a stable and well-defined, surface-confined redox couple at an apparent formal potential of −0.317 V vs. Ag|AgCl with a surface coverage value of 2.239×10^{-10} mol cm^{-2}. Compared with HN, HN-GO and HN-RGO, the HN-RGO/AuNP-modified electrode exhibits excellent electrocatalytic activity towards H_2O_2. Under optimum conditions, the HN-RGO/AuNP-modified electrode shows a wide linear response ranges from 0.05 mM to 518.15 mM towards H_2O_2 with a fast response time (3 s). The calculated sensitivity and limit of detection (LOD) of the biosensor were 3.99 mA mM^{-1} cm^{-2} and 16 nM, respectively. In addition, the Michaelis-Menten constant value of the biosensor is 0.13 mM, which indicates the high affinity of HN towards the reduction of H_2O_2.

Gao et al. (2014) fabricated a nonenzymatic sensor based on Ni(OH)2/ERGO–multiwalled carbon nanotube (MWNT) nanocomposites via convenient electrodeposition of Ni(OH)2 nanoparticles on ERGO–MWNT film modified GCE. GO sheets can serve as surfactants to stabilize the dispersion of pristine MWNTs in aqueous solution, rendering a fine coverage of ERGO–MWNT film on GCE during the fabrication process. MWNTs perform as conducting bridges between ERGO sheets to enhance the electron transfer rate in the substrate. By combining the advantages of ERGO and MWNTs, together with electrocatalytic effect of Ni(OH)2 nanoparticles, the well-designed nanocomposites exhibit excellent sensing behavior towards glucose and H_2O_2. The linear detection ranges for glucose and H_2O_2 are 10–1500 μM and 10–9050 μM while the detection limits are 2.7 μM and 4.0 μM, respectively. Furthermore, a very high sensitivity is achieved with 2042 μA m M^{-1} cm^{-2} estimated for glucose and 711 μA m M^{-1} cm^{-2} for H_2O_2.

Luo et al. (2014) used Cu_2O/Cu NC nanocomposite catalysts on glass carbon electrodes have been synthesized by electrochemical deposition at −0.2 V versus silver/silver chloride to construct an electrochemical sensor for detection of hydrogen peroxide. The effects of deposition time and pH were investigated in detail. In 0.1 M phosphate buffer saline (PBS, pH = 6.5), the Cu2O/Cu NC modified electrode exhibits a wide linear dependence (R = 0.996) at a concentration of H_2O_2 from 4.0×10^{-7} M to 1.0×10^{-2} M, a high sensitivity of 870.4 mA mM^{-1} cm^{-2} and a detection limit of 2.0×10^{-7} M.

Bas (2015) presented the preparation of gold nanoparticle functionalized graphene oxide (AuNPs-GO) as a new bio-compatible material for sensor applications. The electrocatalytic activity of AuNPs-GO towards electrooxidation of H_2O_2 was also described by using electrochemical techniques. The fabricated biosensor showed a linear range from 0.1 mMto 3.8 mM with a sensitivity of 17.68 μA mM^{-1} cm^{-2} and a detection limit of 0.075 mM for the detection of glucose.

Yang et al. (2016) directly deposited highly efficient electrocatalytic polyoxometalate (POM) on polymeric ionic liquid (PIL)-functionalized reduced graphene oxide (rGO) in a simple manner. The nano-sized POM with PIL functional groups was uniformly distributed on the surface of rGO sheets. The unique nanostructure of the resultant POM-g-rGO nanohybrids enabled well-defined multiple redox reaction of POMs and rapid electron transfer.

4.4.3.1. Cholesterol graphene-based biosensor. Cholesterol is a major modifiable risk factor in cardiovascular disease and can be effectively managed by a combination of medication and monitoring. There continues to be a need for new point-of-care diagnostics to measure lipid panels, including total cholesterol (Ahmadraji and Killard, 2016). Several researches on the preparation and application of a cholesterol enzyme biosensor based on novel graphene materials have been reported by various research groups:

Wu et al. (2016) successfully prepared a novel graphene nanocomposite, functionalized by polymeric ionic liquids (PILs) and poly (sodium-p-styrenesulfonate) (PSS) and exhibited excellent conductivity, favorable biocompatibility and good film-forming properties as an electrode material. TEM showed that the nanocomposite possessed an individual nanosheet-like structure. Owing to the surface modification of graphene, PSS/PILs-GP can not only be well dispersed in aqueous solution, but also possesses a strong negative charge. Due to electrostatic interactions, positively charged ChOx can be immobilized onto the surface of PSS/PILs-GP to form the ChOx/PSS/PILs-GP/GC electrode material. UV–vis and FT-IR spectroscopy were used to monitor the assembly process of the nanocomposite. Due to the conductivity and biocompatibility of PSS/PILs-GP, the immobilized ChOx exhibited enhanced DET at a glassy carbon (GC) electrode. Furthermore, the ChOx/PSS/PILs-GP/GC electrode displayed excellent catalytic performance with a wide linear range of 10.5×10^{-6} to 10.4×10^{-3} mol L^{-1}, and a low detection limit of 3.5 m mol L^{-1} for the detection of cholesterol.

Siddique et al. (2017) reported the electrical performance of graphene devices with the immobilization of cholesterol molecules. In electrical transport measurements, the Dirac point position is gradually shifted towards negative gate voltage as cholesterol concentration increases which reveal the clear influence of cholesterol molecules on the graphene. These graphene surface modifications induce n-type doping and the charge carrier mobility is increased from ~2000 cm^2 V^{-1} s^{-1} to ~3900 cm^2 V^{-1} s^{-1} by increasing the cholesterol concentration. The detection of cholesterol molecules is further investigated by Raman spectroscopy, FTIR and AFM characterizations.

Wu et al. (2016) fabricated a highly sensitive and selective cholesterol biosensor. Due to excellent conductivity and catalytic activity, silver nanowires (AgNWs) and zinc oxide (ZnO) are modified on an indium tin oxide (ITO) electrode with GO and chitosan (CS) to construct the novel amperometric biosensor. The composite of AgNW-ZnO successfully enhanced electron communication, and the electrochemical performances of the ChOx/ZnO/Ag/GO-CS/ITO electrode were investigated via SEM, CV and impedance measurements. The linear response to cholesterol in the range of the fabricated biosensor is 0.25–400 mg dL^{-1} (6.5 μM to 10 mM) with a sensitivity of 9.2 μA μM^{-1} cm^{-2}. Moreover, the limit of detection (LOD) is 0.287 μM (S/N = 3), and the Michaelis-Menten constant is calculated to be about 0.295 μM in 0.1 M phosphate buffer solution (pH 7).

Abraham et al. (2015) introduced partially reduced graphene oxide (pRGO)-silica (SiO_2) particles hybrid system (pRGOSHs) for sensitive and cost effective free cholesterol detection. Fabricated out of thin layers of pRGOSHs, these proposed ChOx/pRGOSHs/ITO based biosensors have a detection range of 2.6–15.5 mM with an appreciable detection limit of 1.3 mM and sensitivity of 11.1 μA/mM/cm^2. Low Michaelis-Menten constant (K_m) (4.9×10^{-4} mM) and high diffusivity constant (D) (3.2×10^{-10} cm^2/s) values clearly indicate enhanced immobilization of enzyme over the substrate. Additionally, electrochemical impedance studies indicate that the synergistic combination of SiO_2 and pRGO also results in much lower impedance values (40% and 18% decrease in comparison to SiO_2 and pRGO respectively) for an overall enhanced sensing performance.

Nandini et al. (2016) reported a new approach for the synthesis of one dimensional gold nanostructure (AuNs) and its application in the development of cholesterol biosensor. Au nanostructures have been synthesized by exploiting β-diphenylalanine (β-FF) as a sacrificial template, whereas the Au nanoparticles (AuNPs) were synthesized by ultrasound irradiation. XRD, SEM and energy dispersive analysis of X-rays (EDAX) have been employed to characterize the morphology and composition of the prepared samples. With the aim to develop a highly sensitive cholesterol biosensor, ChOx was immobilized on AuNs which were appended on the graphite (Gr) electrode via chemisorption onto thiol-functionalized graphene oxide (GO-SH). This Gr/GO-SH/AuNs/ChOx biosensor has been characterized using CV, electrochemical impedance spectroscopy and chronoamperometry. CV results indicated a direct electron transfer between the enzyme and the electrode surface. A new potentiostat intermitant titration technique (PITT) has been studied to determine the diffusion coefficient and maxima potential value.

Komathi et al. (2016) fabricated a novel electrochemical–photoelectrochemical (PEC) dual-mode cholesterol biosensor based on graphene (G) sheets interconnected-graphene embedded titanium nanowires (TiO_2(G)-NWs) 3D nanostacks (designated as G/Ti (G) 3DNS) by exploiting the beneficial characteristics of G and TiO_2-NWs to achieve good selectivity and high sensitivity for cholesterol detection. The G/Ti(G) 3DNS was fabricated by the reaction between functionalized G and TiO_2(G)-NWs. ChOx was subsequently immobilized in to G/Ti(G) 3DNS using chitosan (CS) as the binder and the dual mode G/Ti(G) 3DNS/CS/ChOx biosensor was fabricated. The electro-optical properties of the G/Ti(G) 3DNS/CS/ChOx bioelectrode were characterized by CV and UV–vis diffuse reflection spectroscopy. The CV of immobilized ChOx showed a pair of well-defined redox peaks indicating DET of ChOx. The amperometric reduction peak current (at −0.05 V) linearly increased with increase in cholesterol concentration. The G/Ti(G) 3DNS/CS/ChOx bioelectrode was selective to cholesterol with a remarkable sensitivity (3.82 μA/cm^2 mM) and a lower detection limit (6 μM). Also, G/Ti(G) 3DNS/CS/ChOx functioned as photoelectrode and exhibited selective detection of cholesterol under a low bias voltage and light irradiation.

Li et al. (2015b) investigated a novel cholesterol biosensor (ChOx/CS-GR/GCE) with enhanced sensitivity and low detection limit. The biosensor based on direct electrochemistry of cholesterol oxidase with an apparent rate constant (ks) of 2.69 s^{-1} was fabricated by immobilizing ChOx on GCE functionalized by chitosan-graphene (CS-GR) nanocomposites. GO was synthesized by a novel microwave method and CS-GR was prepared by simple situ reduction of chitosan-graphene oxide (CS-GO). The results of TEM and FT-IR spectroscopy showed that the GO was successfully prepared and deoxygenized. The presence of the CS-GR nanocomposites not only accelerated direct electron transfer from the enzyme to the electrode surface, but also enhanced the immobilized amount and stability of ChOx. The fabricated electrode exhibited a linear response to cholesterol in the range of 0.005–1.0 mM with a detection limit of 0.715 μM (S/N = 3). The Michaelis-Menten constant (k_m ^{app}) was found as 17.39 μM.

Ruecha et al. (2014) attached ChOx to G/PVP/PANI-modified electrode for the amperometric determination of cholesterol. Under optimum conditions, a linear range of 50 μM to 10 mM is achieved and the limit of detection is found to be 1 μM for cholesterol. The proposed system can be applied for the determination of cholesterol in a complex biological fluid (i.e. human serum).

Huan et al. (2015) constructed (CdTe-MWCNTs@rGONRs), which were prepared by electrostatic interactions. The CdTe QDs decorated on the MWCNTs@rGONRs resulted in the amplified ECL intensity by ~4.5 fold and decreased onset potential by ~100 mV. By immobilization of the ChOx and NIR CdTe-MWCNTs@rGONRs on the electrode surface, a solid-state ECL biosensor for cholesterol detection was constructed. When cholesterol was added to the detection solution, the immobilized ChOx catalyzed the oxidation of cholesterol to generate H_2O_2, which could be used as the co-reactant in the ECL system of CdTe-MWCNTs@rGONRs. The as-prepared biosensor exhibited good performance for cholesterol detection including good reproducibility, selectivity, and acceptable linear range from 1 μM to 1 mM with a relative low detection limit of 0.33 μM (S/N = 3).

Wu et al. (2014) developed a facile approach to synthesize multiwall carbon nanotubes-graphene oxide-thionine-Au (MWCNTs-GO-Thi-Au) nanocomposites with the synergistic effect of GO and Thi, resulting in reducing AuCl4 - to Au nanoparticles (AuNPs). Meanwhile, the AuNPs reduced by GO and Thi promoted the electrochemiluminescence (ECL) of luminol-H_2O_2 system and offered active sites for immobilization of numerous enzymes. Additionally, it was also found that the synergetic interactions of Thi with MWCNTs and GO was employed for enhancing ECL of luminol-H_2O_2, which was applied to develop an ECL biosensor for the first time. Using ChOx as model enzyme, the proposed biosensor employed by MWCNTs-GO-Thi-Au nanocomposites showed a high sensitivity for cholesterol in a concentration range of 0.15–828 μM with a detection limit of 50 nM (signal-to-noise ratio of 3).

Ahmadraji and Killard (2016) demonstrated the application of printed electrochemical sensors to the measurement of total cholesterol in serum. The assay uses the surfactant Triton X-100 to provide electrocatalytic enhancement of a silver paste screen-printed electrode to hydrogen peroxide, while also achieving effective solubilisation of total cholesterol from lipoprotein. The resulting biosensors employed 0.5% (v/v) Triton X-100 in PBS with 156 U mL^{-1} cholesterol esterase and 60 U mL^{-1} cholesterol oxidase. Measurement of total cholesterol in serum in the range of 0–10 mM had a sensitivity of 2.24 × 10^{-8} A mM^{-1}, with coefficient of determination of 0.984, detection limit of at least 2 mM and average relative standard deviation of 10.8% (n = 3).

4.4.3.2. Non enzymatic cholesterol graphene–based biosensor. Recently, researchers have reported and fabricated several non enzymatic cholesterol graphene-based biosensors:

Lakshmi et al., (2016) studied a nanocomposite of polyaniline nanofiber-graphene microflowers (PANInf-GMF), prepared by an in situ rapid mixing polymerization method. The structural and morphological studies of the nanocomposite (PANInf-GMF) were carried out by SEM, TEM, FTIR and Raman spectroscopy. The mesoporous, nanofibrous and microflower structures were observed by SEM. The functional groups and synergetic effects were observed by FTIR and micro-Raman measurements. The water wettability was carried out by a contact angle measurement technique and found to be super hydrophilic in nature towards water. This nanocomposite was deposited onto indium-tin-oxide coated glass substrate by a drop casting method and used for the detection of cholesterol using an electrochemical technique. The differential pulse voltammetry studies show the appreciable increase in the current with the addition of 1.93–464.04 mg dl^{-1} cholesterol concentration. The sensitivity of the sensor is estimated as 0.101 μA mg^{-1} dl cm^{-2} and the lower detection limit as 1.93 mg dl^{-1}.

Another enzymeless approach is by (Agnihotri et al., 2015) who chemically converted Graphene modified with β-CD, being hydrophilic, electroactive and high surface area material, provides a platform for the electrochemical detection of cholesterol using Methylene Blue as redox indicator. Methylene Blue (MB) forms an inclusion complex with Grp-β-CD and emerges as a cholesterol sensing matrix. MB molecule is replaced by cholesterol molecule and moves out in the buffer solution, hence, detected electrochemically using DPV technique. The sensing matrix is characterized using FT-IR, TEM and Raman spectroscopy.

Alexander et al. (2017) reported the development of cost effective sensor material prepared from modified graphene oxide based molecular imprinted polymer (GO-MIP). Firstly GO prepared from modified Hummers method undergoes acid functionalization to form GOACOOH. It further undergoes surface modification with glycidyl methacrylate (GMA) in presence of N,N0-dicyclohexylcarbodiimide (DCC), dimethylaminopyridine (DMAP) and dimethyl sulfoxide (DMSO) to form GOACH@CH2. The obtained GOACH@CH2 undergoes molecular imprinting process with methacrylic acid (MAA) as themonomerand ethylene glycol dimethacrylate (EGDMA) as the cross–linker, a,a0-azobisisobutyronitrile (AIBN) as the initiator and cholesterol as the template molecule. The different preparatory stages of materials were characterized by FTIR, XRD, Raman and TEM techniques to understand the formation. The obtained GO-MIP used as an active material for cholesterol sensing where the sensor demonstrate a lower limit detection of 0.1 nM and response time of 2 min with maximum sensing performance at pH 5.0. The repeatability of the sensor is checked up to eight cycles and interference of cholesterol with ascorbic acid (AA), uric acid (UA) and glucose were also studied.

4.4.4. Dihydronicotinamide adenine dinucleotide dehydrogenase (NADH) graphene - Based biosensor

Several researches on the preparation and application of a NADH biosensor based on novel graphene materials have been reported by various research groups:

Breczko et al. (2016) developed a biosensor containing three types of structures: GO silica nanoparticles (SNs) and gold nanoparticles (GNPs) for effective electrochemical and optical determination of NADH. The subsequent steps in biosensor formation, the manner of structure organization and the layer thickness were verified by different methods. Electrochemical oxidation of NADH was performed with the usage of DPV. Results show that obtained biosensor catalyzes the process of NADH electrochemical oxidation. The shift of oxidation potential toward less positive values and the increment of oxidation current were clearly noted. Additionally, the oxidized NAD form was found to exhibit an electrostatic affinity to the top layer of sensor giving a possibility to SPR detection. DPV and SPR signals registered for different amount of NADH were correlated with its concentration into linear relationship: y = 8.6388x - 0.0109; R^2 = 0.9997 and y = 1305.8x - 74.098; R^2 = 0.9913, respectively. Enhancement of the electrochemical sensitivity toward NADH, as a result of electrode modification, was proved by lower values of LOD (0.0236 mM) and LOQ (0.0707 mM) in comparison with corresponding parameters calculated for non-modified gold electrode.

Aydoğdu Tığ (2017) fabricated a novel NADH sensor using gold-silver bimetallic nanoparticles (Au-AgNPs), poly(L-Cysteine) (P(L-Cys)) and ERGO modified glassy carbon electrode (GCE/Au-AgNPs/P(L-Cys)-ERGO). The composite electrode exhibited an excellent electrocatalytic response towards NADH at a low oxidation potential (+ 0.35 V) and minimization of surface contamination due to the synergistic effects of the Au-AgNPs, polymer and ERGO. Under optimum conditions, modified sensors allowed the detection of NADH with a wide linear range from 0.083 μM to 1.05 mM with a low detection limit of 9.0 nM (S/N = 3). Moreover, this modified electrode was also used as a sensitive ethanol biosensor, which was prepared with alcohol dehydrogenase (ADH) via glutaraldehyde, bovin serum albumin and nafion (Naf). There was a linear response for ethanol in the concentration range from 0.017 to 1.845 mM with a low detection limit of 5.0 μM (S/N = 3).

Mutyala and Mathiyarasu (2016) described the fabrication of highly sensitive and selective NADH sensor using nitrogen doped graphene (NDG). NDG modified GCE exhibits strong and stable electrocatalytic response towards NADH oxidation. A substantial (253 mV) decrease in the overpotential for NADH oxidation reaction (compared to GCE) is observed at NDG/GCE. NDG was prepared using hydrothermal procedure and characterized using spectroscopy and microscopy techniques. Furthermore, amperometric responses of NDG/GCE have high sensitivity towards NADH oxidation at lower oxidation potential and minimization of surface contamination. The fabricated NADH biosensor exhibited enhanced and reproducible sensitivity of 0.16 μA/μM (S/N = 3) with a response time of < 3 s and the calculated limit of detection is 0.37 μM. A linear dynamic range from 0.5 to 12 μM was observed for the fabricated biosensor with a correlation coefficient (R^2) of 0.99. Moreover, the biosensor exhibited strong stability after prolonged usage. The oxidation peak potential at the NDG/GCE remained unchanged even after 15 days, with minimum surface contamination.

Sangamithirai et al. (2015) explored the electrocatalytic oxidation of dihydronicotinamide adenine dinucleotide (NADH) based on poly(o-anisidine)/graphene (POA/GR) nanocomposites GCE. POA/GR nanocomposites were synthesized via chemical oxidative polymerization method. X-ray diffraction (XRD), field emission scanning electron microscopy (FESEM), high resolution transmission electron microscopy (HRTEM), FTIR, Raman spectroscopy, and UV–Vis spectroscopy results demonstrate that nanocomposites are successfully synthesized. An intriguing composite structure was observed using different ratios of o-anisidine monomer and graphene. The electrical properties and electrochemical properties of these nanocomposites are investigated by impedance spectroscopy technique and CV method, respectively. The synthesized nanocomposites were used to modify GCE, and the modified electrodes were found to exhibit electrocatalytic activity for oxidation of NADH at low potential range of + 0.045 V in a neutral environment. The fabricated sensor based on POA/GR31-modified GCE exhibited enhanced current response with very high sensitivity of 47.1 μA μM^{-1} for the detection of NADH.

Li et al. (2015a) reported a graphene-DNA tetrahedron-gold nanoparticle modified gold disk electrode for highly sensitive NADH detection. By assembling the DNA tetrahedron/graphene composite film on the gold disk electrode surface which prior harnessed electrochemical deposition of gold nanoparticles to enhance the effective surface area, the oxidation potential of NADH was substantially decreased to 0.28 V (vs. Ag/AgCl) and surface fouling effects were successfully eliminated. Furthermore, the lower detection limit of NADH by the presented platform was reduced down to 1.0 fM, with an upper limit of 10 p.M.

Y. Han et al. (2015), S. Han et al. (2015) fabricated and modified a self-assembly composite of graphene-pyrroloquinoline quinone (PQQ) won GCE for sensitive detection of NADH. Chitosan (CTS) was applied to disperse graphene to form a stable robust film on GCE. A synergistic effect between PQQ and graphene was observed during the electrocatalytic oxidation of NADH, with about 260 mV reductions in the oxidation potential and 2.5-fold increase in the oxidation current compared with those on the bare GCE. The electrochemical sensors based on the modified electrodes allowed the detection of NADH with a good linear dependence from 0.32 to 220 μM with a high sensitivity of 0.421 μA μM^{-1} cm^{-2} and a low detection limit of 0.16 μM (S/N = 3).

Govindhan et al. (2015) reported on a facile, rapid, sensitive, selective and highly stable electrochemical sensing platform for NADH based on uncapped Au nanoparticle/ rGO) nanocomposites without the aid of any redox mediators and enzymes. The Au nanoparticle/rGO composite sensing platform was directly formed on a glassy carbon electrode through an in situ electrochemical reduction of GO and Au^{3+} with a 100% usage of the precursors. The as-prepared Au nanoparticle/rGO composites demonstrated excellent direct electrocatalytic oxidation toward NADH, providing a large electrochemical active surface area as well as a favorable environment for electron transfer from NADH to the electrode via the enhanced mobility of charge carriers. The Au nanoparticle/rGO composites offered a ~2.3 time's higher electrocatalytic current density with a negative of 112 mV, in comparison to Au nanoparticles. The sensor developed in this study displayed a high sensitivity of 0.916μA/μM cm^2 and a wide linear range of from 50 nM to 500 μM with a limit of detection of 1.13 nM (S/N = 3).

Tabrizi and Zand (2014) reported a green and eco-friendly approach to synthesize rGO via a mild hydrothermal process NADH as a reducing agent. The obtained rGO was characterized by UV–vis, XRD, AFM and scanning electron SEM. Electrochemical experiments indicated that the rGO/GC electrode exhibited an excellent electrocatalytic activity towards the oxidation of NADH, which can be attributed to the excellent electrical conductivity and high specific surface area of the rGO composite. The resulting biosensor showed highly sensitive amperometric response to NADH with a low detection limit (0.6 μM).

Gai et al. (2014) designed a novel electrochemical biosensing platform for NAD^+-dependent dehydrogenase catalysis using the nitrogen-doped graphene (NG), which had properties similar to NADH dehydrogenase (CoI). NG mimicked flavin mononucleotide (FMN) in CoI and efficiently catalyzed NADH oxidation. NG also acted as an electron transport "bridge" from NADH to the electrode due to its excellent conductivity. In comparison with a bare gold electrode, an 800 mV decrease in the overpotential for NADH oxidation and CoI-like behavior were observed at NG-modified electrode, which is the largest decrease in overpotential for NADH oxidation reported to date. The catalytic rate constant (k) for the CoI-like behavior of NG was estimated to be 2.3 × 10^5 M^{-1} s^{-1}, which is much higher than that of other previously reported FMN analogs. The Michaelis-Menten constant (K_m) of NG was 26 μM, which is comparable to the K_m of CoI (10 μM).

4.4.5. Graphene based immunosensor

In recent years, tremendous advances have been made in biosensors based on nanoscale electrochemical immunosensors for use in the fields of agriculture, food safety, biomedicine, quality control, and

environmental and industrial monitoring. Electrochemical immunosensors have the potential to transform analytical procedures in biosensing by providing highly specific, rapid, and inexpensive determination of pathogen, protein cancer biomarkers and bone biomarkers (Ronkainen and Okon, 2014). Significant progresses have been made in the study of electrochemical immunosensor that based on GR, especially in the fields of clinical screening and diagnosis of cancer field.

Recently Lim and Ahmed (2016) reviewed recent advances in signal amplification strategies for electrochemical immunosensing applications, with a particular focus on nanotechnology. The strategies employed and their general principles to increase sensitivity, as well as the advantages and limitations of electrochemical immunosensors developed to date were also considered.

In another recent review by Yáñez-Sedeño et al. (2016), it was observed that Single- or multi-walled nanotubes and graphene have been largely applied to the construction of electrochemical (bio)sensors improving two key aspects in this field: surface nanostructuration allowing the preparation of electrode platforms more conductive, selective and suitable for biomolecules immobilization, and the ability to design suitable strategies for signal amplification. Besides the above mentioned carbon nanomaterials, more recently new carbon nanoforms have appeared as suitable nanostructuration tools. Carbon nanohorns, double-walled carbon nanotubes, fullerene (C60), carbon nanoparticles, and graphene quantum dots are examples of novel nanomaterials whose particular characteristics make them well suited for the construction of bioelectrochemical devices.

In a more recent review by Duffy and Moore (2017) recent advances in this area were outlined. In particular, attention was paid to new methods that have been developed for the modification of working electrode surfaces. Many advances have been related to the use of novel nanomaterials such as carbon nanotubes, graphene, and metallic nanoparticles, often used in conjunction with each other or polymers. The use of these materials has generally provided superior sensor sensitivity. The application of immunosensors to the detection of a range of pathogens in real samples is then investigated to establish whether they provide solutions in practical applications.

Similarly (Sharma et al., 2016) also reviewed technological advancements, challenges and trends in immunoassay technologies for ovarian cancer diagnosis. Emphasis is placed on the principles of the technologies, their merits and limitations and on the evolution from laboratory-based methods to point-of-care devices. While the current market is predominantly associated with clinical immunoassay kits, over the last decade a major thrust in development of immunosensors is evident due to their potential in point-of-care devices. Technological advancements in immunosensors, extending from labeled to label-free detection, with and without mediators, for enhancing proficiencies and reliability have been dealt with in detail. Aspects of the utilisation of nanomaterials and immobilization strategies for enhancing sensitivity and altering the detection range were also addressed. Several researches on the preparation and application of immunosensor based on novel graphene materials have been reported by various research groups:

Borisova et al. (2017) reported the assembly of a novel disposable amperometric immunosensor for the detection of the red wine spoilage yeast Brettanomyces bruxellensis. The nanostructured sensing interface was prepared by first coating carbon screen printed electrodes with a gold nanoparticles-reduced graphene oxide hybrid nanomaterial, which was then modified with 3-mercaptopropionic acid to further immobilize specific antibodies for B. bruxellensis via a carbodiimide-coupling reaction. The functionalized electrode allowed the amperometric detection of B. bruxellensis in buffered solutions and red wine samples in the range of 10–10^6 CFU/mL and 10^2–10^6 CFU/mL, with low detection limits of 8 CFU/mL and 56 CFU/mL, respectively.

Zhang et al. (2016a) used $CoFe_2O_4$/graphene nanohybrid ($CoFe_2O_4$/rGO) as support for preparing electrochemical biosensor, and with the addition of Au@Pd nanorods (NRs) as mimic enzyme, a label-free electrochemical immunosensor was prepared. Due to the high electrical conductivity, open porous structure and large loading capacities of $CoFe_2O_4$/rGO, the enhanced signal amplification between Au@Pd NRs and $CoFe_2O_4$/rGO was studied. Fabricated as a novel substrate, the prepared immunosensor had a good analytical performance and exhibited a wide linear range from 0.01 to 18.0 ng mL^{-1} with a low detection limit of 3.3 pg mL^{-1} for estradiol, which was succeeded in applying to detect estradiol in the natural water.

Özcan and Sezgintürk (2016) designed a label free immunosensor for determination of HSP70 (heat shock protein 70). Glassy carbon electrode was used as a working electrode. Graphene oxide was covered on the working electrode surface. AntiHSP70 as a biorecognition element of the biosensor was covalently immobilized onto the graphene oxide layer by using EDC/NHS chemistry. The immobilization of antiHSP70 and binding of HSP70 protein onto the electrode surface were monitored by CV and electrochemical impedance spectroscopy. Single frequency technique was also utilized to monitor binding characterization of HSP70 and antiHSP70. Surface morphology was defined by using SEM. A linear detection range of HSP70 was determined between 12 and 144 fg/mL. Moreover, Kramer's Kronig transform was applied on impedance data.

Mehta et al. (2016) fabricated a graphene based impedimetric immunosensor and employed for highly sensitive and specific detection of parathion. The fabrication proceeded through the modification of the screen-printed carbon electrodes (SPE) with graphene sheets, followed by their functionalization with 2-aminobenzyl amine (2-ABA) via an electrochemical reaction. These amine functionalized graphene electrodes were then bio-interfaced with the anti-parathion antibodies. In the impedimetric mode, this biosensor detected parathion in a broad linear range, i.e. 0.1–1000 ng/L with a very low limit of detection (52 pg/L).

Akter et al. (2016) fabricated an ultrasensitive electrochemical nanostructured immunosensor for a breast cancer biomarker carbohydrate antigen 15-3 (CA 15-3) using non-covalent functionalized graphene oxides (GO/Py-COOH) as sensor probe and multiwalled carbon nanotube (MWCNTs)-supported numerous ferritin as labels. The immunosensor was constructed by immobilizing a monoclonal anti-CA 15-3 antibody on the GO modified cysteamine (Cys) self-assembled monolayer (SAM) on an Au electrode (Au/Cys) through the amide bond formation between the carboxylic acid groups of GO/Py-COOH and amine groups of anti-CA 15-3. Secondary antibody conjugated MWCNT-supported ferritin labels (Ab2-MWCNT-Ferritin) were prepared through the amide bond formation between amine groups of Ab2 and ferritin and carboxylic acid groups of MWCNTs. The detection of CA 15-3 was based on the enhanced bioelectrocatalytic reduction of hydrogen peroxide mediated by hydroquinone (HQ) at the GO/Py-COOH-based sensor probe. The GO/Py-COOH-based sensor probe and Ab2-MWCNT-Ferritin labels were characterized using CV, EIS, SEM, TEM, and XPS techniques. Using DPV technique, CA 15-3 can be selectively detected as low as 0.01 ± 0.07 U mL^{-1} in human serum samples.

Zhang et al. (2015) fabricated a simple and highly sensitive amperometric immunosensor for the determination of alpha-fetoprotein (AFP) based on multi-functional gold nanoparticles-polydopamine-Prussian blue-graphene oxide nanocomposites (Au-PDA-PB-GO). GO as a template was employed to situ synthesized PB nanoparticle, then PB-GO surface was functionalized by one-step oxidative polymerization of dopamine in basic solution at environment friendly condition to obtain the polydopamine (PDA) modified reduced PB-GO nanoparticles. Via in situ deposition, the Au NPs deposited on the polydopamine functionalized PB-GO nanocomposites. The Au-PDA-PB-GO nanocomposites not only enhance the stability of Prussian blue and provided a favorable microenvironment to maintain the activity of the immobilized biomolecules due to the excellent biocompatibility of PDA, but also increased the loading capacity of the biomolecules due to the large surface area of

nanocomposites, and the present of gold nanoparticles enhanced the conductivity and charge-transport properties of the composites. The dynamic range of the resulted immunosensor for the detection of AFP is from 0.01 ng mL^{-1} to 80.0 ng mL^{-1} with a detection limit of 0.007 ng mL^{-1} (S/N = 3).

Li et al. (2017b) fabricated a novel and sensitive sandwich-type electrochemical immunosensor for quantitative monitoring of prostate specific antigen (PSA). The mesoporous core-shell Pd@Pt nanoparticle loaded by amino group functionalized graphene (M-Pd@Pt/NH2-GS) with high specific surface area, high indexed facets, and good biocompatibility was not only as the carriers of secondary antibodies (Ab2) but also catalyzed the reduction of H_2O_2, which effectually amplified the current signal in detection of PSA. The as-proposed immunosensor exhibited high sensitivity and stability on the detection of PSA. A linear relationship between current signals and the concentrations of PSA was obtained in the range from 10 fg/mL to 50 ng/mL and the detection limit of PSA was 3.3 fg/mL (signal-to-noise ratio of 3).

Yang et al. (2015c) designed a facile and feasible sandwich-type electrochemical immunosensor for ultrasensitive determination of Carbohydrate antigen 19-9 (CA19-9) by using Au@Pd-Gra/Thi-Ab2/HRP bioconjugate which exhibited satisfying electrochemical redox activity, high electrocatalytic activity and friendly biocompatibility. Under optimal conditions, the electrochemical immunosensor exhibited desirable performance for determination of CA19-9 with a wide linearity in the range from 0.015 to 150 U mL^{-1} and a relatively low detection limit of 0.006 U mL^{-1}.

Tian et al. (2015) developed a novel and ultrasensitive sandwich-type electrochemical immunosensor for the quantitative detection of prostate specific antigen (PSA), a well-known prostatic tumor biomarker. A 3D-structured reduced graphene oxide-multiwalled carbon nanotube-palladium nanoparticle (NP) nanocomposite (rGO-MWCNT-Pd) was prepared in a simple and environmentally friendly way and utilized for the adsorption of secondary antibodies (Ab2). It is used as a novel enzyme-mimicking label to develop a sandwich-type electrochemical immunosensor for signal amplification, and shows better electrocatalytic activity for the reduction of H_2O_2 than rGO-CNT or rGO-Pd due to the synergetic effect of the rGO-MWCNT-Pd nanocomposite. The nanocomposite of Au NPs decorated on animated graphene (Au-NH2-GS) is used as a platform for the immobilization of primary antibobies (Ab1) via an amide reaction between the -NH_2 group of the Au-NH2-GS and the -COOH groups of Ab1. Due to the excellent electrocatalytic activity of rGO-MWCNT-Pd for the reduction of H_2O_2, electrochemical amperometric changes at different concentrations of PSA were studied after the immunoreaction. Under the optimum experimental conditions, the proposed electrochemical sandwich-type immunosensor exhibits a low detection limit (0.17 pg mL^{-1}), and a wide linear range (from 0.5 pg mL^{-1} to 15 ng mL^{-1}) for the detection of PSA.

Liu et al. (2015b) developed a high performance three-dimensional (3D) electrochemical immunosensor for sensitive detection of the tumor biomarker, carcinoembryonic antigen (CEA). Monolithic and macroporous graphene foam grown by CVD served as the scaffold of the free-standing 3D electrode. Immuno-recognition interface was fabricated via simple and non-covalent immobilization of antibody using lectin-mediated strategy. Briefly, the well-known lectin macromolecule (concanavalin A, Con A) monolayer was functionalized on 3D graphene (3D-G) using in-situ polymerized polydopamine as the linker. Then the widely used horseradish peroxidase (HRP)-labeled antibody (anti-CEA) in immunoassays was efficiently immobilized to demonstrate the recognition interface via the biospecific affinity of lectin with sugarprotein. The 3D immunosensor is able to detect CEA with a wide linear range (0.1–750.0 ng ml^{-1}), low detection limit (~90 pg ml^{-1} at a signal-to-noise ratio of 3), and short incubation time (30 min).

Zhong et al. (2014) developed a facile electrochemical immunosensor based on graphene-three dimensional nanostructure gold nanocomposites (G-3D Au) using simple and rapid one-step electrochemical co-reduction technique for sensitive detection of topoisomerase. The resultant G-3D Au nanocomposites were characterized by SEM, CV and electrochemical impedance spectroscopy, and then were used as a substrate for construction of the "sandwich-type" immunosensor. Amperometric current-time curve was employed to monitor the immunoreaction on the protein modified electrode. The proposed method could respond to topoisomerase with a linear calibration range from 0.5 ng mL^{-1} to 50 ng mL^{-1} with a detection limit of 10 pg mL^{-1}. This new biosensor exhibited a fast amperometric response, high sensitivity and selectivity, and was successfully used in determining the topoisomerase which was added in human serum with a relative standard deviation (n = 5) < 5%.

4.4.5.1. Non enzymatic graphene based immunosensor. Recently, researchers have reported and fabricated several non enzymatic immunosensor:

M. Li et al. (2017), Y. Li et al. (2017) designed and fabricated a sensitive sandwich-type non-enzymatic electrochemical immunosensor for quantitative detection of squamous cell carcinoma antigen (SCCA). Gold nanoparticles/graphene nanoribbons (Au NPs/NH_2-GNRs) are used as the platform of electrochemical immunosensor to accelerate electron transfer and increase the specific surface area. The Au NPs with good biocompatibility can increase the probability of capturing primary antibodies (Ab_1) to further improve the sensitivity. The silver nanoflower-molybdenum disulfide/multiwalled carbon nanotubes (SNFs-NH_2-MoS_2/MWCNTs) were used as labels of secondary antibodies (Ab_2) and exhibit remarkable multiple-signal amplification effects. The silver nanoflowers with many branches can provide abundant active sites for the electrochemical reaction to further improve the sensitivity. Under the optimal conditions, the immunosensor shows a wide linear range between 0.1 pg mL^{-1} and 20 ng mL^{-1} with a limit of detection 0.03 pg mL^{-1}.

Jian et al. (2016) constructed a novel nonenzymatic electrochemical immunosensor for quantitative detection of α-fetoprotein (AFP). The immunosensor was constructed by modifying gold electrode with electrochemical reduction of graphene oxide-carboxyl multi-walled carbon nanotube composites (ERGO-CMWCNTs) and electrodeposition of gold nanoparticles (AuNPs) for effective immobilization of primary antibody (Ab1). Ferroferric oxide-manganese dioxide-reduced graphene oxide nanocomposites ($Fe_{3O}4$@MnO_2-rGO) were designed as labels for signal amplification. On one hand, the excellent electroconductivity and outstanding electron transfer capability of ERGO-CMWCNTs/AuNPs improved the sensitivity of the immunosensor. On the other hand, introduction of rGO could not only increase the specific surface area for immobilization of secondary antibody (Ab2) but also build a synergetic effect to reinforce the electrocatalytic properties of catalysts. $Fe_{3O}4$@MnO_2-rGO nanocomposites were characterized by SEM, FTIR and X-ray photoelectron spectroscopy. Using AFP as a model analyte, the proposed sandwich-type electrochemical immunosensor exhibited a wide linear range of 0.01–50 ng mL^{-1} with a low detection limit of 5.8 pg mL^{-1}. Moreover, the Fe_3O_4@MnO_2-rGO-based peroxidase mimetic system displayed an excellent analytical performance with low cost, satisfactory reproducibility and high selectivity, which could be further extended for detecting other disease-related biomarkers.

4.4.6. DNA graphene based biosensor

As the carriers of genetic information, DNA has attracted much attention in life sciences. Electrochemistry offers sensitivity, selectivity and low cost for fabrication of sensors capable of detection of selected DNA targets or mutated genes associated with human disease.

The single stranded DNA (ss-DNA) molecules in DNA-biosensors serve as the target recognition element and are known as the probe ss-DNA. The principle is based on the hybridization of the probe ss-DNA with complementary target ss-DNA or the disruption of the structural integrity of probe ss-DNA by the analyte molecules. Both ways lead to

changes in the mass transport, light absorption, emission, or proton concentration, which results in the generation of a signal. Then, the signal is converted into a measurable response via an appropriate transducer element such as optical, electrochemical or thermal element, making the signal measurable as light, current, potential (Saidur et al., 2017). Several researches on the preparation and application of a DNA based on novel graphene materials have been reported by various research groups:

Yardım et al. (2017) modified a GCE by ERGO for subsequent dsDNA immobilization. The interaction of cisplatin with dsDNA was studied at this modified electrode. Quantitative investigations were performed by adsorptive transfer stripping voltammetry (AdTSV) using differential pulse voltammetry (DPV). The morphology and structure of GO and ERGO modified GCEs (GO/GCE and ERGO/GCE, respectively) were characterized by UV–vis, FT-IR, Raman spectroscopy and CV. Compared with the bare GCE and the GO/GCE, the ERGO/GCE exhibited excellent electrocatalytic activity towards the oxidation of dsDNA due to guanine and adenine groups, testified by high oxidation peak currents and decreased oxidation potentials. The interaction of micromolar concentrations of cisplatin with surface confined dsDNA was readily detected as inferred from the decrease of the voltammetric oxidation peaks of guanine and adenine. This trend was significantly greater at the ERGO/GCE compared to the GO/GCE. The interaction of cisplatin with dsDNA was also studied in solution phase by AdTSV with detection at the ERGO/GCE.

Yan et al. (2017) developed a high performance electrochemical DNA sensor with three-dimensional graphene (3DGR) and gold (Au) nanocomposite modified electrode for sensitive analysis of specific hly gene of Listeria monocytogenes. Nanocomposite was synthesized by electrochemical deposit ion of 3DGR and Au in turn on carbon ionic liquid electrode (CILE). Mercaptoacetic acid (MAA) was self-assembled on Au/3DGR/CILE by the specific binding of Au-S bond, which was used for the covalently linkage of ssDNA probe sequences. The fabricated ssDNA/MAA/Au/3DGR/CILE could interact with the target ssDNA sequence and the hybridization was recorded by using electrochemical indicator methylene blue (MB). Based on the reduction current of MB, this electrochemical DNA sensor was able to detect the target ssDNA sequence of hly gene with a wide linear concentration range (1.0×10^{-14} to 1.0×10^{-6} mol L^{-1}) and a low detection limit (3.3×10^{-15} mol L^{-1}, 3σ).

Xu et al. (2017) presented a simple and sensitive electrochemical DNA biosensor based on graphene oxide (GO)/chitosan (CS) hybrid nanocomposites modified GCE for detection of Escherichia coli O157:H7 (E.coli O157:H7). The morphology and composition of GO and hybrid nanocomposites were characterized by TEM, X-ray powder diffraction (XRD), field emission scanning electron microscopy (FESEM), and FTIR. CV investigations indicated that the GO/CS/GCE showed excellent electron transfer ability and good linear relation. Under the optimal hybridization conditions, EIS responses of ssDNA/GO/CS/GCE biosensor were in linear with the target DNA in the concentration range from 1×10^{-14} to 1×10^{-8} M with the detection limit as 3.584×10^{-15} M (3σ). Moreover, differential pulse voltammetry (DPV) studies revealed good specificity and excellent ability of ssDNA/GO/CS/GCE biosensor to distinguish complementary, 1-base mismatched DNA, 2-base mismatched DNA and multi-base mismatched DNA. The developed strategy in this research revealed that the GO/CS modified electrode possess excellent performance for detecting of Escherichia coli O157:H7 DNA

Wang et al. (2017) constructed a novel and ultrasensitive electrochemical biosensor for DNA detection based on functionalized gold clusters/graphene nanohybrids (AuNCs/GR nanobybrids) and exonuclease III (Exo III)-aided cascade target recycling. By utilizing the capacity of GR as universal template, different metal nanoclusters including AuNCs/GR nanobybrids and PtNCs/GR nanohybrids were synthesized through convenient ultrasonic method. Exo III-aided cascade recycling was initiated by target DNA, generating the final cleavage product (S2), which acted as a linkage between capture probe and the functionalized metal nanoclusters/GR conjugates in the construction of the biosensor. The AuNCs/GR-DNA-enzyme conjugates acted as interfaces of enzyme-catalyzed silver deposition reaction, achieving DNA detection ranging from 0.02 fM to 20 p.M. with a detection limit of 0.057 fM. In addition, PtNCs/GR-DNA conjugates presented peroxidase-like activity and the functionalized PtNCs/GR nanohybrids-based electrochemical biosensor also realized DNA detection by catalyzing the 3,3′,5,5′-tetramethylbenzidine-hydrogen peroxide (TMB-H_2O_2) system to produce electrochemical signal. This metal clusters/GR-based multiple-amplified electrochemical biosensor provided a universal method for DNA detection.

Teymourian et al. (2017) developed a novel label-free, indicator-free strategy of electrochemical DNA sensor based on Fe_3O_4 nanoparticles/reduced graphene oxide (Fe_3O_4/r-GO) nanocomposite modified electrode. By using Fe_3O_4/r-GO nanocomposite as a substrate to immobilize probe DNA and subsequent hybridization with target sequence to form dsDNA, a great signal amplification was achieved through measuring changes in DPV peak current of underlying Fe(II)/Fe(III) redox system.

Pan et al. (2017) reported a novel fabrication method for producing a dual-modality biosensor that can simultaneously detect vascular endothelial growth factor (VEGF) and prostate-specific antigen (PSA) in human serum for early diagnosis of PCa. This biosensor was constructed by coating graphene oxide/ssDNA (GO-ssDNA) on an Au-electrode for VEGF detection, and incorporated with poly-$_L$-lactide nanoparticles (PLLA NPs) for signal amplification and PSA detection. The results showed that this biosensor has wide liner detection ranges (0.05–100 ng/mL for VEGF and 1–100 ng/mL for PSA), as well as high levels of sensitivity and selectivity (i.e., resisting interference from external factors, such as glucose, ascorbic acid human serum protein, immunoglobulin G, and immunoglobulin M), and demonstrated a high correlation with an enzyme-linked immunosorbent assay for sample detection in patients. Therefore, this biosensor could be utilized for early clinical diagnosis of PCa in the future.

Moghaddam et al. (2017) used DPV, for an electrochemical investigation of the interaction between TMX and salmon-sperm double-stranded DNA (ds-DNA) which was conducted with a graphene paste electrode (GPE). To determine TMX, a simple and sensitive biosensor was fabricated through this interaction. A linear dynamic range between 8.0×10^{-7} and 8.5×10^{-5} M was exhibited by DPV for TMX. Finally this modified electrode was used for determination of TMX in TMX tablet, serum and urine samples.

Lin et al. (2017) developed an electrochemical biosensor capable of direct detection of DNA damage induced by clenbuterol (CLB). A GCE was modified using reduced graphene oxide-Nafion and dsDNA to produce a dsDNA/RGO-Nafion/GCE sensor. The modified electrode was characterized by EIS and CV, and the results at each stage of the electrode construction were interpreted. They indicated that the electrochemical oxidation peak currents of guanine and adenine at the electrode (dsDNA/RGO-Nafion/GCE) significantly increased as compared with those at the untreated electrode (dsDNA/GCE). Based on this, the sensor was used to measure the change of the oxidation peak currents for guanine and adenine between the intact and damaged dsDNA in the sensor films, and the DNA damage was successfully detected. Furthermore, the plot of peak current decline for the guanine and adenine versus the concentration of CLB was linear in the range of 5.0×10^{-7} to 4.0×10^{-6} mol L^{-1}, with a limit of detection (LOD) of 3.2×10^{-7} mol L^{-1}, which provided a good method to determine CLB indirectly.

Gong et al. (2017) developed an impedimetric HIV-1 gene biosensor based on graphene-Nafion composite film. The biosensor was fabricated by adsorbing the single-stranded DNA (ssDNA) on graphene-Nafion modified on the surface of glassy carbon electrode via the π–π stacking interactions. As the negative ssDNA and the steric hindrance, the electron transfer resistance of the electrodes toward the $[Fe(CN)_6]^{3-/4}$ redox couple was difficult, the electron transfer resistance value

increased. In the measurement of HIV gene, ssDNA probe with the target DNA to form double-stranded DNA (dsDNA), the formation of helix induced dsDNA to release from the surface of the biosensor. The decrease in the electron transfer resistance was in logarithmically direct proportion to the concentration of HIV-1 gene over a range from 1.0×10^{-13} to 1.0×10^{-10} M. The detection limit of this sensor was 2.3×10^{-14} M.

Gao et al. (2017) presented a simple and highly sensitive biosensing interface for DNA detection on the basis of graphene oxide nanosheets (GONs) directed in-situ deposition of silver nanoparticles (AgNPs). The fabrication process and electrochemical properties of the biosensing interface were probed by electrochemical techniques and scanning electron microscopy. The results indicate that GONs can specifically adsorb at the single-stranded DNA probe surface, and induces the deposition of highly electroactive AgNPs. Upon hybridization with complementary oligonucleotides to generate the duplex DNA on the electrode surface, the GONs with the deposited AgNPs will be liberated from the sensing interface due to the inferior affinity of GONs and duplex DNA, resulting in the reduction of the electrochemical signal. Such a strategy combines the superior recognition of GONs toward single-stranded DNA and double-stranded DNA, and the strong electrochemical response of in-situ deposited AgNPs. Under optimal conditions, the biosensor can detect target DNA over a wide range from 10 fM to 10 nM with a detection limit of 7.6 fM.

Chen et al. (2017a) described the construction of a sandwich-type of DNA biosensor for detecting a specific DNA sequence of Mycobacterium tuberculosis (MTB). A polyaniline-reduced graphene oxide (PANI-rGO) composite with favorable electrochemical activity was used as a redox nanoprobe for the generation of the voltammetric signal. The composite was decorated with gold nanoparticles (AuNPs) onto which the signal probe was immobilized to form the tracer label. After hybridization between target DNA and tracer label, the voltammetric signal resulting from the polyaniline-reduced graphene oxide (PANI-rGO) redox probe can be apparently observed. The biosensor can detect the specific IS6110 DNA sequence of MTB in the 0.1 p.M. to 10 nM concentration range, and the detection limit is as low as 50 fM (at an S/N ratio of 3).

X. Chen et al. (2017), M. Chen et al. (2017) developed a new, sensitive electrochemical deoxyribonucleic acid (DNA) biosensor to detect specific target sequences. The biosensor was constructed using a modified nanocomposite consisting of three-dimensional (3D) nitrogen-doped graphene (NG) and Fe_3O_4 nanoparticles. These 3D NG-Fe_3O_4 nanoparticles formed a unique sensing film with strong synergistic effects; the highly porous 3D NG provided a large surface area, whereas Fe_3O_4 was uniformly deposited on the 3D graphene hydrogel (GH), facilitating electron transfer for sensitive detection of DNA with excellent selectivity, fast responses, and a low detection limit. Immobilization of the probe ssDNA sequences on the electrode was greatly improved owing to the unique synergistic effects of 3D NG and Fe_3O_4. Differential pulse voltammetry (DPV) was used to survey the DNA hybridization event with methylene blue (MB) as an electrochemical indicator. Under optimal conditions, the proposed biosensor could detect target DNA concentrations down to 3.63×10^{-15} M (signal/noise ratio of 3) with a linear range from 1.0×10^{-14} to 1.0×10^{-6} M, showing high sensitivity.

Ruiyi et al. (2016) reported on the synthesis of a composite consisting of thionin-functionalized multiple graphene aerogel and gold nanostars (termed TF-MGA/GNSs). The composite displays an enhanced electrochemical performance compared to the classical graphene aerogel. The performance can be further improved by increasing number of the graphene oxide gelation cycles. The composite was deposited on a glassy carbon electrode to obtain a biosensor for the direct detection of dsDNA. The interaction of thionin with dsDNA causes a specific electrochemical response, best at a working voltage of −228 mV (vs. Ag/AgCl). The enhanced electrocatalytic activity of the composite strongly improves sensitivity. The differential pulse voltammetric signal linearly decreases with increasing dsDNA concentration in the range from 100 fg·mL^{-1} to 10 ng·mL^{-1}, and the detection limit is 39 fg·mL^{-1} (at an S/N ratio of 3).

Ba Hashwan et al. (2017) demonstrated thin films of reduced graphene oxide–multiwalled carbon nanotube (rGO–MWCNT) composites as sensing membrane electrodes for single-stranded DNA (ssDNA) detection. The morphology of the rGO–MWCNT composite thin films was observed via field emission scanning electron microscopy. The GO sheet and MWCNTs were clearly obtained, and the MWCNTs were uniformly distributed on the surface of the GO. The chemical bonding of the rGO–MWCNTs was examined using Fourier transform infrared spectroscopy. The element compositions of carbon, silicon, and oxygen were confirmed via energy-dispersive X-ray spectroscopy and X-ray powder diffraction analysis. The biosensor demonstrated high sensitivity to the ssDNA target with a linear range from 500 to 100 p.M.

Ahour and Shamsi (2017) constructed a novel label-free electrochemical biosensor for rapid and facile detection of short sequences ss-DNA molecules related to hepatitis C virus 1a using graphene oxide modified pencil graphite electrode. The sensing mechanism is based on the superior adsorption of single-stranded DNA to GO over double stranded DNA (ds-DNA). The intrinsic guanine oxidation signal measured by differential pulse voltammetry (DPV) has been used for duplex DNA formation detection. The probe ss-DNA adsorbs onto the surface of GO via the π– π* stacking interactions leading to a strong background guanine oxidation signal. In the presence of complementary target, formation of helix which has weak binding ability to GO induced ds-DNA to release from the electrode surface and significant variation in differential pulse voltammetric response of guanine bases. The results indicated that the oxidation peak current was proportional to the concentration of complementary strand in the range of 0.1 nM to 0.5 μM with a detection limit of 4.3×10^{-11} M.

Benvidi et al. (2015) designed a simple and novel electrochemical biosensor based on GCE for DNA detection. GCE was modified with RGO and gold nanoparticles (AuNPs) by the electrochemical method, which is helpful for immobilization of thiolated bioreceptors. The electrode modification processes were characterized by scanning electron microscopy (SEM) and electrochemical methods. Then a single-stranded DNA (ssDNA) probe for BRCA1 5382 insC mutation detection was immobilized on the modified electrode for a specific time. The experimental conditions, such as probe immobilization time and target DNA (complementary DNA) hybridization time and temperature with probe DNA, were optimized using electrochemical methods. The electrochemical response for DNA hybridization and synthesis was measured using EIS and CV methods. The calibration graph contains two linear ranges; the first part is in the range of 3.0×10^{-20} to 1.0×10^{-12} M, and the second segment part is in the range of 1.0×10^{-12} to 1.0×10^{-7} M.

Báez and Bollo (2016) reported a comparative study about the electrochemical response of glassy carbon electrode modified with four different carbon nanomaterial (CNM) against dsDNA is reported. The CNM used were oxidized and nonoxidized multiwalled carbon nanotubes (MWNT-OX and MWNT, respectively), GO and chemically RGO and dispersed in 3:1 chitosan/water mixture. The electrodes were characterized by CV, SEM, and contact angle measurements. The results showed that the type and degree of oxidation have a strong effect on the electroactivity of the modified electrode. GCE/RGO clearly exhibited the most electroactive surface among the CNMs, demonstrating that the graphitic structure is highly important. A more sensitive electrochemical response against dsDNA was obtained when GCE/RGO electrode was used.

Song et al. (2014) developed an ultrasensitive and selective electrochemical immunosensor for the detection of Epstein Barr virus nuclear antigen 1 (EBNA-1). Firstly, a suspension of graphene sheets (GS) and multi-walled carbon nanotubes (MWCNTs) was prepared with the aid of chitosan (CS) solution and then modified on a GCE. Gold nanoparticles (AuNPs) were then electrodeposited onto the surface of the GS-MWCNTs film by CV to immobilize the captured antibodies. After

that, specific sandwich immunoreactions were formed among the captured antibody, EBNA-1, and secondary antibody, DNA-coated carboxyl multi-wall carbon nanotubes (DNA-MWCNTs-Ab2). DNA initiator strands (S0) and secondary antibodies linked to the MWCNTs and double-helix DNA polymers were obtained by hybridization chain reaction (HCR), and here S0 on the MWCNTs propagates a chain reaction of hybridization events between two alternating hairpins to form a nicked double-helix. Finally, electroactive indicator doxorubicin hydrochloride was intercalated into the CG-GC steps between the HCR products and could produce an electrochemical signal, which was monitored by differential pulse voltammetry (DPV). Under optimum conditions, the amperometric signal increased linearly with the target concentrations (0.05–6.4 ng mL^{-1}), and the immunosensor exhibited a detection limit as low as 0.7 pg mL^{-1} (S/N = 3).

Shi et al. (2015) proposed a label-free DNAzyme biosensor for the detection of oligonucleotides related to a hepatitis B virus (HBV) DNA segment. The novel DNAzyme biosensor was based on the electrochemical reduction of graphene oxide-carboxyl multi-walled carbon nanotube composites (GO-CMWCNTs) and the electrodeposition of gold nanoparticles (AuNPs) on a GCE. The thiolate hairpin capture probes with a caged G-quadruplex configuration were self-assembled on AuNPs through the well-known Au-thiol binding. Only after hybridization with target DNA, the hairpin configuration could be opened and released the particular guanine-rich nucleic acid sequences which could assemble to G-quadruplexes. In the presence of hemin and K^+, the hemin/G-quadruplex DNAzyme was generated on the electrode surface, triggering the electrochemical H_2O_2-mediated oxidation of 3,3′,5,5′-tetramethylbenzidine (TMB). With the advantages of amplification effects of AuNPs and hemin/G-quadruplex, a linear concentration range from 10 p.M. to 10 nM with a limit of detection of 0.5 p.M. was obtained for the target DNA.

4.4.7. Dopamine, ascorbic acid, uric acid graphene- based biosensor

Dopamine (DA) is one of the most important neurotransmitters in the central nervous system of mammals, and which exists in the tissues and body fluids in the form of cations for controlling the nervous system. Ascorbic acid is a vital component of the human diet. Ascorbate prevents scurvy and it is accepted to be the primary antioxidant in human blood plasma. It is present in the mammalian brain together with various neurotransmitter amines including dopamine, epinephrine and norepinephrine.

Uric acid (UA) and other oxypurines are the principal final products of purine metabolism in the human body. Abnormal levels of UA cause symptoms of several diseases, including gout, hyperuricemia and Lesch–Nyan disease. UA, as vital biological substance, is desirable to be accurate detected in clinical monitoring and diagnosis. In recent years, many graphene nanocomposites have been synthetized and used in fabricating electrochemical sensors for the simultaneous determination of DA, UA and AA. Several researches on the preparation and application of DA, UA and AA based on novel graphene materials have been reported by various research groups:

Wang et al. (2017) synthesized Cu_2O/CuO/reduced graphene oxide (rGO) through a rapid and convenient microwave-assisted hydrothermal method. The crystal structure and morphology of the as-prepared product were characterized using XRD, field-emission-scanning electron microscopy (FESEM), TEM, Raman spectroscopy, and XPS. The electrochemical performance of the novel Cu_2O/CuO/rGO biosensor was investigated via CV. The biosensor was evaluated for AA detection and exhibited a wide linear range of 100–1000 μM, a low detection limit of 0.301 μM, and a sensitivity of 1375.486 μA mM^{-1} cm^{-2}.

Zhang et al. (2016) fabricated a reduced graphene oxide-zinc oxide (RGO-ZnO) composite by a spontaneous reduction of graphene oxide via zinc slice in one-pot approach at room temperature, and used to modify GCE for developing of electrochemical biosensor (RGO-ZnO/GCE). The as-prepared RGO-ZnO was characterized by XRD, XPS, inductively coupled plasma atomic emission spectroscopy (ICP-AES), SEM and TEM. It was revealed that the existence of ZnO in RGO-ZnO/GCE largely enhanced the electroactive surface area (EASA) and therefore the sensitivity for electrochemical sensing. In the mixtures of AA, DA and UA, the biosensor exhibited three well-resolved voltammetric peaks ($\Delta E_{AA\text{-}DA}$ = 236 mV, $\Delta E_{DA\text{-}UA}$ = 132 mV, $\Delta E_{AA\text{-}UA}$ = 368 mV) in the DPV measurements, allowing a simultaneous electrochemical detection of these biomolecules. The liner relationships between current intensities and concentrations were found to be 50–2350 μM, 1–70 μM and 3–330 μM, with detection limits of 3.71 μM, 0.33 μM and 1.08 μM for AA, UA and DA, respectively.

Zhu et al. (2017) developed a new electrochemical sensor for the simultaneous determination of AA, DA and UA using ferrocene hybrid (Fc)/three dimensional graphene hydrogel (3DGH) nanocomposite. The composite materials were characterized using different techniques, such as SEM, AFM, and UV–vis. The electrochemical detection methods using for the individual and simultaneous detection of AA, DA and UA were CV, DPV and amperometric (i–t). Due to the excellent properties and unique structure of the nanocomposite, this sensor exhibited sharp peaks for the oxidation of AA, DA and UA as compared with the bare GCE. The linear responses of AA, DA and UA were observed from 20 to 450 μM, 10–180 μM and 8–400 μM with detection limits (S/N = 3) of 0.183 μM AA, 0.042 μM DA and 0.067 μM UA, respectively. In addition, the developed 3DGH-Fc/GCE electrode showed well anti-interference ability, great stability and excellent reproducibility.

Wang et al. (2017) synthesized Cu_2O/CuO/reduced graphene oxide (rGO) through a rapid and convenient microwave-assisted hydrothermal method. The crystal structure and morphology of the as-prepared product were characterized using X-ray diffraction (XRD), field-emission-scanning electron microscopy (FESEM), transmission electron microscopy (TEM), Raman spectroscopy, and XPS. The electrochemical performance of the novel Cu_2O/CuO/rGO biosensor was investigated via CV. The biosensor was evaluated for AA detection and exhibited a wide linear range of 100–1000 μM, a low detection limit of 0.301 μM, and a sensitivity of 1375.486 μA mM^{-1} cm^{-2}.

Bai et al. (2017) constructed sensitive electrochemical biosensor for detection of UA with cationic poly(diallyldimethylammonium chloride) functionalized reduced graphene oxide (PDDA-rGO) and anionic Au nanoparticles mixed with polyoxometalates clusters $K_8P_2W_{16}V_2O_{62}$ ($P_2W_{16}V_2$-Au). The effective combination of $P_2W_{16}V_2$-Au and PDDA-rGO brings many advantages in electrochemical detection, involving the fast transmission of electric charges, the unimpeded pathways for diffusion and more sensing sites. Under optimized conditions, the proposed sensor showed acceptable analytical performances for UA in terms of good linearity (over the concentration range from 2.5×10^{-7} to 1.5×10^{-4} M) and lower detection limit 8.0×10^{-8} M (S/N = 3).

Muthukumaran et al. (2016) grew marigold flower-like self-assembled β-NiS (nickel sulfide) nanosheets on rGO by a single-step hydrothermal process and then gold nanospheres (AuNS) were electrochemically deposited on the β-NiS@rGO nanostructures. The β-NiS@rGO/AuNS hierarchical hybrid demonstrates excellent electrochemical activities for clinically important analytes such as AA, EP and UA simultaneously. Moreover, the β-NiS@rGO/AuNS/GCE exhibits significant detection of AA by one order and UA by two orders higher sensitivity when compared to a β-NiS@rGO modified electrode. They investigated using this electrocatalyst for individual detection, the linear responses of AA, EP and UA at concentrations in the ranges of 900 nM to 100 μM, 2 μM to 1 mM and 100 nM to 1 mM with low detection limits of 331 nM, 540 nM and 4.5 nM (S/N = 3σ/b), respectively; the resulting non-enzymatic biosensor also retained a good response to simultaneous detection with a wide linear range 1 μM to 1 mM, 2 μM to 1 mM and 100 nM to 1 mM and significantly lower detection limits of 682 nM, 1.3 μM and 6 nM, respectively.

Mao et al. (2016) prepared hydrophilic polymers (HP) functionalized polypyrrole/graphene oxide nanosheets (HP/PPy/GO) by covalently modifying polyacrylamide (PAM), polyacrylic acid (PAA) and polyvinylpyrrolidone (PVP) on the surface of PPy/GO nanosheets

containing vinyl groups. Besides significantly improving the dispersivity of PPy/GO in water, the different chemical properties among the three HP with different hydrophilic groups further resulted in the different performances of the obtained electrochemical biosensors PAM/PPy/GO, PAA/PPy/GO and PVP/PPy/GO modified GCEs in electrocatalytic applications to simultaneously determine DA and AA. PAM/PPy/GO and PAA/PPy/GO modified GCEs exhibited good electrochemical responses to distinguish DA from AA in their mixture at certain concentrations, which cannot be achieved by the PVP/PPy/GO modified GCE, due to their different chemical properties among the three HP with different hydrophilic groups. Particularly, compared to PAA/PPy/GO, PAM/PPy/GO can act as a good steady electrode material with good selectivity and sensitivity that can simultaneously determine the two substrates in their mixture at lower concentrations, which may be due to the different chemical properties between the electron-donating amide groups and electron-withdrawing carboxyl groups. The different electronic effects of the amide group and carboxyl group resulted in the difference in the transmission capability of electrons released from the oxidation reaction of DA and AA.

Guo et al. (2016) investigated GCE modified with 5-(4-Aminophenyl)-10,15,20-triphenylporphyrin]Mn(III) ($MnNH_2TPP$) and GO composite materials (GO-$MnNH_2TPP$) by EIS and successfully employed for the determination of UA. Electrochemical behaviors of UA at various electrodes including the glassy carbon electrode, GO/GCE, $MnNH_2TPP$/GCE and GO-$MnNH_2TPP$/GCE were measured, respectively, which showed GO-$MnNH_2TPP$/GCE had better electrocatalytic activities than other electrodes under the present experimental conditions. The experimental conditions of the UA determination including the effects of scan rate, pH value and the modified amount of GO-$MnNH_2TPP$ on the surface of GCE were optimized when the GO-$MnNH_2TPP$/GCE was used to detect UA. The electrochemical response properties of UA were studied by two electrochemical methods including the differential pulse voltammograms (DPV) and the amperometric i-t curve technique under above optimized experimental conditions. The response of GO-$MnNH_2TPP$/GCE towards UA was excellent line relationship in the concentration ranges from 0.5 to 500 μM and the lowest detection limit was 0.30 μM (S/N = 3) by DPV; the amperometric i-t curve techniques also exhibited excellent line relationship in the concentration ranges from 20 to 290 μM and the lowest detection limit was 1.74 μM (S/N = 3).

Fu et al. (2016) prepared reduced graphene oxide–ZnO (RGO–ZnO) nanorods composite via a simple one-pot hydrothermal approach. The synthesized RGO–ZnO nanorods composite has been successfully applied for GCE surface modification. The RGO–ZnO nanorods composite-modified GCE was applied for sensitive and selective determination of uric UA. The biosensor exhibited a linear dependence on UA concentration ranging from 1 to 800 μM with a detection limit of 0.312 μM (S/N = 3).

Zou et al. (2015) used H-GO modified GCE that showed high electrocatalytic activities for the oxidation of ascorbic acid, dopamine, and uric acid, achieving the simultaneous determination for those three different kinds of biomolecules with detection limits of 0.3, 0.17, and 0.17 $\mu mol\ L^{-1}$ (S/N = 3), respectively.

Zhao et al. (2015) fabricated an electrochemical biosensor for simultaneous detection of AA, DA and UA by electrochemical deposition of MgO nanobelts on a graphene-modified tantalum wire (denoted as MgO/Gr/Ta) electrode. The MgO nanobelts and graphene were verified by SEM and TEM. Electrochemical performances of the electrodes were characterized by EIS, CV and DPV. The CV results show that AA, DA and UA could be detected simultaneously using MgO/Gr/Ta electrode with peak-to-peak separation of 300 mV, 147 mV and 447 mV for AA-DA, DA-UA and AA-UA, respectively. In the threefold co-existence system, the linear calibration plots for AA, DA and UA were obtained over the concentration range of 5.0–350 μM, 0.1–7 μM and 1–70 μM with detection limits of 0.03 μM, 0.15 μM and 0.12 μM respectively.

Ramakrishnan et al. (2015) synthesized platinum nanoparticle-decorated graphene and carbon nanotube (Pt-Gr-CNT) nanocomposites by radio frequency chemical vapour deposition (RF-CVD) from ethanol, using a Pt/MgO catalyst. Morphological analysis showed Pt nanoparticles decorating graphene sheets and double-walled and multi-walled carbon nanotubes. It was observed that, upon encountering Pt nanoparticles, carbon nanotubes unravelled into graphene sheets. This may be due to graphitic carbon atoms from growing CNTs forming bonds with carbon atoms from other CNTs, particularly at the site of another Pt NP. The Pt-Gr-CNT-modified GCE showed high electrocatalytic activity towards the oxidation of AA, DA and UA in 0.1 M phosphate buffer solution (pH 7.0) in CV and differential pulse voltammetry (DPV) studies. CV showed well-separated oxidation peaks of AA (−99 mV), DA (121 mV) and UA (261 mV). In DPV studies, the peak separation between AA-DA, DA-UA and AA-UA was 210 mV, 140 mV and 360 mV respectively. The simultaneous detection of AA, DA and UA using DPV, in respective concentration ranges of 200–900 μM, 0.2–30 μM, 0.1–50 μM, showed good linearity and sensitivities of 0.186 $\mu A\ \mu M^{-1}\ cm^{-2}$ (AA), 9.199 $\mu A\ \mu M^{-1}\ cm^{-2}$ (DA) and 9.386 $\mu A\ \mu M^{-1}\ cm^{-2}$ (UA) respectively.

4.4.8. Metals ions graphene- based biosensor

The presence of heavy metal in food chains due to the rapid industrialization poses a serious threat on the environment. As heavy metal ions severely harm human health, it is important to develop simple, sensitive and accurate methods for their detection in environment and food. Electrochemical detection featured with short analytical time, low power cost, high sensitivity and easy adaptability for in-situ measurement is one of the most developed methods. Therefore, detection and monitoring of heavy metals contamination are gaining more attention in recent times. But, the current analytical methods (based on spectroscopy) for the detection of heavy metal contamination are often very expensive, tedious and can only be handled by trained personnel (Saidur et al., 2017). The heavy metal ions, especially Cd^{2+}, Pb^{2+} and Hg^{2+}, show extremely hazard to the environment and human being. Heavy metals such as cadmium and lead, due to their high toxicity, represent a serious threat to health and the environment. Even exposure to low levels of cadmium and lead can be life-threating. The measurement of heavy metal ions using sensors is attracting great attention for its advantages of high sensitivity and selectivity, low-cost, convenience to handle and rapid detection. In recent years, graphene and its nanocomposite materials are applied in sensors to investigate heavy metal ions, in particular, Cd^{2+}, Pb^{2+} and Hg^{2+}(Liu et al., 2017a). Many kinds of heavy metal ions such as Ag^{+}, Au^{3+}, Cd^{2+}, Cu^{2+}, Fe^{3+}, Hg^{2+}, Mn^{2+} and Pb^{2+} have been detected with the use of graphene-based sensors in recent years (Zhang et al., 2017) (Table 2).

Several researches on the preparation and application of a metal biosensor based on novel graphene materials have been reported by various research groups:

Zhang et al. (2016) prepared a novel DNA-modified nanocomposite of three-dimensional reduced graphene oxide and chitosan particles (CS@3D-rGO@DNA) by one-step method and used as a new electrochemical biosensing strategy to detect Hg^{2+} in drinking water. This biosensor was fabricated by the chemical coordination of T-Hg^{2+}-T between the T-rich oligonucleotide strands contained in the as-prepared CS@3D-rGO@DNA nanocomposite and Hg^{2+}, thereby varying the electrochemical signals. The developed electrochemical biosensor exhibited high sensitivity toward the determination of Hg^{2+} with a low detection limit of 0.016 nM, ranging from 0.1 nM to 10 nM.

Xue et al. (2016) used integrated with DNAzyme highly specific to metal ions, hemin@reduced graphene oxide (hemin@rGO) functionalized with flower-like MnO_2 and hollow AuPd (hAuPd-fMnO_2-hemin@rGO) as electroactive probe and electrocatalyst to construct a universal platform for metal ion detection (lead ion Pb^{2+} as the model). The proposed strategy with generality was mainly based on two aspects. Firstly, the designed probe not only showed high stability and excellent peroxidase-like activity originating from hemin, fMnO_2 and hAuPd, but also possessed intrinsic redox performance from hemin, which resulted

Table 2
The detections of specific heavy metal ions and corresponding bioelectronics devices based on graphene.

Ions	Methods	Sensors	Detection limit	Linear range	Reference
Hg^{2+}	Piezoelectric	Graphene nanostructures	0.031 nM	1–500 nM	(Wang et al., 2014a)
	Liquid-ion FET	FET Graphene aptasensor	10 p.M.	$10–10^3$ pM	
	Electrochemiluminescence	Micropatterned rGO films	~1 nM		
	Electrochemical	GPC/graphene/luminol	0.005 nM	0.01–100 nM	(Guo et al., 2015b)
	Electrochemical	Nanoparticles/graphene	< 0.3 ppb	0.008–0.05ppb/0.1–60 ppb	
	Electrochemical	3DG/PPy composite	0.03 nM	0.1–110 nM	(Wang et al., 2014b)
	Electrochemical	GO/ionic liquid/AuNPs	0.03 nM	0.1–100 nM	
	Electrochemical	Graphene-DNA biosensor	5 nM	8–100 nM	
	Electrochemical	GO		1–300 nM	
	Electrochemical	GO/gold nanoparticles	0.78 nM	5–110 nM	
	Electrochemical	Porous Cu microspheres/rGO	8.62 p.M.	0.05–40 nM	(Fang et al., 2014)
	Electrochemical	Graphene nanostructures	0.017 nM	0.1–100 nM	(Wang et al., 2014a)
	Electrochemical	3DGH/polyaniline	0.035 nM	0.1–100 nM	(Yang et al., 2015a, 2015b, 2015c, 2015d)
	Electrochemical	GO/4-Aminophenyl/Au	5 nM		(Zhang et al., 2015b)
	Electrochemical	GQD/functionalized Au NPs	0.02 nM	0.02–1.5 nM/1.5–100 nM	(Ting et al. 2015)
	Electrochemical	SnO_2/rGO nanocomposites	122 p.M.	0.4–1.2 μM	
	Chemiluminescence	PPy/rGO	15 nM		
	Electrochemical	GO-assisted exonuclease	2 nM		
Ag^{+}	Electrochemical	GNs/thionine/molecular wire	4.17 nM	8×10^{-3}~10 mM	(Afkhami et al. 2015)
Cu^{2+}	Electrochemical	Graphene/Au electrode		1.5–20 nM	
	Electrochemical	Alkyl GO	2.7 μM		
	Electrochemical	Rhodamine B/GO	0.061 nM	0.1–50 nM	(Kang et al., 2015)
	Electrochemical	Graphene /porous Au electrode		0.009–4 μM	(Zhu et al., 2015)
	Electrochemical	GO/Au electrode	10 nM		(Zhang et al., 2015b)
	Electrochemical	GQD functionalized AuNPs	0.05 nM		(Ting et al. 2015)
	Electrochemical	SnO2/rGO nanocomposites	226.9 p.M.	0.2–0.6 μM	
	Electrochemical	Metallo-graphene platform	0.07 μg L^{-1}	1–7 μg L^{-1}	
Pb^{2+}	Electrochemical	Graphene/polyaniline	0.1 μg L^{-1}	1–300 μg L^{-1}	(Ruecha et al. 2015)
	Electrochemical	PPy/rGO	4 p.M.		
	Electrochemical	graphene/Au electrode	0.4 ± 0.05 nM	0.4–20 nM	
	Electrochemical	rGO/GCE	0.5 nM	3–15 nM	(Hamsawahini et al. 2015)
	Electrochemical	Graphene/ porous Au electrode		0.006–2.5 M	(Zhu et al., 2015)
	Electrochemical	GO/Au Electrodes	1 nM		(Zhang et al., 2015b)
	Electrochemical	AlOOH-rGO Nanocomposites	76 μM	0.3–1.1 μM	
	Electrochemical	SnO_2/rGO Nanocomposites	18.39 p.M.	0.4–1.2 μM	
	Electrochemical	Metallo-graphene platform	0.07 μg L^{-1}	1–7 μg L^{-1}	
Zn^{2+}	Electrochemical	Graphene/polyaniline	1 μg L^{-1}	1–300 μg L^{-1}	(Ruecha et al. 2015)
	Electrochemical	Metallo-graphene platform	0.07 μg L^{-1}	1–7 μg L^{-1}	
Cd^{2+}	Electrochemical	Graphene/polyaniline	0.1 μg L^{-1}	1–300 μg L^{-1}	(Ruecha et al. 2015)
	Electrochemical	nanographene-based sensor	3.5 ng L^{-1}	0.25–5 μg L^{-1}	(Wu et al., 2014a)
	Electrochemical	AlOOH-rGO Nanocomposites	44.6 p.M.	0.1–0.8 μM	
	Electrochemical	SnO_2/rGO nanocomposites	0.08 μg L^{-1}		
	Electrochemical	Metallo-graphene platform	0.07 μg L^{-1}	1–7 μg L^{-1}	

in the promotion of electron transfer and the enhancement of the response signal readout. Secondly, due to the introduction of Pb^{2+}, Pb^{2+}-dependent DNAzyme bound in the electrode surface could be specifically identified and cleaved by Pb^{2+}, and the remained fragment (its supplementary sequence is a single-strand DNA S3) captured the nanocomposites S3-hAuPd-fMnO_2-hemin@rGO by the hybridization reaction. Therefore, combined the cooperative catalysis of fMnO_2, hAuPd and hemin to H_2O_2 reduction with highly specific interaction of Pb^{2+}-dependent DNAzyme, the proposed Pb^{2+} biosensor showed significant improvement of electrochemical analytical performance, which was involved in wide dynamic response in the range of 0.1 p.M. to 200 nM, low detection limit of 0.034 p.M., high sensitivity and high specificity.

Mishraa et al. (2017) presented an electrospinning of GO onto screen printed carbon electrodes (SPCE) for heavy metals (HMs) bio-sensing. The GO was dispersed in poly (vinyl alcohol) (PVA) diluted aqueous solution, and the mixture was electrospun into GO/PVA composite nanofibers. The morphology of GO and SPCE modified with electrospun nanofiber was studied using SEM micrographs and confirmed the uniform distribution of GO sheets in nanofibers. The Alkaline Phosphatase (ALP) was immobilized ontonanofibers grown on the SPCE and activity was checked using 1-napthyl phosphate (1-NP) by applying differential pulse voltammetry (DPV). The ALP activity was inhibited in the presence of HMs and a difference in activity was recorded after inhibition. The inhibition was calculated based on the data of pre and post inhibition current values. The inhibition of ALP was observed with mercury (Hg2+), lead (Pb2+) and cadmium (Cd2+) with a detection limit of 0.0075, 0.015 and 0.0312 ppb respectively. Excellent HM recoveries were obtained in the range 94.6–99.75 with %RSD value of 3.77.

Zhang et al. (2017) developed an ultrasensitive electrochemical biosensor for detection of Ag+ based on magnetic Fe3O4@gold core-shell nanoparticles (Fe3O4@Au NPs) labeling with hybridization chain reaction (HCR) amplification strategy. In this sensing strategy, the magnetic Fe_3O_4@Au NPs were selected for labeling with HCR product and enrichment on the surface of magnetic gold electrode. Thiolated-oligonucleotide (S1) was firstly immobilized on the surface of Fe3O4@Au NPs through Au–S chemical bond. In the presence of Ag+, cytosine-rich DNA oligonucleotide S2 hybridized with S1 to form an intramolecular duplex, in which Ag+ can selectively bind to cytosine–cytosine mismatches forming C–Ag+–C complex. The exposed stem of the C–Ag+–C complex opened two alternating ferrocene-labeled DNA hairpins (H1 and H2) in turn and triggered HCR to form a supersandwich DNA structure on the surface of Fe3O4@Au NPs. The HCR products modified Fe3O4@Au NPs were brought to the surface of magnetic gold electrode for direct electrochemical measurements. The proposed strategy led to a low detection limit of 0.5 fM and a wide dynamic range of 1 fM^{-100} pM for target Ag+.

Tang et al. (2016) fabricated a novel label free electrochemical biosensor by the use of GO as catalytic probe and deposition substrate

for sensitive detection of Pb^{2+}. As a result of Pb^{2+} induced conformational change of aptamer, GO can be captured on electrode surface. The Ag^{+} reduction process can be accelerated by the captured GO, which resulted in the formation of silver nanoparticles (AgNPs) on GO surface. Through detecting the oxidation signal of the formed AgNPs by voltammetry, highly sensitive detection of Pb^{2+} can be realized. The detection limit of this assay for Pb^{2+} was 80 p.M. with a linear range from 0.1 nM to 10.0 μM.

4.4.9. Pesticides graphene-based biosensor

Oganophosphorus (OPs) and organophosphate (OP) pesticides are toxic to human and most animals through inhibition of the enzymes in neurosynapses—acetylcholinesterases

(AChE), resulting in accumulation of acetylcholine in human body. Acetycholine over stimulate its receptors in synapses and eventually damaging the nervous system. OPs have been widely used in the past several decades to protect crops from insects (Long et al., 2015). Several researches on the preparation and application of a pesticides biosensor based on novel graphene materials have been reported by various research groups:

Cui et al. (2018a) developed a highly stable electrochemical AChE biosensor for detection of organophosphorus pesticides (OPs) simply by adsorption of AChE on chitosan (CS), TiO2 sol-gel, and reduced graphene oxide (rGO) based multi-layered immobilization matrix (denoted as CS@TiO2-CS/rGO). The biosensor fabrication conditions were optimized, and the fabrication process was probed and confirmed by scanning electron microscopy and electrochemical techniques. The matrix has a mesoporous nanostructure. Incorporation of CS and electrodeposition of a CS layer into/on the TiO2 sol-gel makes the gel become mechanically strong. The catalytic activity of the AChE immobilized CS@TiO2-CS/rGO/glassy carbon electrode to acetylthiocholine is significantly higher than those missing any one of the component in the matrix. The detection linear range of the biosensor to dichlorvos, a model OP compound, is from 0.036 μM (7.9 ppb) to 22.6 μM, with a limit of detection of 29 nM (6.4 ppb) and a total detection time of about 25 min.

Guler et al. (2017) developed a facile electrochemical AChE (EC 3.1.1.7; AChE) biosensor based on nafion (NA) and Ag nanoparticles supported on amine functionalized reduced graphene oxide (rGO-NH_2). The Ag@rGO-NH_2 nanocomposite was characterized using FouFT-IR, TEM, and XRD. After being optimized, the biosensor exhibited excellent electrochemical response to the oxidation of thiocholine, the hydrolysis product of acetylthiocholine chloride (ATCl) catalyzed by AChE. An apparent Michealis-Menten value of 20.5 μM was obtained. Under optimized conductions, the biosensor detected malation, methidathion, and chlorpyrifos ethyl in the linear range from 0.0063 to 0.077 μg/mL, from 0.012 to 0.105 μg/mL, and from 0.021 to 0.122 μg/mL, respectively. The detection limit (LoD) was 4.5 ng/mL for malation, 9.5 ng/mL for methidathion, and 14 ng/mL for chlorpyrifos ethyl.

Zhou et al. (2016) obtained a sensitive and fast sensor for quantitative detection of organophosphorus pesticides (OPs) using AChE biosensor based on graphene oxide (GO)-chitosan (CS) composite film. This new biosensor was prepared via depositing GO-CS composite film on GCE and then assembling AChE on the composite film. The GO-CS composite film shows an excellent biocompatibility with AChE and enhances immobilization efficiency of AChE. GO homogeneously disperses in the GO-CS composite films and exhibits excellent electrocatalytic activity to thiocholine oxidation, which is from acetylthiocholine catalyzed by AChE. The results show that the inhibition of carbaryl/trichlorfon on AChE activity is proportional to the concentration of carbaryl/trichlorfon. The detection of linear range for carbaryl is from 10 nM to 100 nM and the correlation coefficients of 0.993. The detection limit for carbaryl is calculated to be about 2.5 nM. In addition, the detection of linear range for trichlorfon is from 10 nM to 60 nM and the correlation coefficients of 0.994. The detection limit for trichlorfon is calculated to be about 1.2 nM.

Zhang et al. (2015) developed a sensitive electrochemical AChE biosensor based on a rGO and silver nanocluster (AgNC) modified GCE. rGO and AgNC nanomaterials with excellent conductivity, catalytic activity and biocompatibility offered an extremely hydrophilic surface, which facilitated the immobilization of AChE to fabricate the organophosphorus pesticide biosensor. Carboxylic chitosan (CChit) was used as a cross-linker to immobilize AChE on a rGO and AgNC modified GCE. The AChE biosensor showed favorable affinity to acetylthiocholine chloride (ATCl) and could catalyze the hydrolysis of ATCl. Based on the inhibition effect of organophosphorus pesticides on the AChE activity, using phoxim as a model compound, the inhibition effect of phoxim was proportional to its concentration ranging from 0.2 to 250 nM with a detection limit of 81 p.M. estimated at a signal-to-noise ratio of 3.

Sansuk and Sritongkham (2015) constructed a disposable electrochemical biosensor based on enzyme inhibition for detection of organophosphate and carbamate pesticides. The nanocomposite film of gold nanoparticles and graphene/PEDOT-PSS were prepared on the surface of screen-printed carbon based electrodes (SPCEs). Acetylcholinesterase enzyme was immobilized onto the film via cross-linking method. The composite film provides specific surface area and high conductivity. A significant synergistic effect of nanocomposites on the biosensor performance was observed in sensing of acetylthiocholine chloride and the inhibition of paraoxon and carbofuran. Graphene/PEDOT-PSS/AuNPs enhanced electron transfer reaction at a lower potential and catalyzed the electrooxidation of thiocholine. Based on the inhibition of paraoxon on the AChE activity, a Unear range of 10–400 ppb were obtained. For carbofuran determination, two Unear ranges at 0.5–10 and 200–500 ppb can be found.

Yang et al. (2014) constructed a nanohybrid of gold nanoparticles, polypyrrole, and reduced graphene oxide sheets (named as Au-PPy-rGO) by electrochemical deposition of reduced graphene oxide with pyrrole and the introduction of gold nanoparticles. AChE was further encapsulated in a silica matrix and immobilized on the Au-PPy-rGO nanocomposite by co-deposition with $(NH_4)_2SiF_6$. The presence of PPy helped to avoid the aggregation of rGO caused by van der Waals interactions between individual sheets and significantly increased the surface area of the modified electrode. The obtained Au-PPy-rGO nanocomposite not only showed excellent conductivity but also exhibited a high electrocatalytic activity and specific affinity for thiocholine, the hydrolysis product of the enzyme, and thus an improved detection sensitivity. Since AChE molecules were protected by the circumambient silica matrix, which provided a biocompatible environment and facilitated mass transport, the fabricated AChE biosensor displayed high stability and excellent activity together with a fast response to organophosphorus pesticides. Under optimum conditions, the biosensor led to the rapid and sensitive detection of paraoxon-ethyl from 1.0 nM to 5 μM with a detection limit of 0.5 nM

Zhan et al. (2015) developed a fast and stable organophosphate pesticide (OP) biosensor with enhanced sensitivity has been developed for the detection of OPs by using Au-Pd bimetallic nanoparticles and ionic liquid functionalized graphene-chitosan nanocomposites (Au-Pd/IL-GR-CHI). An electrodeposition method was first applied to form Au-Pd nanoparticles on the surface of IL-GR-CHI, which were characterized by scanning electron microscopy and electrochemical methods. The electron transfer resistance of the Au-Pd/IL-GR-CHI modified electrode was smaller than that of the Au/IL-GR-CHI (or Pd/IL-GR-CHI) modified electrode, indicating that the presence of Au-Pd/IL-GR-CHI hybrid nanocomposites on the electrode surface could improve the reactive sites, reduce the interfacial resistance, and make the electron transfer easier. The Au-Pd/IL-GR-CHI hybrid nanocomposites with excellent conductivity, catalytic activity and biocompatibility offered an extremely hydrophilic surface for AChE adhesion. Under optimal conditions, based on the inhibition of organophosphate pesticides (OPs) on the AChE activity, using phorate as a model compound, the biosensor detected phorate in the linear range from 5.0×10^{-16} to 2.5×10^{-13} M and from 4.9×10^{-13} to 9.5×10^{-6} M, with a detection limit of 2.5×10^{-16} M (S/N = 3).

4.4.10. Mycotoxin graphene-based biosensor

Toxins caused by pathogenic bacteria have always been a serious threat to the health of people and to the economy of nations. Food safety is threatened by toxins which could give rise to foodborne diseases, seriously affecting human health and the profits of food businesses. Toxins can also be used in bioterrorism. Shiga toxin-producing E. coli (STEC) serotype O157:H7 are the most commonly mentioned in E. coli group in association with foodborne outbreaks (Xua, Ronghui Wanga et al., 2017). Ochratoxin A (OTA), a toxin produced by *Aspergillus ochraceus and Penicillium verrucosum*, is one of the most abundant food-contaminating mycotoxins worldwide (Hao et al., 2016; Hu et al., 2017; Lv et al., 2017). Aflatoxin is the most harmful mycotoxin which is ubiquitous in foods and agricultural supplies and aflatoxin can put the safety of people in jeopardy and lead to some fatal disease (Eivazzadeh-Keihan et al., 2017). Aflatoxin B1 (AFB1) is a carcinogenic substance produced by fungi of genus *Aspergillus,* especially *Aspergillus flavus* (Joo et al., 2017).

Recently, researchers have reported and fabricated several mycotoxin biosensors:

Sun et al. (2017) developed a simple and feasible homogeneous electrochemical sensing protocol for the detection of ochratoxin A (OTA) in foodstuff on the immobilization-free aptamer–graphene oxide nanosheets coupling with DNase I-based cycling signal amplification. Under optimal conditions, graphene-based aptasensing platform could exhibit good electrochemical responses for the detection of OTA at a concentration as low as 5.6 pg mL^{-1}.

Loo et al. (2015) developed an electrochemical aptasensor for ochratoxinA (OTA) by utilizing graphene-oxide nanoplatelets (GONPs) as electroactive labels. OTA aptamer (OTA-apt), which serves as the recognition element, was first immobilized onto the electrode surface before the modified electrode underwent exposure to OTA. Subsequently, incubation with GONPs was performed and the nanoplatelets conjugated to the immobilized OTA-apt through π-π interactions. The principle of detection lies in the ability of these nanoplatelets to be electrochemically reduced, thereby producing a well-defined reduction peak that was then employed as the analytical signal. The fabricated aptasensor is capable of detecting OTA in the concentration range of 310fM to 310 p.M., with good selectivity against common interferences.

Lu et al. (2016b) developed an electrochemical immunosensing method for rapid and sensitive detection of two mycotoxins, fumonisin B1 (FB1) and deoxynivalenol (DON). A disposable screen-printed carbon electrode (SPE) was used as sensing platform. The working electrode part of SPE was modified by gold nanoparticles (AuNPs) and polypyrrole (PPy)-ErGO nanocomposite film for effective anti-toxin antibody immobilization, enhanced electrical conductivity, and biocompatibility. Under optimized test conditions, the limit of detection and linear range achieved for FB1 were 4.2 ppb and 0.2–4.5 ppm (% RSD = 4.9%); and the corresponding values for DON were 8.6 ppb and 0.05–1 ppm (%RSD = 5.7%).

Khoshfetrat et al. (2018) developed a sensitive electrochemiluminescence (ECL) aptasensor for aflatoxin M1 (AFM1) detection by a closed bipolar electrode (BPE) array. The thiolated AFM1 aptamer was immobilized on gold nanoparticle-coated magnetic Fe_3O_4 nanoparticles (Apt-GMNPs). Luminol-functionalized silver nanoparticle-decorated graphene oxide (GO-L-AgNPs) participates in π-π interactions with the unpaired bases of the immobilized aptamer (Apt-GMNPs-GO-L-AgNPs). After the Apt-GMNPs-GO-L-AgNPs were introduced to a gold anodic BPE array, the individual electrodes were subjected to different concentrations of AFM1. Upon the interaction of AFM1 with the aptamers, the GO-L-AgNPs detach from the aptamer; the resulting ECL of luminol and H_2O_2 at the anodic poles is monitored using a photomultiplier tube (PMT) or smartphone, and the images are analyzed using ImageJ software. This process triggers thionine reduction at the cathodic poles. Under the optimal conditions obtained by a face-centered central composite design (FCCD), the PMT-based detection of the BPE-ECL aptasensor exhibit a linear response over a wide dynamic range from 5 to 150 ng mL^{-1}, with a detection limit of 0.01 ng mL^{-1}. Additionally, smartphone-based detection shows a linear relationship between the ECL image gray value and the logarithmic concentration of the AFM1 target over a range of 10–200 ng mL^{-1}, with a detection limit of 0.05 ng mL^{-1}.

Wang et al. (2015) nanocomposed rGO with polypyrrole (PPy) and pyrrolepropylic acid (PPa) as a unique sensing platform, in which rGO greatly improves the conductivity and stability, PPa provides covalent linkers for probe immobilization and PPy endows the film electroactivity from its inherent electrochemical doping/dedoping property for impedance measurements, thus significantly improving the sensitivity to detect AFB_1 in a range of 10 fg mL^{-1} to 10 pg mL^{-1} with high specificity and good reproducibility.

Ma et al. (2016) reported a general overview of development situations and application prospects of electrochemical biosensors in aflatoxins detection, focusing on the electrochemical sensing mechanisms, fabrication methods and detection performances. Compared with the traditional methods for detecting aflatoxins, electrochemical biosensors have the advantages of fast, simple, low-cost, easy of miniaturization and so on. The use of gold nanoparticles, carbon nanotubes and other nanomaterials will further increase the sensitivity of the electrochemical biosensors and the immobilization efficiency of the antigens or antibodies.

Karapetis et al. (2016) described a miniaturized potentiometric cholera toxin sensor on graphene nanosheets with incorporated lipid films. Ganglioside GM1, the natural cholera toxin receptor, immobilized on the stabilized lipid films, provided adequate selectivity for detection over a wide range of toxin concentrations, fast response time of ca. 5 min, and detection limit of 1 nM. The proposed sensor is easy to construct and exhibits good reproducibility, reusability, selectivity, long shelf life and high sensitivity of ca. 60 mV/decade of toxin concentration.

Bratakou et al. (2017) described a miniaturized potentiometric saxitoxin sensor on graphene nanosheets with incorporated lipid films and Anti-STX, the natural saxitoxin receptor, immobilized on the stabilized lipid films. An adequate selectivity for detection over a wide range of toxin concentrations, fast response time of ca. 5–20 min, and detection limit of 1 nM have been achieved. The proposed sensor is easy to construct and exhibits good reproducibility, reusability, selectivity, long shelf life and high sensitivity of ca. 60 mV/decade of toxin concentration.

5. Challenges and conclusion

Graphene and its composites have shown great potentials in biosensing (Zhang and Wei, 2016, Qiu et al., 2017, Wang et al., 2017a; Wang and Dai, 2015), but they have following challenges in their technologies : a), the reproducibility, selectivity and stability of the bioelectronics devices based on graphene and its composite materials should be improved. b), the possible toxicity of graphene have been written in the international nanotechnology guidelines. Current challenge will be how to assess and overcome the toxicity of graphene.

This review has highlighted significant advances in functionalized graphene-based biosensors and has offered an overview of the electrochemical sensors developed for sensing biomolecules during the last 4 years. Electrochemical sensors provide a powerful analytical tool for the sensitive, simple, rapid and selective determination of biomolecules, while remaining inexpensive. Additionally, these biosensors are capable of being incorporated into robust, portable, or miniaturized devices, enabling tailoring the detection of biomolecules and toxins for particular applications in clinical and diagnostic fields as biomarkers of several diseases, such as Alzheimer's disease and Parkinson's disease.

References

Abdalhai, M.H., Fernandes, A.M., Xia, X., Musa, A., Ji, J., Sun, X., 2015. J. Agric. Food Chem. 63 (20), 5017–5025.

Abdalla, S., Al-Marzouki, F.M., Al-Ghamdi, A.A., 2017. Braz. J. Phys. 47 (1), 34–41.
Abraham, S., Srivastava, S., Kumar, V., Pandey, S., Rastogi, P.K., Nirala, N.R., Kashyap, S., Srivastava, S.K., Singh, V.N., Ganesan, V., Saxena, P.S., Srivastava, A., 2015. J. Electroanal. Chem. 757, 65–72.
Adhikari, B.R., Govindhan, M., Chen, A., 2015. Sensors 15 (9), 22490–22508.
Afkhami, A., Soltani-Felehgari, F., Madrakian, T., 2014. Talanta 128, 203–210.
Agnihotri, N., Chowdhury, A.D., De, A., 2015. Biosens. Bioelectron. 63, 212–217.
Ahmadraji, T., Killard, A.J., 2016. Anal. Methods 8 (13), 2743–2749.
Ahour, F., Ahsani, M.K., 2016. Biosens. Bioelectron. 86, 764–769.
Ahour, F., Shamsi, A., 2017. Anal. Biochem. 532, 64–71.
Akiba, U., Anzai, J.I., 2016. Sensors 16, 12.
Akter, R., Jeong, B., Choi, J.S., Rahman, M.A., 2016. Biosens. Bioelectron. 80, 123–130.
Alexander, S., Baraneedharan, P., Balasubrahmanyan, S., Ramaprabhu, S., 2017. Eur. Polym. J. 86, 106–116.
Ali Tahir, A., Ullah, H., Sudhagar, P., Asri Mat Teridi, M., Devadoss, A., Sundaram, S., 2016. Chem. Rec. 1591–1634.
Aliakbarinodehi, N., De Micheli, G., Carrara, S., 2015) Optimized electrochemical detection of anti-cancer drug by carbon nanotubes or gold nanoparticles. In: 2015 Proceedings of the 11th Conference on Ph.D. Research in Microelectronics and Electronics, PRIME 2015.
Aliakbarinodehi, N., De Micheli, G., Carrara, S., 2016. Anal. Chem. 88 (19), 9347–9350.
Altuntas, D.B., Tepeli, Y., Anik, U., 2016. Graphene-metallic nanocomposites as modifiers in electrochemical glucose biosensor transducers. 2D Mater. 3, 3.
Amano, Y., Koto, A., Matsuzaki, S., Sakamoto, H., Satomura, T., Suye, S.I., 2016. Mater. Lett. 174, 184–187.
Amatatongchai, M., Sroysee, W., Chairam, S., Nacapricha, D., 2015. Talanta.
Amatatongchai, M., Sroysee, W., Chairam, S., Nacapricha, D., 2017. Talanta 166, 420–427.
Ambrosi, A., Chua, C.K., Latiff, N.M., Loo, A.H., Wong, C.H.A., Eng, A.Y.S., Bonanni, A., Pumera, M., 2016. Chem. Soc. Rev. 45 (9), 2458–2493.
Amjad, M.S., Sadiq, N., Qureshi, H., Fareed, G., Sabir, S., 2015. Asian Pac. J. Trop. Dis. 5 (10), 767–771.
Antonios, K., 2015. Curr. Opin. Coll. Interface Sci. 20, 354–361.
Arduini, F., Cinti, S., Scognamiglio, V., Moscone, D., 2016a. Microchim. Acta 183 (7), 2063–2083.
Arduini, F., Micheli, L., Moscone, D., Palleschi, G., Piermarini, S., Ricci, F., Volpe, G., 2016b. TrAC Trends Anal. Chem. 79, 114–126.
Arkan, E., Saber, R., Karimi, Z., Mostafaie, A., Shamsipur, M., 2014. J. Pharm. Biomed. Anal. 92, 74–81.
Arkan, E., Saber, R., Karimi, Z., Shamsipur, M., 2015. Anal. Chim. Acta 874, 66–74.
Arvand, M., Hemmati, S., 2017. Sens. Actu. B: Chem. 238, 346–356.
Asadian, E., Shahrokhian, S., Iraji Zad, A., Ghorbani-Bidkorbeh, F., 2017. Sens. Actu. B: Chem. 239, 617–627.
Asif, S.A.B., Khan, S.B., Asiri, A.M., 2017. J. Taiwan Instit. Chem. Eng. 74, 255–262.
Aslan, S., Anik, Ü., 2016. Microbial glucose biosensors based on glassy carbon paste electrodes modified with Gluconobacter Oxydans and graphene oxide or graphene-platinum hybrid nanoparticles. Microchim. Acta 183 (1), 73–81.
Aydoğdu Tığ, G., 2017. Talanta 175, 382–389.
Ba Hashwan, S.S., Ruslinda, A.R., Fatin, M.F., Arshad, M.K.M., Hashim, U., 2016. Micro-Technology 1–8.
Ba Hashwan, S.S., Ruslinda, A.R., Fatin, M.F., Arshad, M.K.M., Hashim, U., 2017. Micro-Technology 23 (8), 3421–3428.
Báez, D.F., Bollo, S., 2016. J. Solid State Electrochem. 20 (4), 1059–1064.
Bahadir, E.B., Sezgintürk, M.K., 2016. TrAC – Trends Anal. Chem. 76, 1–14.
Bahrami, S., Abbasi, A.R., Roushani, M., Derikvand, Z., Azadbakht, A., 2016. Talanta 159, 307–316.
Bai, J., Sun, C., Jiang, X., 2016. Anal. Bioanal. Chem. 408 (17), 4705–4714.
Bai, Z., Li, G., Liang, J., Su, J., Zhang, Y., Chen, H., Huang, Y., Sui, W., Zhao, Y., 2016. Biosens. Bioelectron. 82, 185–194.
Bai, Z., Zhou, C., Xu, H., Wang, G., Pang, H., Ma, H., 2017. Polyoxometalates-doped Au nanoparticles and reduced graphene oxide: a new material for the detection of uric acid in urine. Sens. Actuators B: Chem. 243, 361–371.
Balamurugan, J., Thanh, T.D., Kim, N.H., Lee, J.H., 2016. Biosens. Bioelectron. 83, 68–76.
Baldantoni, D., De Nicola, F., Alfani, A., 2014. Atmos. Pollut. Res. 5 (2), 262–269.
Bandodkar, A.J., Jeerapan, I., You, J.M., Nuñez-Flores, R., Wang, J., 2016. Nano Lett. 16 (1), 721–727.
Bao, J., Hou, C., Zhang, Y., Li, Q., Huo, D., Yang, M., Luo, X., 2015. J. Electrochem. Soc. 162 (3), B47–B51.
Bao, S., Du, M., Zhang, M., Zhu, H., Wang, P., Yang, T., Zou, M., 2014. Chem. Eng. J. 258, 281–289.
Baptista-Pires, L., Pérez-López, B., Mayorga-Martinez, C.C., Morales-Narváez, E., Domingo, N., Esplandiu, M.J., Alzina, F., Torres, C.M.S., Merkoçi, A., 2014. Biosens. Bioelectron. 61, 655–662.
Barberis, A., Spissu, Y., Fadda, A., Azara, E., Bazzu, G., Marceddu, S., Angioni, A., Sanna, D., Schirra, M., Serra, P.A., 2015. Biosens. Bioelectron. 67, 214–223.
Barbosa, F.H.F., Menezes, H.C., de Carvalho Teixeira, A.P., Serp, P., Antipoff, V., de Lourdes Cardeal, Z., 2017. Talanta 167, 538–543.
Barsan, M.M., Brett, C.M., 2015. Stud. Univ. Babes-Bolyai Chem. 60 (3), 31–52.
Baryeh, K., Takalkar, S., Lund, M., Liu, G., 2017. Introduction to Medical Biosensors for Point of Care Applications Medical Biosensors for Point of Care (POC) Applications. Woodhead Publishing, pp. 3–25.
Bas, S.Z., 2015. Mater. Lett. 150, 20–23.
Behera, T.K., Sahu, S.C., Satpati, B., Bag, B., Sanjay, K., Jena, B.K., 2016. Electrochim. Acta 206, 238–245.
Beiranvand, S., Abbasi, A.R., Roushani, M., Derikvand, Z., Azadbakht, A., 2016. J. Electroanal. Chem. 776, 170–179.
Beiranvand, Z.S., Abbasi, A.R., Dehdashtian, S., Karimi, Z., Azadbakht, A., 2017. Anal. Biochem. 518, 35–45.
Benítez-Martínez, S., Valcárcel, M., 2015. TrAC – Trends Anal. Chem. 72, 93–113.
Benjamin, M., Manoj, D., Thenmozhi, K., Bhagat, P.R., Saravanakumar, D., Senthilkumar, S., 2017. Biosens. Bioelectron. 91, 380–387.
Benvidi, A., Firouzabadi, A.D., Moshtaghiun, S.M., Mazloum-Ardakani, M., Tezerjani, M.D., 2015. Anal. Biochem. 484, 24–30.
Benvidi, A., Tezerjani, M.D., Jahanbani, S., Mazloum Ardakani, M., Moshtaghioun, S.M., 2016. Talanta 147, 621–627.
Bharath, G., Madhu, R., Chen, S.-M., Veeramani, V., Balamurugan, A., Mangalaraj, D., Viswanathan, C., Ponpandian, N., 2015. J. Mater. Chem. B 3 (7), 1360–1370.
Bilgi, M., Ayranci, E., 2016. Sens. Actuators B: Chem. 237, 849–855.
Bing, X., Wang, G., 2017. Int. J. Electrochem. Sci. 12 (7), 6304–6314.
Bo, X., Zhou, M., Guo, L., 2016. Biosens. Bioelectron. 273, 567–572.
Borisova, B., Sánchez, A., Jiménez-Falcao, S., Martín, M., Salazar, P., Parrado, C., Pingarrón, J.M., Villalonga, R., 2016. Sens. Actuators B: Chem. 232, 84–90.
Borisova, B., Villalonga, M.L., Arévalo-Villena, M., Boujakhrout, A., Sánchez, A., Parrado, C., Pingarrón, J.M., Briones-Pérez, A., Villalonga, R., 2017. Anal. Bioanal. Chem. 1–8.
Boujakhrout, A., Sánchez, E., Díez, P., Sánchez, A., Martínez-Ruiz, P., Parrado, C., Pingarrón, J.M., Villalonga, R., 2015. ChemElectroChem 2 (11), 1735–1741.
Boujakhrout, A., Díez, P., Sánchez, A., Martínez-Ruíz, P., Pingarrón, J.M., Villalonga, R., 2016. J. Colloid Interface Sci. 482, 105–111.
Bratakou, S., Nikoleli, G.P., Siontorou, C.G., Nikolelis, D.P., Karapetis, S., Tzamtzis, N., 2017. Electroanalysis 29 (4), 990–997.
Breczko, J., Regulska, E., Basa, A., Baran, M., Winkler, K., Plonska-Brzezinska, M.E., 2016. ECS J. Solid State Sci. Technol. 5 (8), M3018–M3025.
Buber, E., Yuzer, A., Soylemez, S., Kesik, M., Ince, M., Toppare, L., 2017. Int. J. Biol. Macromole. 96, 61–69.
Cai, B., Huang, L., Zhang, H., Sun, Z., Zhang, Z., Zhang, G.-J., 2015. Biosens. Bioelectron. 74, 329–334.
Campuzano, S., Pedrero, M., Nikoleli, G.P., Pingarrón, J.M., Nikolelis, D.P., 2017. Biosens. Bioelectron. 89, 269–279.
Cao, F., Zhang, L., Tian, Y., 2016. J. Electroanal. Chem. 781, 278–283.
Casalino, M., Coppola, G., De Stefano, L., Caliò, A., Rea, I., Mocella, V., Dardano, P., Romano, S., Rao, S., Rendina, I., 2015. J. Eur. Opt. Soc. 10, 346.
Castrignanò, S., Valetti, F., Gilardi, G., Sadeghi, S.J., 2016. Biotechnol. Appl. Biochem. 63 (2), 157–162.
Celine, I.L., Ana, R., Armando, C.D., Teresa, A.P., 2017. Trends Anal. Chem. 91 (2017), 53e66.
Cernat, A., Tertiş, M., Săndulescu, R., Bedioui, F., Cristea, A., Cristea, C., 2015. Anal. Chim. Acta 886, 16–28.
Chabot, V., Higgins, D., Yu, A., Xiao, X., Chen, Z., Zhang, J., 2014. Energy Environ. Sci. 7 (5), 1564–1596.
Chang, J., Mao, S., Zhang, Y., Cui, S., Steeber, D.A., Chen, J., 2013. Biosens. Bioelectron. 42 (1), 186–192.
Chatterjee, J., Cardenal, J., Shellikeri, A., 2015. J. Biomed. Nanotechnol. 11 (1), 150–156.
Chauhan, N., Narang, J., Jain, U., 2015. Analyst 140 (6), 1988–1994.
Chauhan, N., Chawla, S., Pundir, C.S., Jain, U., 2017. Biosens. Bioelectron. 89, 377–383.
Chen, C., Hong, X., Xu, T., Chen, A., Lu, L., Gao, Y., 2016. Synth. Met. 212, 123–130.
Chen, G., Liu, Y., Liu, Y., Tian, Y., Zhang, X., 2015. J. Electroanal. Chem. 738, 100–107.
Chen, M., Hou, C., Huo, D., Bao, J., Fa, H., Shen, C., 2016a. Biosens. Bioelectron. 85, 684–691.
Chen, M., Hou, C., Huo, D., Fa, H., Zhao, Y., Shen, C., 2017. Sens. Actuators B: Chem. 239, 421–429.
Chen, X., Yan, H., Shi, Z., Feng, Y., Li, J., Lin, Q., Wang, X., Sun, W., 2017. Polym. Bull. 74 (1), 75–90.
Chen, Y., Tan, C., Zhang, H., Wang, L., 2015. Chem. Soc. Rev. 44 (9), 2681–2701.
Chen, Y., Li, Y., Yang, Y., Wu, F., Cao, J., Bai, L., 2017a. Microchim. Acta 184 (6), 1801–1808.
Chen, Y., Zhou, S., Li, L., Zhu, J.-j., 2017b. Nano Today 12, 98–115.
Cheng, H., Lai, G., Fu, L., Zhang, H., Yu, A., 2015. Biosens. Bioelectron. 71, 353–358.
Chia, J.S.Y., Tan, M.T.T., Khiew, P.S., Chin, J.K., Siong, C.W., 2015. Sens. Actuators B: Chem. l 210, 558–565.
Chiang Lin, K., Yu Lai, S., Ming Chen, S., 2014. Analyst 139 (16), 3991–3998.
Chinnappan, A., Baskar, C., Kim, H., Ramakrishna, S., 2016. J. Mater. Chem. A 4 (24), 9347–9361.
Church, J., Wang, X., Calderon, J., Lee, W.H., Cho, H.J., Zhai, L., 2016. J. Nanosci. Nanotechnol. 16 (2), 1620–1623.
Cinti, S., Arduini, F., 2016. Biosens. Bioelectron.
Correa, D.S., Pavinatto, A., Mercante, L.A., Mattoso, L.H.C., Oliveira, J.E., Riul Jr, A., 2017. Chemical Sensors Based on Hybrid Nanomaterials for Food Analysis A2 - Grumezescu. Academic Press, Alexandru Mihai. Nanobiosensors, pp. 205–244.
Cui, H.F., Wu, W.W., Li, M.M., Song, X., Lv, Y., Zhang, T.T., 2018a. Biosens. Bioelectron. 99, 223–229.
Cui, L., Wu, J., Li, J., Ge, Y., Ju, H., 2014. Biosens. Bioelectron. 55, 272–277.
Cui, L., Wu, J., Ju, H., 2015. Biosens. Bioelectron. 63, 276–286.
Cui, L., Li, Y., Lu, M., Tang, B., Zhang, C.-y., 2018b. Biosens. Bioelectron. 99, 1–7.
Cui, X., Liu, J., Yang, A., Fang, X., Xiao, C., Zhao, H., Ren, H., Li, Z., 2017. Colloids Surf. A: Physicochem. Eng. Asp. 520, 668–675.
Dagar, K., Pundir, C.S., 2017. Enzym. Microb. Technol. 96, 177–186.
Dago, A., Navarro, J., Ariño, C., Díaz-Cruz, J.M., Esteban, M., 2015. J. Chromatrogr. A 1409, 210–217.
Dahal, D., Gumbs, G., 2017. J. Phys. Chem. Solids 100, 83–91.
Dalkıran, B., Erden, P.E., KılıÃ§, E., 2016. Anal. Bioanal. Chem. 408 (16), 4329–4339.
Dalkıran, B., Erden, P.E., Kılıç, E., 2017a. Artif. Cells Nanomed. Biotechnol. 45 (2), 340–348.

Dalkıran, B., Esra Erden, P., Kılıç, E., 2017b. Talanta 167, 286–295.
Dar, R.A., Naikoo, G.A., Kalambate, P.K., Giri, L., Khan, F., Karna, S.P., Srivastava, A.K., 2015. Electrochim. Acta 163, 196–203.
David, M., Barsan, M.M., Florescu, M., Brett, C.M.A., 2015. Electroanalysis 27 (9), 2139–2149.
Deb, A.K., Das, S.C., Saha, A., Wayu, M.B., Hensley Marksberry, M., Baltz, R.J., Chusuei, C.C., 2016. J. Appl. Electrochem. 46 (3), 289–298.
Del Valle, M., Bonanni, A., 2014. Biosens. Nanotechnol. 81–110.
Deng, W., Liu, F., Ge, S., Yu, J., Yan, M., Song, X., 2014. Analyst 139 (7), 1713–1720.
Deng, Y., Zhang, M., Yuan, F., Li, Z., Zhou, W., 2016. Nano 11, 5.
Dervisevic, M., Dervisevic, E., Şenel, M., 2018. Sens. Actuators B: Chem. 254, 93–101.
Devasenathipathy, R., Mani, V., Chen, S.M., Huang, S.T., Huang, T.T., Lin, C.M., Hwa, K.Y., Chen, T.Y., Chen, B.J., 2015. Enzym. Microb. Technol. 78, 40–45.
Dezfuli, A.S., Ganjali, M.R., Naderi, H.R., 2017. Appl. Surf. Sci. 402, 245–253.
Dhull, V., Dilbaghi, N., Hooda, V., 2015. Inter. J. Pharm. Pharm. l Sci. 7 (2), 17–24.
Ding, J., Guo, Y., Jia, H., Qiao, L., Sun, X., Wang, X., 2014. Sens. Transducer J. 172 (6), 27–33.
Dong, J., Zhao, H., Qiao, F., Liu, P., Wang, X., Ai, S., 2013. Anal. Methods 5 (11), 2866–2872.
Dridi, F., Marrakchi, M., Gargouri, M., Saulnier, J., Jaffrezic-Renault, N., Lagarde, F., 2017. Nanomaterial-based Electrochemical Biosensors for Food Safety and Quality Assessment A2 - Grumezescu. Academic Press, Alexandru Mihai. Nanobiosensors, pp. 167–204.
Du, X., Jiang, D., Chen, S., Dai, L., Zhou, L., Hao, N., You, T., Mao, H., Wang, K., 2017. Biosens. Bioelectron. 89, 681–688.
Duffy, G.F., Moore, E.J., 2017. Anal. Lett. 50 (1), 1–32.
Eftekhari-Sis, B., Aliabad, M.A., Karimi, F., 2016. Mater. Lett. 183, 441–443.
Eguílaz, M., Gutiérrez, A., Rivas, G., 2016a. Sens. Actuators B: Chem. 225, 74–80.
Eguílaz, M., Gutierrez, F., González-Domínguez, J.M., Martínez, M.T., Rivas, G., 2016b. Biosens. Bioelectron. 86, 308–314.
Eguílaz, M., Venegas, C.J., Gutiérrez, A., Rivas, G.A., Bollo, S., 2016c. Microchem. J. 128, 161–165.
Eivazzadeh-Keihan, R., Pashazadeh, P., Hejazi, M., de la Guardia, M., Mokhtarzadeh, A., 2017. TrAC Trends Anal. Chem. 87, 112–128.
Ertek, B., Dilgin, Y., 2016. Bioelectrochemistry 112, 138–144.
Fan, X., Chen, X., Dai, L., 2015. Curr. Opin. Colloid Interface Sci. 20 (5–6), 429–438.
Fan, Z., Li, S., Yuan, F., Fan, L., 2015a. RSC Adv. 5 (25), 19773–19789.
Fan, Z., Lin, Q., Gong, P., Liu, B., Wang, J., Yang, S., 2015b. Electrochim. Acta 151, 186–194.
Farka, Z., Jurík, T., Kovář, D., Trnková, L., Skládal, P., 2017. Chem. Rev. 117 (15), 9973–10042.
Fedorovskaya, E.O., Bulusheva, L.G., Kurenya, A.G., Asanov, I.P., Rudina, N.A., Funtov, K.O., Lyubutin, I.S., Okotrub, A.V., 2014. Electrochim. Acta 139 (0), 165–172.
Feng, D., Li, L., Fang, X., Han, X., Zhang, Y., 2014. Electrochim. Acta 127, 334–341.
Feng, X., Gan, N., Zhang, H., Yan, Q., Li, T., Cao, Y., Hu, F., Yu, H., Jiang, Q., 2015. Electrochim. Acta 170, 292–299.
Fenzl, C., Hirsch, T., Baeumner, A.J., 2016. Nanomaterials as versatile tools for signal amplification in (bio)analytical applications. TrAC Trends Anal. Chem. 79, 306–316.
Fu, L., Zheng, Y., Wang, A., Cai, W., Deng, B., Zhang, Z., 2016. Arab. J. Sci. Eng. 41 (1), 135–141.
Gai, P.P., Zhao, C.E., Wang, Y., Abdel-Halim, E.S., Zhang, J.R., Zhu, J.J., 2014. Biosens. Bioelectron. 62, 170–176.
Gan, X., Zhao, H., 2015. Sens. Mater. 27 (2), 191–215.
Gao, N., Gao, F., He, S., Zhu, Q., Huang, J., Tanaka, H., Wang, Q., 2017. Anal. Chim. Acta 951, 58–67.
Gao, W., Tjiu, W.W., Wei, J., Liu, T., 2014. Talanta 120 (0), 484–490.
Ge, S., Lan, F., Yu, F., Yu, J., 2015. New J. Chem. 39 (4), 2380–2395.
Ghorbani-Bidkorbeh, F., 2015. Iran. J. Pharm. Res. 14 (3), 663–664.
Ghosh*, S., Gupta, B., Ganesan, K., Das, A., Kamruddin, M., Dash, D., Tyagi, A.K., 2016. Mater.- Today-Proc. 3, 1686–1692.
Gokoglan, T.C., Kesik, M., Soylemez, S., Yuksel, R., Unalan, H.E., Toppare, L., 2017. J. Electrochem. Soc. 164 (6), G59–G64.
Gong, Q., Wang, Y., Yang, H., 2017. Biosens. Bioelectron. 89, 565–569.
Goryacheva, I.Y., Speranskaya, E.S., Goftman, V.V., Tang, D., De Saeger, S., 2015. TrAC - Trends Anal. Chem. 66, 53–62.
Govindasamy, M., Mani, V., Chen, S.M., Karthik, R., Manibalan, K., Umamaheswari, R., 2016. Int. J. Electrochem. Sci. 11 (4), 2954–2961.
Govindhan, M., Amiri, M., Chen, A., 2015. Biosens. Bioelectron. 66, 474–480.
Green, N.S., Norton, M.L., 2015. Anal. Chim. Acta 853 (1), 127–142.
Gu, C.J., Kong, F.Y., Chen, Z.D., Fan, D.H., Fang, H.L., Wang, W., 2016. Biosens. Bioelectron. 78, 300–307.
Guler, M., Turkoglu, V., Basi, Z., 2017. Electrochim. Acta 240, 129–135.
Güner, A., Çevik, E., Şenel, M., Alpsoy, L., 2017. Food Chem. 229, 358–365.
Guo, J., Han, X., Wang, J., Zhao, J., Guo, Z., Zhang, Y., 2015. Anal. Biochem. 491, 58–64.
Guo, X.M., Guo, B., Li, C., Wang, Y.L., 2016. J. Electroanal. Chem. 783, 8–14.
Guy, O.J., Walker, K.A.D., 2016. Graphene Functionalization for Biosensor Applications. Silicon Carbide Biotechnology: A Biocompatible Semiconductor for Advanced Biomedical Devices and Applications: Second Edition, pp. 85–141.
Han, H.S., Lee, H.K., You, J.M., Jeong, H., Jeon, S., 2014. Sens. Actuators B: Chem. 190, 886–895.
Han, J., Li, Y., Feng, J., Li, M., Wang, P., Chen, Z., Dong, Y., 2017. J. Electroanal. Chem. 786, 112–119.
Han, S., Du, T., Jiang, H., Wang, X., 2015. Biosens. Bioelectron.
Han, Y., Chabu, J.M., Hu, S., Deng, L., Liu, Y.N., Guo, S., 2015. Chem. Eur. J. 21 (37), 13045–13051.
Hao, N., Jiang, L., Qian, J., Wang, K., 2016. J. Electroanal. Chem. 781, 332–338.
Hasanzadeh, M., Shadjou, N., Lin, Y., de la Guardia, M., 2017. TrAC - Trends Anal. Chem. 86, 185–205.
Hayat, A., Haider, W., Raza, Y., Marty, J.L., 2015. Talanta 143, 157–161.
He, J., Sunarso, J., Zhu, Y., Zhong, Y., Miao, J., Zhou, W., Shao, Z., 2017. Sens. Actuators B: Chem. 244, 482–491.
Holzinger, M., Goff, A.L., Cosnier, S., 2014. Front. Chem. 2.
Hong, S.G., Kim, J.H., Kim, R.E., Kwon, S.J., Kim, D.W., Jung, H.T., Dordick, J.S., Kim, J., 2016. Biotechnol. Bioprocess Eng. 21 (4), 573–579.
Hossain, M.F., Park, J.Y., 2016a. RSC Adv. 6 (78), 74453–74461.
Hossain, M.F., Park, J.Y., 2016b. Sci. Rep. 6.
Hossain, M.F., Heo, M., Shin, J.H., Park, J.Y., 2015. Int. J. Electrochem. Sci. 10 (8), 6803–6819.
Hou, W., Xingzhong, Y., Guangming, Z., YanWuc, Y., Qian, J., Shansi, G., 2015. Adv. Colloids Interface Sci. 221, 41–49.
Hu, S., Ouyang, W., Guo, L., Lin, Z., Jiang, X., Qiu, B., Chen, G., 2017. Biosens. Bioelectron. 92, 718–723.
Huan, J., Liu, Q., Fei, A., Qian, J., Dong, X., Qiu, B., Mao, H., Wang, K., 2015. Biosens. Bioelectron. 73, 221–227.
Huang, J., Tian, J., Zhao, Y., Zhao, S., 2015. Sens. Actuators B: Chem. 206, 570–576.
Huang, J., Chen, H., Jing, L., Fam, D., Tok, A.I.Y., 2016. Biomed. Microdevices 18 (4).
Huang, W., Hao, Q., Lei, W., Wu, L., Xia, X., 2015. Mater. Res. Expr. 1 (4).
Hughes, G., Pemberton, R.M., Fielden, P.R., Hart, J.P., 2017. Methods Mol. Biol. 1572, 1–12.
Hui, Y., Ma, X., Hou, X., Chen, F., Yu, J., 2015. Ionics 21 (6), 1751–1759.
Jain, U., Chauhan, N., 2017. Biosens. Bioelectron. 89, 578–584.
Jakubus, A., Paszkiewicz, M., Stepnowski, P., 2017. Crit. Rev. Anal. Chem. 47 (1), 76–91.
Jamil, A., Lim, H.N., Yusof, N.A., Tajudin, A.A., Huang, N.M., Pandikumar, A., Golsheikh, A.M., Lee, Y.H., Andou, Y., 2015. Sens. Actuators B: Chem. 221, 1423–1432.
Jariwala, D., Sangwan, V.K., Lauhon, L.J., Marks, T.J., Hersam, M.C., 2013. Chem. Soc. Rev. 42 (7), 2824–2860.
Ji, Xuqiang, Xu, Yuanhong, Zhang, Wenling, Cui, Liang, Liu, J., 2016. Composites 87, 29–45.
Jian, W., Wang, C., Chen, Z., Yu, Y., Sun, D., Han, L., Shi, L., 2016. Nano 11 (10).
Jiang, B., Zhou, K., Wang, C., Sun, Q., Yin, G., Tai, Z., Wilson, K., Zhao, J., Zhang, L., 2018. Sens. Actuators B: Chem. 254, 1033–1039.
Joo, M., Baek, S.H., Cheon, S.A., Chun, H.S., Choi, S.-W., Park, T.J., 2017. Colloids Surf. B: Biointerfaces 154, 27–32.
Justino, C.I.L., Gomes, A.R., Freitas, A.C., Duarte, A.C., Rocha-Santos, T.A.P., 2017. TrAC - Trends Anal. Chem. 91, 53–66.
Kakatkar, A., Abhilash, T.S., De Alba, R., Parpia, J.M., Craighead, H.G., 2015. Nanotechnol 26 (12).
Kakhki, S., Barsan, M.M., Shams, E., Brett, C.M.A., 2013. Anal. Methods 5 (5), 1199–1204.
Kangkamano, T., Numnuam, A., Limbut, W., Kanatharana, P., Thavarungkul, P., 2017. Sens. Actuators B: Chem. 246, 854–863.
Karapetis, S., Nikoleli, G.P., Siontorou, C.G., Nikolelis, D.P., Tzamtzis, N., Psaroudakis, N., 2016. Electroanalysis 28 (7), 1584–1590.
Kazemi, S.H., Ghodsi, E., Abdollahi, S., Nadri, S., 2016. Mater. Sci. Eng. 69, 447–452.
Khoshfetrat, S.M., Bagheri, H., Mehrgardi, M.A., 2018. Biosens. Bioelectron. 100, 382–388.
Kim, J.H., Hong, S.G., Wee, Y., Hu, S., Kwon, Y., Ha, S., Kim, J., 2017. Biosens. Bioelectron. 87, 365–372.
Komathi, S., Muthuchamy, N., Lee, K.P., Gopalan, A.I., 2016. Biosens. Bioelectron. 84, 64–71.
Komori, K., Terse-Thakoor, T., Mulchandani, A., 2016. Bioelectrochemistry 111, 57–61.
Kong, B., Liu, W., Li, Q., Chen, L., Liu, X., Zhou, J., 2015. Sens. Lett. 13 (4), 267–272.
Kong, F.-Y., Li, W.-W., Wang, J.-Y., Fang, H.-L., Fan, D.-H., Wang, W., 2015. Anal. Chim. Acta 884, 37–43.
Kong, L., Du, Z., Xie, Z., Chen, R., Jia, S., Dong, R., Sun, Z., Sun, W., 2017. Inter. J. Electrochem. Sci. 12 (3), 2297–2305.
Krzyczmonik, P., Socha, E., Skrzypek, S., 2015. Bioelectrochemistry 101 (0), 8–13.
Kulkarni, T., Slaughter, G., 2017. Self-powered Glucose Biosensor Operating under Physiological Conditions.
Kurbanoglu, S., Ozkan, S.A., Merkoçi, A., 2017a. Biosens. Bioelectron. 89 (Part 2), 886–898.
Kurbanoglu, S., Rivas, L., Ozkan, S.A., Merkoçi, A., 2017b. Biosens. Bioelectron. 88, 122–129.
Lakshmi, G.B.V.S., Sharma, A., Solanki, P.R., Avasthi, D.K., 2016. Nanotechnology 27 (34).
Lebedev, A.A., Davydov, V.Y., Novikov, S.N., Litvin, D.P., Makarov, Y.N., Klimovich, V.B., Samoilovich, M.P., 2016. Tech. Phys. Lett. 42 (7), 729–732.
Lee, J., Kim, J., Kim, S., Min, D.-H., 2017. Adv. Drug Deliv. Rev.
Lee, S.W., Lee, K.Y., Song, Y.W., Choi, W.K., Chang, J., Yi, H., 2016. Adv. Mater. 28 (8), 1577–1584.
Lei, W., Wu, L., Huang, W., Hao, Q., Zhang, Y., Xia, X., 2014. J. Mater. Chem. B 2 (27), 4324–4330.
Li, C., Zhang, H., Wu, P., Gong, Z., Xu, G., Cai, C., 2011. Analyst 136 (6), 1116–1123.
Li, J., Jiang, Y., Zhai, Y., Liu, H., Li, L., 2015. Anal. Lett. 48 (17), 2786–2798.
Li, M., Wang, P., Li, F., Chu, Q., Li, Y., Dong, Y., 2017. Biosens. Bioelectron. 87, 752–759.
Li, Q., Kang, C., Li, K., Chen, A., Zhang, W., Zhao, Y.S., 2017a. Sci. China Chem. 60 (5), 642–648.
Li, Q., Wang, Q., Yang, X., Wang, K., Zhang, H., Nie, W., 2017b. Talanta 174, 521–526.
Li, S.M., Wang, Y.S., Hsiao, S.T., Liao, W.H., Lin, C.W., Yang, S.Y., Tien, H.W., Ma, C.C.M., Hu, C.C., 2015. J. Mater. Chem. C 3 (36), 9444–9453.
Li, X., Zhao, T., Sun, L., Aifantis, K.E., Fan, Y., Feng, Q., Cui, F., Watari, F., 2016. J. Biomed. Mater. Res. - Part A 104 (1), 322–339.

Li, Y., Zhang, Y., Han, J., Chu, P.K., Feng, J., Dong, Y., 2017. RSC Adv. 7 (4), 2242–2248.
Li, Z., Su, W., Liu, S., Ding, X., 2015a. Biosens. Bioelectron. 69, 287–293.
Li, Z., Xie, C., Wang, J., Meng, A., Zhang, F., 2015b. Sens. Actuators B: Chem. 208, 505–511.
Li, Z., Zhang, W., Guo, J., Yang, B., Yuan, J., 2015c. Vacuum 117, 35–39.
Li, Z.J., Yang, B.C., Lv, X.W., Li, Y.C., Wang, L., 2016. Appl. Surf. Sci. 370, 508–513.
Liang, B., Guo, X., Fang, L., Hu, Y., Yang, G., Zhu, Q., Wei, J., Ye, X., 2015. Electrochem. Commun. 50, 1–5.
Liepmann, D., Aran, K., Ajayan, P.M., Viswanathan, S., Li, P., Renugopalakrishnan, V., 2015. Graphene protein field effect biomedical sensor for glucose measurements. Materials Research Society Symposium Proceedings.
Lim, S.A., Ahmed, M.U., 2016. RSC Adv. 6 (30), 24995–25014.
Lin, X., Ni, Y., Pei, X., Kokot, S., 2017. Anal. Methods 9 (7), 1105–1111.
Lin, Y., Li, L., Hu, L., Liu, K., Xu, Y., 2014. Sens. Actuators B: Chem. 202, 527–535.
Liu, H., Chen, X., Su, X., Duan, C., Guo, K., Zhu, Z., 2015. J. Electrochem. Soc. 162 (12), B312–B318.
Liu, H., Guo, K., Duan, C., Dong, X., Gao, J., 2017. Biosens. Bioelectron. 87, 473–479.
Liu, J., Wang, X., Wang, T., Li, D., Xi, F., Wang, J., Wang, E., 2014. ACS Appl. Mater. Interfaces 6 (22), 19997–20002.
Liu, J., Bo, X., Zhao, Z., Guo, L., 2015a. Biosens. Bioelectron. 74, 71–77.
Liu, K., Dong, H., Deng, Y., 2016. J. Nanosci. Nanotechnol. 16 (7), 6648–6656.
Liu, N., Nie, D., Tan, Y., Zhao, Z., Liao, Y., Wang, H., Sun, C., Wu, A., 2017. Microchim. Acta 184 (1), 147–153.
Liu, S., Zheng, Y., Qiao, K., Su, L., Sanghera, A., Song, W., Yue, L., Sun, Y., 2015. J. Nano Res. 17 (12), 1–13.
Liu, S., Lai, G., Zhang, H., Yu, A., 2017. Microchim. Acta 184 (5), 1445–1451.
Liu, W., Ma, Y., Sun, G., Wang, S., Deng, J., Wei, H., 2017. Biosens. Bioelectron. 92, 305–312.
Liu, Y., Wang, G., Li, C., Zhou, Q., Wang, M., Yang, L., 2014. Mater. Sci. Eng.: C 35, 253–258.
Liu, Y., Han, Y., Chen, R., Zhang, H., Liu, S., Liang, F., 2016a. PLoS One 11 (7).
Liu, Y., Zhang, X., He, D., Ma, F., Fu, Q., Hu, Y., 2016b. RSC Adv. 6 (22), 18654–18661.
Liu, Y., Deng, Y., Dong, H., Liu, K., He, N., 2017a. Sci. China Chem. 60 (3), 329–337.
Liu, Y., Liu, X., Guo, Z., Hu, Z., Xue, Z., Lu, X., 2017b. Biosens. Bioelectron. 87, 101–107.
Long, Q., Li, H., Zhang, Y., Yao, S., 2015. Biosens. Bioelectron. 68, 168–174.
Loo, A.H., Bonanni, A., Pumera, M., 2015. ChemElectroChem 2 (5), 743–747.
Lorencova, L., Bertok, T., Dosekova, E., Holazova, A., Paprckova, D., Vikartovska, A., Sasinkova, V., Filip, J., Kasak, P., Jerigova, M., Velic, D., Mahmoud, K.A., Tkac, J., 2017. Electrochim. Acta 235, 471–479.
Lou, J., Liu, S., Tu, W., Dai, Z., 2015. Anal. Chem. 87 (2), 1145–1151.
Low, S.S., Tan, M.T.T., Khiew, P.S., Loh, H.S., Chiu, W.S., 2015. Mater. Tehnol. 49 (5), 837–840.
Lu, L., Li, W., Zhou, L., Zhang, Y., Zhang, Z., Chen, Y., Liu, J., Liu, L., Chen, W., Zhang, Y., 2016a. Electrochim. Acta 219, 463–469.
Lu, L., Seenivasan, R., Wang, Y.-C., Yu, J.-H., Gunasekaran, S., 2016b. Electrochim. Acta 213 (Supplement C), S89–S97.
Luo, B., Li, X., Yang, J., Li, X., Xue, L., Li, X., Gu, J., Wang, M., Jiang, L., 2014. Anal. Methods 6 (4), 1114–1120.
Luong, J.H.T., Glennon, J.D., Gedanken, A., Vashist, S.K., 2017. Microchim. Acta 184 (2), 369–388.
Lv, L., Li, D., Cui, C., Zhao, Y., Guo, Z., 2017. Biosens. Bioelectron. 87, 136–141.
Ma, H., Zhang, Y., Zhen, T., Sun, J., Xia, S., 2016. J. Chin. Cereals Oils Assoc. 31 (2), 132–140.
Ma, Y., Shen, X.L., Zeng, Q., Wang, H.S., Wang, L.S., 2017. Talanta 164, 121–127.
Macwan, I., Khan, M.D.H., Aphale, A., Singh, S., Liu, J., Hingorani, M., Patra, P., 2017. Biosens. Bioelectron. 89, 326–333.
Majumder, T., Mondal, S.P., 2016. J. Electroanal. Chem. 769, 48–52.
Malhotra, B.D., Srivastava, S., Ali, M.A., Singh, C., 2014. Appl. Biochem. Biotechnol. 174 (3), 880–896.
Malhotra, B.D., Srivastava, S., Augustine, S., 2015. Biosensors for food toxin detection: Carbon nanotubes and graphene. Materials Research Society Symposium Proceedings.
Mani, V., Dinesh, B., Chen, S.M., Saraswathi, R., 2014. Biosens. Bioelectron. 53, 420–427.
Manna, B., Retna Raj, C., 2016. J. Mater. Chem. B 4 (26), 4585–4593.
Mao, H., Ji, C., Liu, M., Sun, Y., Liu, D., Wu, S., Zhang, Y., Song, X.M., 2016. RSC Adv. 6 (113), 111632–111639.
Mazaheri, M., Aashuri, H., Simchi, A., 2017. Sens. Actuators B: Chem. 251, 462–471.
Mehmeti, E., Stanković, D.M., Chaiyo, S., Zavasnik, J., Žagar, K., Kalcher, K., 2017. Microchim. Acta 184 (4), 1127–1134.
Mehrotra, P., 2016. J. Oral Biol. Craniofacial Res. 6 (2), 153–159.
Mehta, J., Vinayak, P., Tuteja, S.K., Chhabra, V.A., Bhardwaj, N., Paul, A.K., Kim, K.H., Deep, A., 2016. Biosens. Bioelectron. 83, 339–346.
Meng, L., Xia, Y., Liu, W., Zhang, L., Zou, P., Zhang, Y., 2015. Electrochim. Acta 152, 330–337.
Mercante, L.A., Facure, M.H.M., Sanfelice, R.C., Migliorini, F.L., Mattoso, L.H.C., Correa, D.S., 2017. Appl. Surf. Sci. 407, 162–170.
Metters, J.P., Banks, C.E., 2016. Electrochemical Strategies in Detection Science. The Royal Society of Chemistry, pp. 229–278.
Mijowska, E., Onyszko, M., Urbas, K., Aleksandrzak, M., Shi, X., Moszyński, D., Penkala, K., Podolski, J., El Fray, M., 2015. Appl. Surf. Sci. 355, 587–592.
Mikmeková, E., Frank, L., Müllerová, I., Li, B.W., Ruoff, R.S., Lejeune, M., 2016. Diam. Relat. Mater. 63, 136–142.
Mishraa, R., Nawazb, M.H., Hayatb, Akhtar, Nawazb, Muhammad Azhar Hayat, Sharmac, Vinay, Martya, J.-L., 2017. Sens. Actuators-B-Chem. 247, 366–373.
Mogha, N.K., Sahu, V., Sharma, M., Sharma, R.K., Masram, D.T., 2016. Mater. Des. 111, 312–320.
Moghaddam, H.M., Beitollahi, H., Dehghannoudeh, G., Forootanfar, H., 2017. J. Electrochem. Soc. 164 (7), B372–B376.
Mohammad-Rezaei, R., Razmi, H., 2016. Sens. Lett. 14 (7), 685–691.
Morales-Narváez, E., Sgobbi, L.F., Machado, S.A.S., Merkoçi, A., 2017. Prog. Mater. Sci. 86, 1–24.
Muthuchamy, N., Lee, K.P., Gopalan, A.I., 2017. Biosens. Bioelectron. 89, 390–399.
Muthukumaran, P., Sumathi, C., Wilson, J., Ravi, G., 2016. RSC Adv. 6 (99), 96467–96478.
Mutyala, S., Mathiyarasu, J., 2016. Mater. Sci. Eng. C 69, 398–406.
Naghib, S.M., 2016. Anal. Bioanal. Electrochem. 8 (4), 453–465.
Nanda, S.S., Papaefthymiou, G.C., Yi, D.K., 2015. Crit. Rev. Solid State Mater. Sci. 40 (5), 291–315.
Nandini, S., Nalini, S., Reddy, M.B.M., Suresh, G.S., Melo, J.S., Niranjana, P., Sanetuntikul, J., Shanmugam, S., 2016. Bioelectrochemistry 110, 79–90.
Nayak, P., Santhosh, P.N., Ramaprabhu, S., 2015. J. Nanosci. Nanotechnol. 15 (7), 4855–4862.
Nguyen, K.T., Zhao, Y., 2014. Nanoscale 6 (12), 6245–6266.
Nirala, N.R., Abraham, S., Kumar, V., Bansal, A., Srivastava, A., Saxena, P.S., 2015. Sens. Actuators B: Chem. 218, 42–50.
Noremberg, B.S., Silva, R.M., Paniz, O.G., Alano, J.H., Gonçalves, M.R.F., Wolke, S.I., Labidi, J., Valentini, A., Carreño, N.L.V., 2017. Sens. Actuators B: Chem. 240, 459–467.
Osikoya, A.O., Parlak, O., Murugan, N.A., Dikio, E.D., Moloto, H., Uzun, L., Turner, A.P.F., Tiwari, A., 2016. Biosens. Bioelectron.
Özcan, B., Sezgintürk, M.K., 2016. Talanta 160, 367–374.
Pacheco, J.G., Barroso, M.F., Nouws, H.P.A., Morais, S., Delerue-Matos, C., 2017. Biosensors A2 - Larroche, Christian. current developments. In: Sanromán, M.Á., Du, G., Pandey, A. (Eds.), Biotechnology and Bioengineering. Elsevier, pp. 627–648.
Pakapongpan, S., Poo-arporn, R.P., 2017. Mater. Sci. Engin.: C 76, 398–405.
Palanisamy, S., Devasenathipathy, R., Chen, S.M., Ajmal Ali, M., Karuppiah, C., Balakumar, V., Prakash, P., Elshikh, M.S., Al-Hemaid, F.M.A., 2015. Electroanalysis 27 (10), 2412–2420.
Pan, L.H., Kuo, S.H., Lin, T.Y., Lin, C.W., Fang, P.Y., Yang, H.W., 2017. Biosens. Bioelectron. 89, 598–605.
Paredes, J.I., Villar-Rodil, S., 2016. Nanoscale 8 (34), 15389–15413.
Park, B., Park, H.G., Ji, J.H., Cho, J., Jun, S.C., 2016. Micromachines 7 (8).
Park, C.S., Yoon, H., Kwon, O.S., 2016. J. Ind. Eng. Chem. 38, 13–22.
Park, J.W., Lee, C., Jang, J., 2015. Sens. Actuators B: Chem. 208, 532–537.
Paul, K.B., Singh, V., Vanjari, S.R.K., Singh, S.G., 2017. Biosens. Bioelectron. 88, 144–152.
Pepłowski, A., Janczak, D., Jakubowska, M., 2015. Stabilization of glucose-oxidase in the graphene paste for screen-printed glucose biosensor. Proceedings of SPIE - The International Society for Optical Engineering.
Perreault, F., Fonseca, A., de Faria, Elimelech, M., 2015. Chem. Soc. Rev. 44 (16), 5861–5896.
Pezard, J., Lazar, M., Haddour, N., Botella, C., Roy, P., Brubach, J.B., Wysocka, D., Vilquin, B., Romeo, P.R., Buret, F., 2015. Thin Solid Films.
Piro, B., Shi, S., Reisberg, S., Noël, V., Anquetin, G., 2016. Biosensors 6 (1), 3.
Pittori, M., Santonicola, M.G., Ortolani, L., Gentili, D., Morandi, V., Rizzoli, R., 2015. Graphene-lipids interaction: Towards the fabrication of a novel sensor for biomedical uses. IEEE-NANO 2015 - Proceedings of the 15th International Conference on Nanotechnology.
Pur, M.R.K., Hosseini, M., Faridbod, F., Dezfuli, A.S., Ganjali, M.R., 2016. Anal. Bioanal. Chem. 1–10.
Qi, M., Zhang, Y., Cao, C., Lu, Y., Liu, G., 2016. RSC Adv. 6 (45), 39180–39187.
Qin, Y., Cui, J., Zhang, Y., Wang, Y., Zhang, X., Zheng, H., Shu, X., Fu, B., Wu, Y., 2016. Sci. Bull. 1–8.
Qiu, H.-J., Guan, Y., Luo, P., Wang, Y., 2017. Biosens. Bioelectron. 89 (Part 1), 85–95.
Qu, F., Ma, X., Hui, Y., Hou, X., Yu, J., Zhang, Q., Chen, F., 2015. J. Electrochem. Soc. 162 (1), B27–B35.
Qu, F., Ma, X., Hui, Y., Chen, F., Gao, Y., Chen, Y., 2017. J. Solid State Electrochem. 21 (6), 1545–1557.
Rabti, A., Argoubi, W., Raouafi, N., 2016. Microchim. Acta 183 (3), 1227–1233.
Radhakrishnan, S., Kim, S.J., 2015. RSC Adv. 5 (17), 12937–12943.
Rafighi, P., Tavahodi, M., Haghighi, B., 2016. Sens. Actuators B: Chem. 232, 454–461.
Raicopol, M., Vlsceanu, I., Lupulescu, I., Brezoiu, A.M., Pilan, L., 2016. UPB Sci. Bull. Ser. B: Chem. Mater. Sci. 78 (2), 131–142.
Ramakrishnan, S., Pradeep, K.R., Raghul, A., Senthilkumar, R., Rangarajan, M., Kothurkar, N.K., 2015. Anal. Methods 7 (2), 779–786.
Rashid, M.H.O., Triani, G., Scales, N., in het Panhuis, M., Nghiem, L.D., Ralph, S.F., 2017. J. Memb. Sci. 529, 23–34.
Ravenna, Y., Xia, L., Gun, J., Mikhaylov, A.A., Medvedev, A.G., Lev, O., Alfonta, L., 2015. Anal. Chem. 87 (19), 9567–9571.
Reina, G., Tamburri, E., Orlanducci, S., Gay, S., Matassa, R., Guglielmotti, V., Lavecchia, T., Terranova, M.L., Rossi, M., 2014. BioMatter 4 (3).
Ren, Q., Feng, L., Fan, R., Ge, X., Sun, Y., 2016. Mater. Sci. Eng. C 68, 308–316.
Rengaraj, A., Haldorai, Y., Kwak, C.H., Ahn, S., Jeon, K.J., Park, S.H., Han, Y.K., Huh, Y.S., 2015. J. Mater. Chem. B 3 (30), 6301–6309.
Reverté, L., Prieto-Simón, B., Campàs, M., 2016. Anal. Chim. Acta 908, 8–21.
Ronkainen, N.J., Okon, S.L., 2014. Materials 7 (6), 4669–4709.
Rotariu, L., Lagarde, F., Jaffrezic-Renault, N., Bala, C., 2016. TrAC Trends Anal. Chem. 79, 80–87.
Ruecha, N., Rangkupan, R., Rodthongkum, N., Chailapakul, O., 2014. Biosens. Bioelectron. 52, 13–19.
Ruiyi, L., Jiajia, W., Ling, L., Zaijun, L., 2016. Microchim. Acta 183 (5), 1641–1649.
Sadhukhan, M., Bhowmik, T., Kundu, M.K., Barman, S., 2014. RSC Adv. 4 (10),

4998–5005.
Saeed, A.A., Sánchez, J.L.A., O'Sullivan, C.K., Abbas, M.N., 2017. Bioelectrochemistry 118, 91–99.
Sağlam, O., Dilgin, Y., 2017. Electroanalysis.
Saidur, M.R., Aziz, A.R.A., Basirun, W.J., 2017. Biosens. Bioelectron. 90, 125–139.
Saini, D., 2016. Nanotechnol. Rev. 5 (4), 393–416.
Šakinyte, I., Barkauskas, J., Gaidukevič, J., Razumiene, J., 2015. Talanta 144, 1096–1103.
Sangamithirai, D., Narayanan, V., Muthuraaman, B., Stephen, A., 2015. Mater. Sci. Engin. C. 55, 579–591.
Sansuk, M., Sritongkham, P., 2015. Amperometric detection of organophosphate and carbamate pesticides Based on AuNPs/graphene-PEDOT:PSS nanocomposites modified electrode. BMEiCON 2014 - Proceedings of the 7th Biomedical Engineering International Conference.
Saxena, U., Das, A.B., 2016. Biosens. Bioelectron. 75, 196–205.
Serry, M., Sakr, M.A., 2016. Sens. Actuators A: Phys. 245, 169–179.
Shanbhag, V.K.L., Prasadi, K.S., 2016. Anal. Methods 8 (33), 6255–6259.
Sharma, S., Raghav, R., O'Kennedy, R., Srivastava, S., 2016. Enzym. Microb. Technol. 89, 15–30.
Shi, L., Yu, Y., Chen, Z., Zhang, L., He, S., Shi, Q., Yang, H., 2015. RSC Adv. 5 (15), 11541–11548.
Shim, Jaeho, Kim, JungKyu, Lee, KyuSeung, Lee, Chang-Lyoul, MingMad, W., 2016. Nano Energy 25, 9–17.
Shrivastava, S., Jadon, N., Jain, R., 2016. TrAC Trends Anal. Chem. 82, 55–67.
Shu, J., Shen, W., Cui, H., 2015. Sci. China Chem. 58 (3), 425–432.
Shuai, H.L., Huang, K.J., Xing, L.L., Chen, Y.X., 2016. Biosens. Bioelectron. 86, 337–345.
Siddique, S., Iqbal, M.Z., Mukhtar, H., 2017. Sens. Actuators B: Chem. 253, 559–565.
Sieben, J.M., Ansón-Casaos, A., Montilla, F., Martínez, M.T., Morallón, E., 2014. Electrochim. Acta 135, 404–411.
Śliwak, A., Grzyb, B., Díez, N., Gryglewicz, G., 2017. Appl. Surf. Sci. 399, 265–271.
Sobolewski, P., Piwowarczyk, M., Fray, M.E., 2016. Macromole. Biosci. 944–957.
Soleymani, J., 2015. TrAC – Trends Anal. Chem. 72, 27–44.
Song, C., Xie, G., Wang, L., Liu, L., Tian, G., Xiang, H., 2014. Biosens. Bioelectron. 58, 68–74.
Song, H.S., Kwon, O.S., Kim, J.-H., Conde, J., Artzi, N., 2017. Biosens. Bioelectron. 89 (Part 1), 187–200.
Song, Y., Luo, Y., Zhu, C., Li, H., Du, D., Lin, Y., 2016. Biosens. Bioelectron. 76, 195–212.
Sookhakian, M., Zalnezhad, E., Alias, Y., 2017. Sens. Actuators, B: Chem. 241, 1–7.
Su, Y., Lv, Y., 2014. RSC Adv. 4 (55), 29324–29339.
Sun, A.-L., Zhang, Y.-F., Sun, G.-P., Wang, X.-N., Tang, D., 2017. Biosens. Bioelectron. 89 (Part 1), 659–665.
Sun, W., Hou, F., Gong, S., Han, L., Wang, W., Shi, F., Xi, J., Wang, X., Li, G., 2015. Sens. Actuators B: Chem. 219, 331–337.
Sun, Y., He, K., Zhang, Z., Zhou, A., Duan, H., 2015. Biosens. Bioelectron. 68, 358–364.
Syedmoradi, L., Daneshpour, M., Alvandipour, M., Gomez, F.A., Hajghassem, H., Omidfar, K., 2017. Biosens. Bioelectron. 87, 373–387.
Szabó, T., Magyar, M., Hajdu, K., Dorogi, M., Nyerki, E., Tóth, T., Lingvay, M., Garab, G., Hernádi, K., Nagy, L., 2015. Nanoscale Res. Lett. 10 (1), 1–12.
Tabrizi, M.A., Zand, Z., 2014. Electroanalysis 26 (1), 171–177.
Tajabadi, M.T., Sookhakian, M., Zalnezhad, E., Yoon, G.H., Hamouda, A.M.S., Azarang, M., Basirun, W.J., Alias, Y., 2016. Appl. Surf. Sci. 386, 418–426.
Tang, S., Tong, P., You, X., Lu, W., Chen, J., Li, G., Zhang, L., 2016. Electrochim. Acta 187, 286–292.
Tanmoy, M., Suvra Prakash, M., 2016. J. Electroanal. Chem. 769, 48–52.
Taranejoo, S., Moghri, M., 2014. Russ. J. Appl. Chem. 87 (1), 69–75.
Termehyousefi, A., Tanaka, H., Bagheri, S., 2017. Rev. Chem. Eng. 33 (2), 201–215.
Terse-Thakoor, T., Komori, K., Ramnani, P., Lee, I., Mulchandani, A., 2015. Langmuir 31 (47), 13054–13061.
Teymourian, H., Salimi, A., Khezrian, S., 2017. Electroanalysis 29 (2), 409–414.
Tezerjani, M.D., Benvidi, A., Jahanbani, S., Moshtaghioun, S.M., Mazloum-Ardakani, M., 2016. J. Electroanal. Chem. 778, 23–31.
Thirumalraj, B., Palanisamy, S., Chen, S.M., Yang, C.Y., Periakaruppan, P., Lou, B.S., 2015. RSC Adv. 5 (95), 77651–77657.
Thirumalraj, B., Rajkumar, C., Chen, S.-M., Barathi, P., 2016. J. Mater. Chem. B.
Tian, J., Wang, J., Li, Y., Huang, M., Lu, J., 2017. J. Electrochem. Soc. 164 (7), H470–H476.
Tian, K., Prestgard, M., Tiwari, A., 2014. Mater. Sci. Eng. C 41, 100–118.
Tian, L., Liu, L., Li, Y., Wei, Q., Cao, W., 2015. New J. Chem. 39 (7), 5522–5528.
Tingting, Y., Ruiyi, L., Xiaohuan, L., Zaijun, L., Zhiguo, G., Guangli, W., Junkang, L., 2016. Electrochim. Acta 187, 143–152.
Tonelli, F.M., Goulart, V.A., Gomes, K.N., Ladeira, M.S., Santos, A.K., Lorençon, E., Ladeira, L.O., Resende, R.R., 2015. Nanomedicine 10 (15), 2423–2450.
Tran, T.-T., Mulchandani, A., 2016. TrAC Trends Anal. Chem. 79, 222–232.
Velmurugan, V., Srinivasarao, U., Ramachandran, R., Saranya, M., Grace, A.N., 2016. Mater. Res. Bull. 84, 145–151.
Verma, D., Gope, P.C., Shandilya, A., Gupta, A., 2014. Trans. Indian Inst. Met.
Vijayaraj, K., Hong, S.W., Jin, S.-H., Chang, S.-C., Park, D.-S., 2016. Anal. Methods.
Vilian, A.T.E., Chen, S.-M., 2014. RSC Adv. 4 (99), 55867–55876.
Wang, B., Yan, S., Lin, Z., Shi, Y., Hu, D., Xu, X., 2015. J. Bionanosci. 9 (5), 330–334.
Wang, B., Yan, S., Lin, Z., Shi, Y., Xu, X., Fu, L., Jiang, J., 2016. J. Nanosci. Nanotechnol. 16 (7), 6895–6902.
Wang, B., He, J., Liu, F., Ding, L., 2017. J. Alloy. Comp. 693, 902–908.
Wang, C., Xu, P., Zhuo, K., 2014. Electroanalysis 26 (1), 191–198.
Wang, C., Sun, Y., Yu, X., Ma, D., Zheng, J., Dou, P., Cao, Z., Xu, X., 2016. J. Mater. Sci.: Mater. Electron. 27 (9), 9370–9378.
Wang, D., Hu, W., Xiong, Y., Xu, Y., Ming Li, C., 2015. Biosens. Bioelectron. 63 (Supplement C), S185–S189.
Wang, F., Gong, W., Wang, L., Chen, Z., 2015. Microchim. Acta 182 (11–12), 1949–1956.
Wang, H., Ma, L., Gan, M., Zhou, T., 2017. J. Alloy. Compd. 699, 176–182.
Wang, H.B., Zhang, H.D., Xu, L.L., Gan, T., Huang, K.J., Liu, Y.M., 2014. J. Solid State Electrochem. 18 (9), 2435–2442.
Wang, L., Xiong, Q., Xiao, F., Duan, H., 2017a. Biosens. Bioelectron. 89 (Part 1), 136–151.
Wang, W., Dong, L., Gong, S., Deng, Y., Yu, J., Dong, H., Wang, T., Sun, W., 2015. Arab. J. Chem.
Wang, W., Bao, T., Zeng, X., Xiong, H., Wen, W., Zhang, X., Wang, S., 2017. Biosens. Bioelectron. 91, 183–189.
Wang, X., Wang, L., Yang, W., Ai, S., 2014. Sens. Actuators B: Chem. 194, 276–282.
Wang, X., Liu, L., Zheng, W., Chen, W., Li, G., Sun, W., 2016. Inter. J. Electrochem. Sci. 11 (3), 1821–1830.
Wang, Y., Bi, C.Y., 2014. RSC Adv. 4 (60), 31573–31580.
Wang, Y., Mao, P., Yan, F., Gao, C., Liu, Y., Ding, J., Wu, W., Liu, Y., 2016. Synth. Met. 222, 198–204.
Wang, Y., Sauriat-Dorizon, H., Korri-Youssoufi, H., 2017a. Sens. Actuators B: Chem. 251, 40–48.
Wang, Y., Yang, S., Wang, H., Zhang, L., Cheng, H., He, B., Li, W., Zou, B., 2017b. Curr. Appl. Phys. 17 (3), 343–350.
Wang, Z., Dai, Z., 2015. Nanoscale 7 (15), 6420–6431.
Wang, Z., Yu, J., Gui, R., Jin, H., Xia, Y., 2016. Biosens. Bioelectron. 79, 136–149.
Wen, J., Xu, Y., Li, H., Lu, A., Sun, S., 2015. Chem. Commun. 51 (57), 11346–11358.
Wen, Z., Zhao, W., Li, X., Niu, X., Wang, X., Yan, L., Zhang, X., Li, G., Sun, W., 2017. Inter. J. Electrochem. Sci. 12 (3), 2306–2314.
Weng, X., Neethirajan, S., 2016. Biosens. Bioelectron. 85, 649–656.
Wu, F., Xu, F., Chen, L., Jiang, B., Sun, W., Wei, X., 2016. Chem. Res. Chin. Univ. 32 (3), 468–473.
Wu, H., Huang, D., Jin, X., Luo, C., Dong, Q., Sun, B., Zong, R., Li, J., Zhang, L., Zhang, H., 2016. Anal. Methods 8 (14), 2961–2966.
Wu, H., Yu, Y., Gao, W., Gao, A., Qasim, A.M., Zhang, F., Wang, J., Ding, K., Wu, G., Chu, P.K., 2017. Sens. Actuators B: Chem. 251, 842–850.
Wu, L., Yin, W., Tang, K., Li, D., Shao, K., Zuo, Y., Ma, J., Liu, J., Han, H., 2016. Enzymatic biosensor of horseradish peroxidase immobilized on Au-Pt nanotube/Au-graphene for the simultaneous determination of antioxidants. Anal. Chim. Acta 933, 89–96.
Wu, L., Lu, X., Fu, X., Wu, L., Liu, H., 2017. Gold Nanoparticles dotted reduction graphene oxide nanocomposite based electrochemical aptasensor for selective, rapid, sensitive and congener-specific PCB77 detection. Sci. Rep. 7 (1).
Wu, Q., Hou, Y., Zhang, M., Hou, X., Xu, L., Wang, N., Wang, J., Huang, W., 2016. Anal. Methods 8 (8), 1806–1812.
Wu, S., Wang, Y., Mao, H., Wang, C., Xia, L., Zhang, Y., Ge, H., Song, X.-M., 2016. RSC Adv. 6 (64), 59487–59496.
Wu, S., Su, F., Dong, X., Ma, C., Pang, L., Peng, D., Wang, M., He, L., Zhang, Z., 2017. Appl. Surf. Sci. 401, 262–270.
Wu, X., Chai, Y., Yuan, R., Zhong, X., Zhang, J., 2014. Electrochim. Acta 129, 441–449.
X, W., Zhang, F., Xia, J., Wang, Z., Bi, Z., Xia, L., Li, Y., Xia, Y., Xia, L., Wang, X., 2015. J. Electroanal. Chem. 738, 203–208.
Xi, J., Xie, C., Zhang, Y., Wang, L., Xiao, J., Duan, X., Ren, J., Xiao, F., Wang, S., 2016. ACS Appl. Mater. Interfaces 8 (34), 22563–22573.
Xie, Q., Bao, R., Xie, C., Zheng, A., Wu, S., Zhang, Y., Zhang, R., Zhao, P., 2016a. J. Power Sources 317, 133–142.
Xie, Q., Zheng, A., Xie, C., Fu, W., Wu, S., Zhang, Y., Zhao, P., 2016b. Microporous Mesoporous Mater. 224, 239–244.
Xie, R., Wang, Z., Zhou, W., Liu, Y., Fan, L., Li, Y., Li, X., 2016. Anal. Methods 8 (20), 4001–4006.
Xiong, D., Li, X., Shan, H., Yan, B., Li, D., Langford, C., Sun, X., 2016. Appl. Energy 175, 512–521.
Xu, J., Wang, Y., Hu, S., 2017. Microchim. Acta 184, 1.
Xu, S., Zhang, Y., Dong, K., Wen, J., Zheng, C., Zhao, S., 2017. Int. J. Electrochem. Sci. 12 (4), 3443–3458.
Xu, X., Zheng, Q., Bai, G., Song, L., Yao, Y., Cao, X., Liu, S., Yao, C., 2017. Electrochim. Acta 242, 56–65.
Xu, Z., Cheng, X., Tan, J., Gan, X., 2016. Biotechnol. Appl. Biochem. 63 (6), 757–764.
Xue, Q., Liu, Z., Guo, Y., Guo, S., 2015. Biosens. Bioelectron. 68, 429–436.
Xue, S., Jing, P., Xu, W., 2016. Biosens. Bioelectron. 86, 958–965.
Xue, W., Bo, X., Zhou, M., Guo, L., 2016. J. Electroanal. Chem.
Yan, J., Zhong, T., Qi, W., Wang, H., 2015. J. Inorg. Organomet. Polym. Mater. 25 (2), 275–281.
Yan, L., Zhao, W., Wen, Z., Li, X., Niu, X., Huang, Y., Sun, W., 2017. Int. J. Electrochem. Sci. 12 (5), 4086–4095.
Yan, S., Wang, B., Lin, Z., Sun, B., Pan, L., Wu, J., Shi, Y., 2016. Sci. Adv. Mater. 8 (6), 1165–1171.
Yan, Y., Liu, Q., Du, X., Qian, J., Mao, H., Wang, K., 2015. Anal. Chim. Acta 853 (1), 258–264.
Yáñez-Sedeño, P., González-Cortés, A., Agüí, L., Pingarrón, J.M., 2016. Electroanalysis 28 (8), 1679–1691.
Yang, C., Denno, M.E., Pyakurel, P., Venton, B.J., 2015a. Anal. Chim. Acta 887, 17–37.
Yang, C., Hu, L.W., Zhu, H.Y., Ling, Y., Tao, J.H., Xu, C.X., 2015b. J. Mater. Chem. B 3 (13), 2651–2659.
Yang, F., Yang, Z., Zhuo, Y., Chai, Y., Yuan, R., 2015c. Biosens. Bioelectron. 66, 356–362.
Yang, G., Zhu, C., Du, D., Zhu, J., Lin, Y., 2015d. Nanoscale 7 (34), 14217–14231.
Yang, J.K., Kwak, S.Y., Jeon, S.J., Lee, E., Ju, J.M., Kim, H.I., Lee, Y.S., Kim, J.H., 2016. Nanoscale 8 (24), 12272–12281.
Yang, M., Kim, D.S., Lee, T.J., Lee, S.J., Lee, K.G., Choi, B.G., 2016. J. Colloid Interface Sci. 468, 51–56.
Yang, W., Liu, J., Zhang, X., Chen, L., Zhou, Y., Zou, Z., 2016. Appl. Energy.

Yang, Y., Asiri, A.M., Du, D., Lin, Y., 2014. Analyst 139 (12), 3055–3060.
Yang, Y., Shi, W., Zhang, R., Luan, C., Zeng, Q., Wang, C., Li, S., Huang, Z., Liao, H., Ji, X., 2016. Electrochim. Acta 204, 100–107.
Yang, Y.J., Li, W., 2014. Biosens. Bioelectron. 56, 300–306.
Yanga, Yingkui, Hana, Cuiping, Jianga, Beibei, Iocozziaa, James, Heb, Chengen, Shib, Dean, Jiangb, Tao, Lina, Z., 2016. Mater. Sci. Eng. R 102 (2016), 1–72 (**102:** 1-72).
Yardım, Y., Vandeput, M., Çelebi, M., Şentürk, Z., Kauffmann, J.M., 2017. Electroanalysis 29 (5), 1451–1458.
Yoon, J., Lee, T., Bapurao G, B., Jo, J., Oh, B.-K., Choi, J.-W., 2017. Biosens. Bioelectron. 93, 14–20.
Yu, N., Wang, Z., Wang, C., Han, J., Bu, H., 2017. Anal. Chim. Acta 962, 24–31.
Yu, Y., Chen, Z., He, S., Zhang, B., Li, X., Yao, M., 2014. Biosens. Bioelectron. 52, 147–152.
Yusoff, N., Rameshkumar, P., Mehmood, M.S., Pandikumar, A., Lee, H.W., Huang, N.M., 2017. Biosens. Bioelectron. 87, 1020–1028.
Zaidi, S.A., Shin, J.H., 2016. Talanta 149, 30–42.
Zan, X., Bai, H., Wang, C., Zhao, F., Duan, H., 2016. Chem. – Eur. J. 22 (15), 5204–5210.
Zeng, Y., Zhu, Z., Du, D., Lin, Y., 2016. J. Electroanal. Chem. 781, 147–154.
Zhai, Y., Zhu, Z., Dong, S., 2015. ChemCatChem 7 (18), 2806–2815.
Zhan, H., Li, J., Liu, Z., Zheng, Y., Jing, Y., 2015. Anal. Methods 7 (9), 3903–3911.
Zhan, T., Tan, Z., Wang, X., Hou, W., 2018. Sens. Actuators B: Chem. 255, 149–158.
Zhang, A., Lieber, C.M., 2016. Chem. Rev. 116 (1), 215–257.
Zhang, J., Xiong, Z., Chen, Z., 2017. Sens Actuators B: Chem. 246, 623–630.
Zhang, M., Liao, C., Mak, C.H., You, P., Mak, C.L., Yan, F., 2015. Sci. Rep. 5.
Zhang, Q., Xu, Q., Guo, Y., Sun, X., Wang, X., 2016. RSC Adv. 6 (29), 24698–24703.
Zhang, R., Chen, W., 2015. Biosens. Bioelectron.
Zhang, R.Z., Pan, B.G., Wang, H.N., Dan, J.M., Hong, C.L., Li, H.L., 2015. RSC Adv. 5 (48), 38176–38182.
Zhang, S., Zang, L., Zhang, X., Dai, H., Xu, G., Zhang, Q., Yang, C., Lin, Y., 2016. Electrochim. Acta 196, 67–74.
Zhang, T., Liu, J., Wang, C., Leng, X., Xiao, Y., Fu, L., 2017. Biosens. Bioelectron. 89, 28–42.
Zhang, X., Zhang, Y.C., Ma, L.X., 2016. Sens. Actuators B: Chem. 227, 488–496.
Zhang, X., Wang, J., Liu, J., Wu, J., Chen, H., Bi, H., 2017. Carbon 115, 134–146.
Zhang, Y., Wei, Q., 2016. J. Electroanal. Chem.
Zhang, Y., Liu, H., Yang, Z., Ji, S., Wang, J., Pang, P., Feng, L., Wang, H., Wu, Z., Yang, W., 2015. Anal. Methods 7 (15), 6213–6219.
Zhang, Y., Li, J., Wang, Z., Ma, H., Wu, D., Cheng, Q., Wei, Q., 2016a. Sci. Rep. 6.
Zhang, Y., Shen, J., Li, H., Wang, L., Cao, D., Feng, X., Liu, Y., Ma, Y., Wang, L., 2016b. Chem. Rec. 16 (1), 273–294.
Zhang, Y., Li, H., Chen, M., Fang, X., Pang, P., Wang, H., Wu, Z., Yang, W., 2017. Sens. Actuators B: Chem. 249, 431–438.
Zhang, Z., Fu, X., Li, K., Liu, R., Peng, D., He, L., Wang, M., Zhang, H., Zhou, L., 2016. Sens. Actuators B: Chem. 225, 453–462.
Zhao, B., Chen, D., Xiong, X., Song, B., Hu, R., Zhang, Q., Rainwater, B.H., Waller, G.H., Zhen, D., Ding, Y., Chen, Y., Qu, C., Dang, D., Wong, C.P., Liu, M., 2017. Energy Storage Mater. 7, 32–39.
Zhao, C., Wu, X., Zhang, X., Li, P., Qian, X., 2017. J. Electroanal. Chem. 785, 172–179.
Zhao, H., Ji, X., Wang, B., Wang, N., Li, X., Ni, R., Ren, J., 2015. Biosens. Bioelectron. 65, 23–30.
Zhao, H., Liu, F., Wu, S., Yang, L., Zhang, Y.P., Li, C.P., 2017. Nanoscale 9 (12), 4272–4282.
Zhao, L., Li, H., Gao, S., Li, M., Xu, S., Li, C., Guo, W., Qu, C., Yang, B., 2015. Electrochim. Acta 168, 191–198.
Zhao, R., Liu, X., Zhang, J., Zhu, J., Wong, D.K.Y., 2015. Electrochim. Acta 163, 64–70.
Zheng, H.W., Liang, X., Yu, Y.H., Wang, K., Zhang, X.A., Men, B.Q., Diao, C.L., Peng, C.X., Yue, G.T., 2017. Nanoscale Res. Lett. 12 (1).
Zheng, Y., Liu, Z., Jing, Y., Li, J., Zhan, H., 2015. Sens. Actuators B: Chem. 210, 389–397.
Zhong, G.X., Wang, P., Fu, F.H., Weng, S.H., Chen, W., Li, S.G., Liu, A.L., Wu, Z.Y., Zhu, X., Lin, X.H., Lin, J.H., Xia, X.H., 2014. Talanta 125, 439–445.
Zhou, H., Liu, J., Zhang, S., 2015. TrAC - Trends Anal. Chem. 67, 56–73.
Zhou, N., Li, C., Mo, R., Zhang, P., He, L., Nie, F., Su, W., Liu, S., Gao, J., Shao, H., Qian, Z.J., Ji, H., 2016. Surf. Rev. Lett. 23 (2), 1550103.
Zhu, C., Du, D., Lin, Y., 2015. 2D Mater. 2 (3).
Zhu, C., Du, D., Lin, Y., 2017. Biosens. Bioelectron. 89, 43–55.
Zhu, Q., Bao, J., Huo, D., Yang, M., Wu, H., Hou, C., Zhao, Y., Luo, X., Fa, H., 2017. J. Electroanal. Chem. 799, 459–467.
Zhu, X., Li, J., He, H., Huang, M., Zhang, X., Wang, S., 2015. Biosens. Bioelectron. 74, 113–133.
Zhu, X., Wu, G., Lu, N., Yuan, X., Li, B., 2017. J. Hazard. Mater. 324, 272–280.
Zhu, Y., Lu, S., Gowri Manohari, A., Dong, X., Chen, F., Xu, W., Shi, Z., Xu, C., 2017. J. Electroanal. Chem. 796, 75–81.
Zor, E., Saglam, M.E., Akin, I., Saf, A.O., Bingol, H., Ersoz, M., 2014. RSC Adv. 4 (24), 12457–12466.
Zou, F., Zhou, H., Van Tan, T., Kim, J., Koh, K., Lee, J., 2015. ACS Appl. Mater. Interfaces 7 (22), 12168–12175.
Zou, H.L., Li, B.L., Luo, H.Q., Li, N.B., 2015. Sens. Actuators B: Chem. 207 (Part A), 535–541.